2000

X-ray diffraction and Rietveld structural refinement of selected fluoroperovskites

Ross, Kirk Campbell

X – Ray Diffraction and Rietveld Structural Refinement of Selected Fluoroperovskites

By Kirk C. Ross ©

A thesis submitted in partial fulfillment of the requirements for the degree of Master of Science

Supervisor: Dr. R.H. Mitchell
Lakehead University
Thunder Bay, Ontario, Canada

May 2000

Figure Index

Table Index

Abstract

This study presents an X-ray diffraction analysis and Rietveld structural refinement of selected synthetic fluoroperovskite-type compounds including the $Na_{1-x}K_xMgF_3$ solid solution series in addition to synthetic analogues of cryolite (Na_2NaAlF_6) and simmonsite (Na_2LiAlF_6).

The $Na_{1-x}K_xMgF_3$ solid solution series is comprised of three structurally distinct perovskite phases. In order of increasing potassium they are: orthorhombic (***Pbnm***, a = 5.3609(1), b = 5.4862(1), c = 7.6661(1), Z = 4) in the x = 0 – 0.35 compositional range, tetragonal (***P4/mbm***, a = 5.444(3), c = 3.9217(3), Z = 2) in the x = 0.40 ~ 0.46 compositional range and cubic (***Pm$\bar{3}$m***, a = 3.9903, Z = 1) in the x = 0.50 – 1.0 compositional range. The orthorhombic and tetragonal members are derived from the cubic aristotype by octahedral rotation, $a^-a^-c^+$ and $a^0a^0c^+$ respectively. Introduction of potassium into the Na 4***c*** crystallographic site results in a decrease of octahedral rotation and an overall reduction of structural distortion from f = 4.42 for the neighborite end member to f = 5.0 for cubic members. This is accompanied by an increase in the pseudocubic cell dimension in addition to a reduction in ***A***-site cationic displacement. Angular and bond length distortion of the MgF_6 octahedron are at a maximum in the x = 0.20 intermediate member of the series and decrease linearly with additional potassium. These effects are a direct result of cations approaching special positions in the unit cell as potassium is introduced into the neighborite structure.

Synthetic cryolite (Na_2NaAlF_6) and synthetic simmonsite (Na_2LiAlF_6) investigated exhibited similar structural characteristics such as 1:1 ***B***-site cationic ordering and an $a^+b^-b^-$ octahedral rotation scheme. Synthetic cryolite exhibited the

greatest structural and octahedral distortion (f = 4.07, $\Delta_{B'}$ = 0.016, $\delta_{B'}$ = 11.75) and octahedral rotation ($\Phi_{B'}$ = 18.6) as compared to simmonsite (f = 4.52, $\Delta_{B'}$ = 0.06, $\delta_{B'}$ = 2.74 and $\Phi_{B'}$ = 14.96). These ordered monoclinic perovskites ($\boldsymbol{P2_1/n}$, $\boldsymbol{a \approx b \approx \sqrt{2}a_p}$, $\boldsymbol{c \approx 2a_p}$) are derived from the cubic aristotype by octahedral rotation and ***B***-site cationic ordering.

Acknowledgements

I would like to thank Dr. Roger Mitchell for introducing me to the world of mineralogy and crystallography. He provided vital suggestions, motivation and inspiration. Without his support both academically and financially, this research could not have happened.

I would also like to thank Dr. Anton Chakhmouradian for providing many valuable comments and giving me a great deal of insight into perovskite structures. Anton also taught me a great deal about the Rietveld refinement procedure. His comments and instruction were invaluable to the success of this work.

I would also like to thank Ann and Stuart Ross for their continual support through my entire academic career. They provided essential support financially and mentally for the preceding six years. This work is dedicated to my Mother.

Chapter 1, Introduction and Experimental

1.1 Introduction

The family of fluoro – perovskite compounds includes a wide variety of minerals and synthetic phases. Perovskite – type compounds are so – named because of their structural similarities to perovskite *sensu stricto,* $CaTiO_3$. Perovskite – type compounds conform to ABX_3 stoichiometry, where A and B are cations and X is anionic The ideal structure is based on cubic closest packed ions in a $Pm\bar{3}m$ space group, best described as a corner linked BX_6 octahedral framework where, in the ideal structure, the A – site cations are in 12 – fold coordination. Perovskite compounds are well known for their high tolerance of cationic substitution in both the A and B structural sites, which may result in one or more structural distortions, including: A-site cationic displacement, B – site cationic displacement, octahedral distortion and octahedral rotation. Such structural distortions result in a wide variety of stable perovskite- type compositions.

Perovskites are of interest to both industrial and mineralogical researchers. Industrial applications for synthetic perovskite – type compounds include capacitors and high temperature superconductors, in addition to numerous other electronic applications. Researching, understanding and developing new perovskite phases is crucial to the development of many electronic and computer based technologies. In many cases, insight into the stability of synthetic perovskite – type compounds comes from the study of naturally occurring perovskite – type phases. In addition, perovskite – type compounds are also undergoing investigations to determine their actinide – lanthanide sequestration properties, significant to those who wish to find a repository for nuclear waste. Furthermore, it is widely accepted that magnesium silicate perovskite ($MgSiO_3$) is the main constituent of the lower

mantle of the Earth. Unfortunately, this phase is not stable under ambient conditions. Therefore the study of the geophysical properties, such as seismic velocity and elasticity constants exhibited by low pressure, low temperature analogues of magnesium silicate perovskite is necessary to understand better the characteristics of the lower mantle. Interestingly, neighborite ($NaMgF_3$) is isoelectronic and isostructural with $MgSiO_3$ perovskite. The comparable ionic radii and 1:2 electronic charge ratio in $NaMgF_3$ and $MgSiO_3$ make neighborite an ideal analogue for $MgSiO_3$ perovskite.

Neighborite exists in solid solution with potassium neighborite in a 1995 Oldoinyo Lengai natro - carbonatite lava flow in Tanzania. The dissolution of potassium into naturally-occurring neighborite structure has been documented only by Mitchell (1997). Solubility of potassium into synthetic neighborite has been previously determined by Ross (1998) and Zhao (1999).

1.2 Purpose

The main objective of this work is to determine the crystal chemical effects of the substitution of potassium in the neighborite structure. The system $NaMgF_3$ - $KMgF_3$ is a direct analogue of the fluoroperovskite minerals found in the Oldoinyo Lengai natrocarbonatites. The system is investigated because the naturally - occurring material forms crystals which are far too small to be extracted for X - ray diffraction analysis. In addition, knowledge of the phase transitions induced in neighborite by large cation substitution is important with respect to phase transitions to be expected in the lower mantle.

A second objective is to determine the structure of synthetic simmonsite, Na_2LiAlF_6. The structure of this recently recognized mineral (Foord *et al.*, 1999), which is a 1:1 ordered

double perovskite, has not been solved as natural samples are complexly twinned and intergrown with other fluorides

1.3 Apparatus

1.3.1 Hardware

Powder X-ray diffraction (XRD) patterns of synthesis products were obtained on a Phillips 3710 diffractometer. ($T = 20^0C$; radiation: $CuK\alpha$; range $10\text{-}145^\circ$ 2θ). Data were collected in 0.02° 2θ increments for a duration of 2-6 seconds per step. These data were used as input files and are compared to a mathematically generated XRD pattern created by a Rietveld refinement program such as **FULLPROF** or **DBWS.**

Composition and phase relations of samples were determined by X-ray energy-dispersion spectrometry (EDS) using a Hitachi 570 scanning electron microscope equipped with a **LINK ISIS** analytical system incorporating a super ATW light element detector. The duration of spectra acquisition was in the 30 –120s range, however an accelerating voltage of 20kV and a beam current of $\cong$ 0.86nA was used consistently. Spectra were processed using the **LINK ISIS-SEMQUANT** software package. Well-characterized synthetic and natural standards were employed for compositional determination.

1.3.2 Software

Rietveld Refinement

Structural parameters for compounds synthesized in this study were achieved by the Rietveld refinement procedure for powder X-ray diffractive data. The XRD data were analyzed using two similar refinement programs: **DBWS,** and **FULLPROF** (Rodriguez – Carvajal, 1990). Both of these programs are based on the **DBW** code written by Young and Wiles (1981), which in turn is based on the original Rietveld refinement program written by

Rietveld and Hewit (Young, 1981). The versions used in this study were **FP 98 -** V 0.2 and **DB24k** for **FULLPROF** and **DBWS** respectively. They are nearly identical in input control cards, matrix operations and output files; however, they differ in that **FULLPROF** has the ability to generate *h,k,l* dependant **FWHM** parameters to account for size and strain effects, in addition to *h,k,l* dependant shifts or asymmetry caused by special defect types. Although these features did not prove to be particularly advantageous in this study, structural parameters and final agreement factors given herein are derived by **FULLPROF**. The peaks were modeled using a pseudo – Voigt profile function corrected for asymmetry to 45^0 2θ. Thermal isotropic parameters for contaminant phases were fixed at previously determined values.

Coordination and Bond Valence analysis

Atomic and cell parameters obtained from the Rietveld refinement procedure were used in an input file for the coordination analysis software package: **IVTON**. (Balic – Zunic and Vikovic 1996) When executed, this program creates an output file consisting of: bond lengths, bond angles, polyhedral volumes, bond valence parameters in addition to other crystallo-chemical information based on parameters specified by the user in the input file.

Graphics

Graphical representations of structures are drawn from **ATOMS** (Dowty 1970) and **CARINE** (Boudias *et al.* 1997, V3.1) software programs. **ATOMS** provides the user with a windows driven interface which allows the user to export the structure in one of several graphical formats including VRML. **ATOMS** also provides a coordination analysis feature providing redundancy for the validation of parameters given by **IVTON**. In contrast, **CARINE** does not provide the various export features that **ATOMS** does, however,

CARINE gives the user a more direct interface with the observed structure. For example, individual bond lengths and angles in addition to coordination spheres and polyhedral identification may be obtained by a "point and click" interface.

1.4 Synthesis

1.4.1 Aqueous Synthesis

Part of this research project included several syntheses of low – temperature, aqueous neighborite perovskite, a technique which has not been previously documented. Data in figure 1.4.1 are from synthesis products obtained from the low temperature reaction

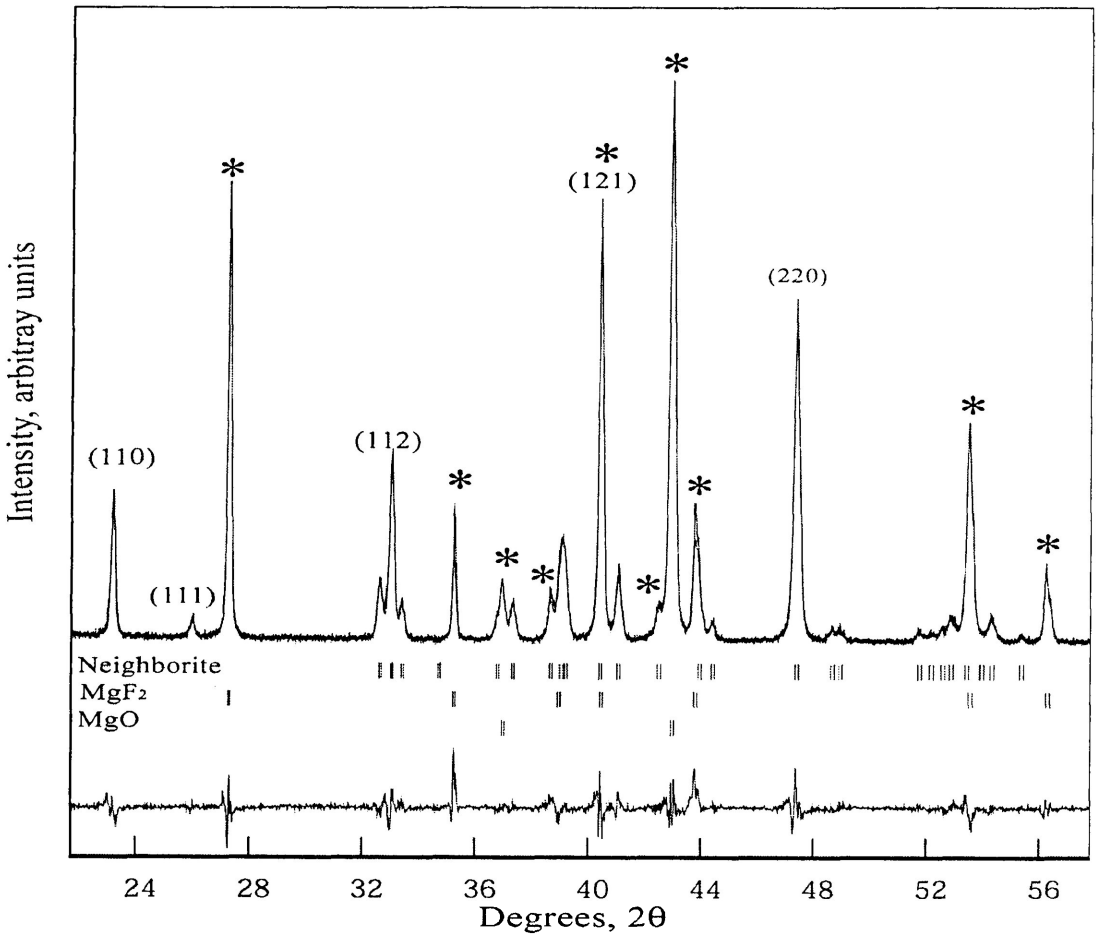

Figure 1.4.1
XRD pattern showing major peaks from neighborite (indexed) synthesized by aqueous methods. * indicate reflections caused by contaminants. CuKα radiation

$$NaOH + MgO + HF = NaMgF_3 + H_2O$$

The reagents were mixed under water in an agate mortar and pestle and washed into a Teflon crucible. Next, an excess of HF was added. The mixture was stirred for several minutes and allowed to dry over a 24h period under low heat. The residuum was then analyzed by the X – ray diffraction techniques outlined in section 1.3.1. Inspection of figure 1.4.1 shows clearly resolvable neighborite perovskite peaks and proves that this synthesis was successful in the production of neighborite. Additional phases present consist mainly of initial reagents. The relatively large content of contaminants made these samples unfavorable for structural refinement and they were therefore not analyzed by Rietveld refinement. Note that these data indicate that neighborite can be made by low -temperature aqueous synthesis *i.e.* an environment similar to that of the type locality in the Green River Formation, South Ouray, Utah (Chao *et al.* 1961).

1.4.2 Ceramic synthesis

Synthesis methods involving the mixture of stoichiometric quantities of NaF, KF and MgF_2 are referred to here as ceramic synthesis. Initial reagents were mixed under acetone in an agate mortar and pestle, dried under heat and synthesized at 750 ^{0}C. Several samples were synthesized in different environments to determine the effects of air on the synthesis products. Sellite (MgF_2) was occasionally present in trace amounts, whereas periclase (MgO) was commonly present in amounts less than or equal to 5 volume percent. In an attempt to produce a synthesis product free of contaminants, several different methods were employed. Initially stoichiometric quantities of NaF, KF, and MgF_2 were mixed as above, placed in an alumina crucible and annealed at 750 ^{0}C for 5 hours at 1 atm. This technique was successful

in the production of neighborite solid solution members, however, periclase was nearly always present. Diffraction data from MgF_2 used in this study did not reveal the presence of MgO as a contaminant; therefore, the MgO in the final products was attributed to the volatilization of F and the subsequent oxidation of Mg to MgO. To remedy this problem, samples identical to the ones above were placed in a tube oven (fig1.4.2) under a constant flow of N_2 gas at 1atm at 750 ^{0}C for 5 hrs. Although cumbersome, this method was successful in the reduction of MgO observed in the XRD patterns.

It was noted that as charges approached end member composition the amount of MgO observed in the XRD spectra was less than that for members of intermediate compositions. On this basis, a third method was employed. Intermediate members were made by mixing stoichiometric quantities of pre - synthesized end members. The end – member mixture method was the most successful in producing samples virtually free of periclase (<2 vol%). Data reported herein are from samples synthesized in this manner.

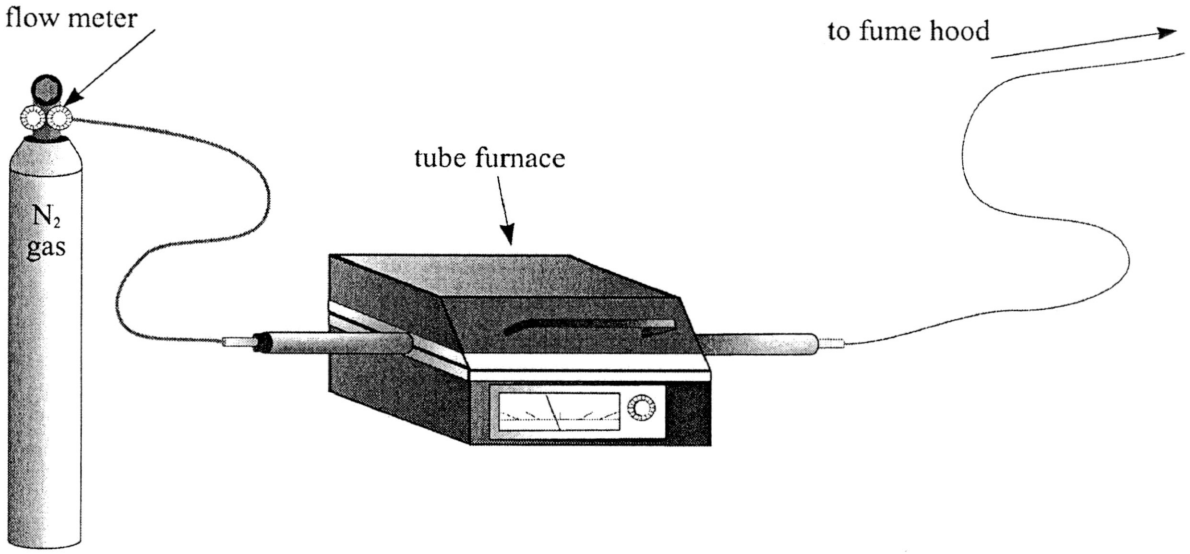

Figure 1.4.2,
A schematic diagram of the tube oven employed to reduce the amount of periclase contamination by synthesizing members in an anoxic environment.

Alumino – fluorides were synthesized by mixing pre – dried stoichiometric quantities of binary fluorides under acetone with an agate mortar and pestle. The mixture was placed in a silica tube fused at one end. This tube was then evacuated of air and subsequently collapsed, sealed at the remaining end and placed in the furnace illustrated in figure 1.4.2 at 600^0C for 24h. The low pressure synthesis environment does not appear to have an effect on the structure at 1 atm. It should be noted that if water is present in the sealed tube during synthesis bursting may occur.

Chapter 2, End – Member Fluoroperovskites

2.1.1$KMgF_3$

Potassium - bearing neighborite occurs naturally as 2 – 10 μm anhedral grains in the 1995 Oldoinyo Lengai lava flow (Mitchell, 1997; Dawson *et al.* 1995). The potassium content in neighborite from Oldoinyo Lengai ranges from 15.6 – 16.8 wt.% K (Mitchell, 1997). Chemically pure end member $KMgF_3$ is the potassium analogue of neighborite and has not been observed in nature.

2.1.2 XRD Data

Synthetic $KMgF_3$ was analyzed by the X – ray diffraction techniques outlined in section 1.3.1 and 1.3.2. Figure 2.1.2 shows a Rietveld refinement difference plot for X –ray diffraction data acquired from $KMgF_3$. The presence of peaks indexed with both odd and even indices indicates a primitive unit cell. R- Bragg for the refinement is 3.90%. All available final agreement parameters are given in appendix A-1.

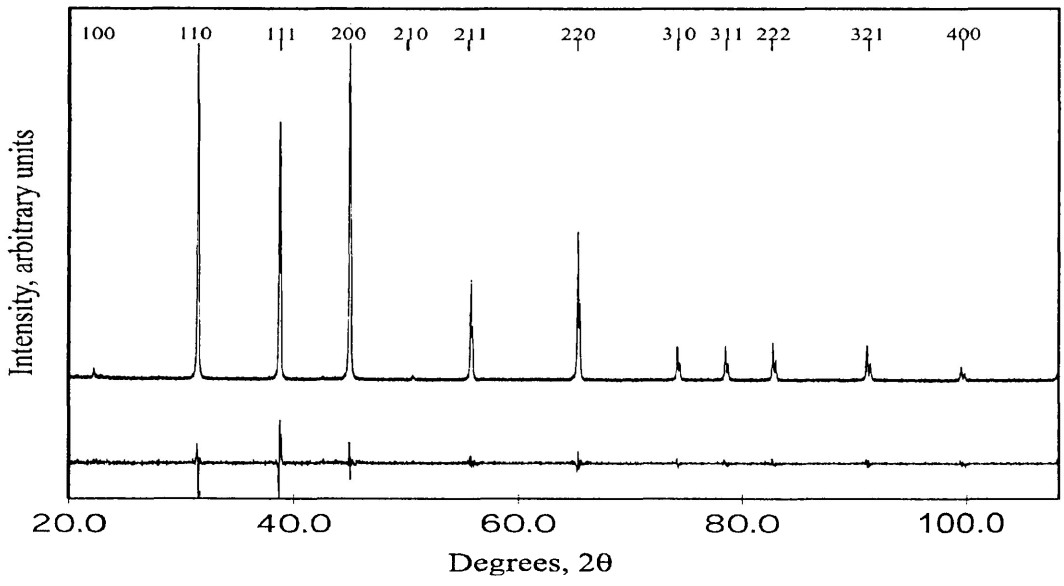

Figure 2.1.2
XRD diffraction pattern and Rietveld difference plot for $KMgF_3$ perovskite. (This work). CuKα radiation, 20 – 110^0 2θ shown.

2.1.3 Structure

Least squares Rietveld structural refinement from this work (**DBWS** and **FULLPROF**) and previous studies (Burns *et al.* 1996) show that $KMgF_3$ crystallizes in a cubic $\boldsymbol{Pm\bar{3}m}$ ($\boldsymbol{a}$ = 3.9903(0) Å) perovskite arrangement at ambient temperatures and pressures. Structural solution and refinement methods (section 1.3.1) included atomic positions, cell dimensions and thermal isotropic parameters. Final cell parameters given by the refinement were in good agreement with those derived by Burns *et al.* (1996).

Cubic $KMgF_3$ perovskite has 3 crystallographically distinct atoms in its structure: potassium (1*b*), magnesium (1*a*) and fluorine (3*d*). The absence of octahedral tilts in $KMgF_3$ results in cubic symmetry (Figure 2.2.1). Thus, the description of the octahedral tilt scheme would be $\boldsymbol{a^0\ a^0\ a^0}$ (Glazer 1977) and $\Phi = 0$ (Zhao *et al.*1993a, defined below). Table 2.1.3 gives crystallographic parameters for $KMgF_3$ ($\boldsymbol{Pm\bar{3}m}$, $\boldsymbol{Z}$ = 1) from this study and Burns *et al.* (1996) and shows that all atoms in this structure are in special positions.

The holosymmetric character results in perfect cubic coordination of both cations. The 12 – coordinated potassium atoms are centralized in a coordination sphere of radius 2.822(1)Å, and magnesium cations are in octahedral coordination by six fluorine anions at a distance of 1.995(1)Å. The first coordination sphere for fluorine contains only two magnesium atoms and reflects the $\boldsymbol{B - X - B}$ angle of 180^0 illustrated in table 2.1.3.

Bond valence parameters (BVP) were computed utilizing the **IVTON** software package. Submitted (Sub) and calculated (Calc) values for each crystallographically distinct ion are in reasonable agreement and are given in adjacent columns in the fifth row of table 2.1.3.

Table 2.1.3 Comparison of crystallographic characteristics of $KMgF_3$ from this work and Burns *et al.*(1997)

Atom			K		Mg		F	
site			1*a*		1*b*		3*c*	
coordination #			6		12		2	
Point Symmetry			***m-3m***		***m-3m***		***4/mmm***	
BVP	Sub	Calc	1.0	1.0	2.0	2.0	-1.0	-1.0
Atomic Coordinates		*x*	1/2		0		1/2	
		y	1/2		0		1/2	
		z	1/2		0		0	
N			1/48		1/48		1/48	
Z			1					
Crystal System			cubic					
Point Group			m-3m					
Space Group			$Pm\bar{3}m$					
Reflection limiting conditions			none					
a (Å)			3.9903(0)		3.9859			
			This study		Burns *et al.*(1997)			
V ($Å^3$)			63.536(3)					
ϕ			0					
θ			0					
Φ			0					
Bond length (Å)								
K – F			2.822(1)					
Mg – F			1.995(2)					
Bond Angle ^{0}								
B - X - B			180					

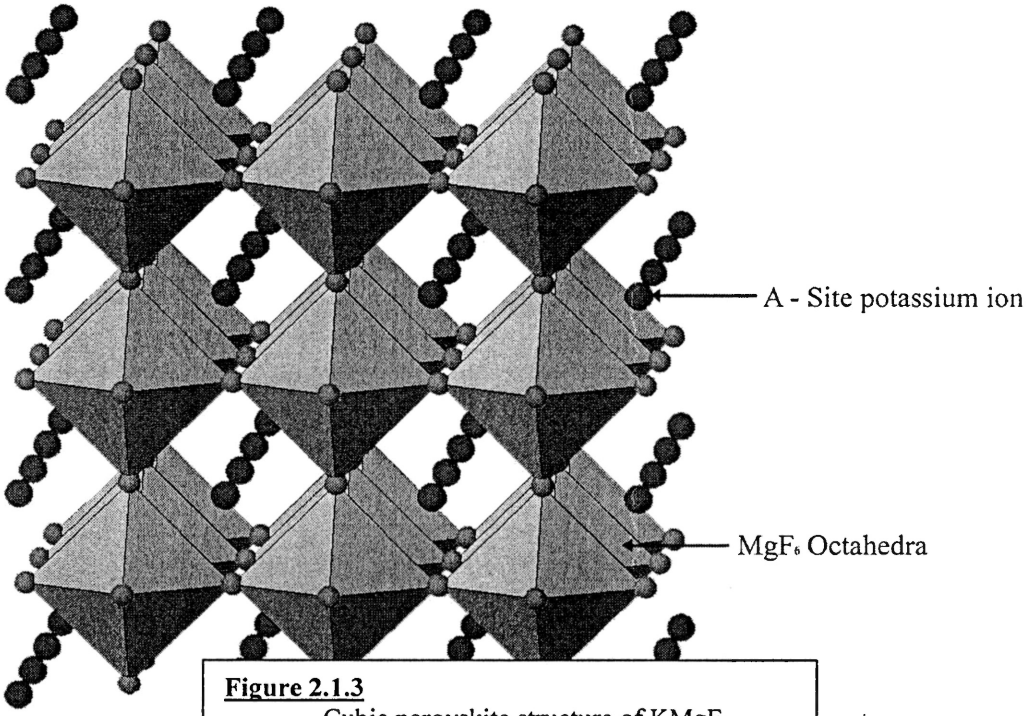

Figure 2.1.3
Cubic perovskite structure of $KMgF_3$

2.2.1 Neighborite ($NaMgF_3$)

Neighborite ($NaMgF_3$) was discovered in 1961 in the Green River formation South Ouray, Utah by Frank Neighbor, a geologist for the Sun Oil Company (Chao *et al.* 1961). Initially characterized by Chao *et al.* (1961), neighborite is of particular interest to mineralogists because it possesses structural, chemical and electronic properties similars to those of $MgSiO_3$ – perovskite, the phase believed to constitute the bulk of the lower mantle (Zhao *et al.* 1993).

Table 2.2.1 gives a comparison of cell dimensions and atomic coordinates of neighborite as determined from this and previous studies (Chao *et al.* 1961, Zhao *et al.* 1993a, b, 1998).

Table 2.2.1Comparison of crystallographic characteristics of $NaMgF_3$ (*Pbnm*, Z=4) from this work and previous studies.

WYCKOFF POSITION	N		This study	Zhao*et al.*	Chao *et al.*	Leutgert (1992)
		a	5.3609(1)	5.3596(1)	5.363(1)	5.325(3)
		b	5.4862(1)	5.4867(1)	5.503(1)	5.484(3)
		c	7.6661(1)	7.6657(1)	7.676(1)	7.654(3)
		Volume	225.46(1)	225.42(1)	226.54(1)	223.5
4*c*	0.5	Na				
		x	0.9897(3)	0.9893(3)		0.9896(3)
		y	0.0439(2)	0.0443(3)		0.0441(2)
		z	0.25	0.25		0.25
4*b*	0.5	Mg				
		x	0	0		0
		y	0.5	0.5		0.5
		z	0	0		0
4*c*	0.5	F(1) apical				
		x	0.0897(3)	0.0865(4)		0.0886(4)
		y	0.4723(3)	0.4716(4)		0.473(3)
		z	0.25	0.25		0.25
8*d*	1	F(2) Equatorial				
		x	0.7035(2)	0.7013(3)		0.7027(2)
		y	0.2961(2)	0.2953(3)		0.2948(2)
		z	0.0474(1)	0.0468(2)		0.0459(1)

Note. Final agreement factors for synthetic neighborite are R_B= 4.93, R_P =10.78, R_{WP} =14.25, S=1.77, D-W D= 0.59 (This work). N = Wyckoff number/ Multiplicity of the general position.

The space group of neighborite is conventionally given as ***Pbnm,*** which is the ***cab*** setting of space group no.62 (Zhao *et al.* 1993a,b). This setting normally places the longest unit cell dimension parallel to the ***c***-axis, the shortest parallel to the ***a***-axis and the intermediate parallel to the ***b***-axis. Arrangements of the six symmetrically equivalent settings are illustrated in figure 2.2.1 (O'Keefe and Hyde 1996).

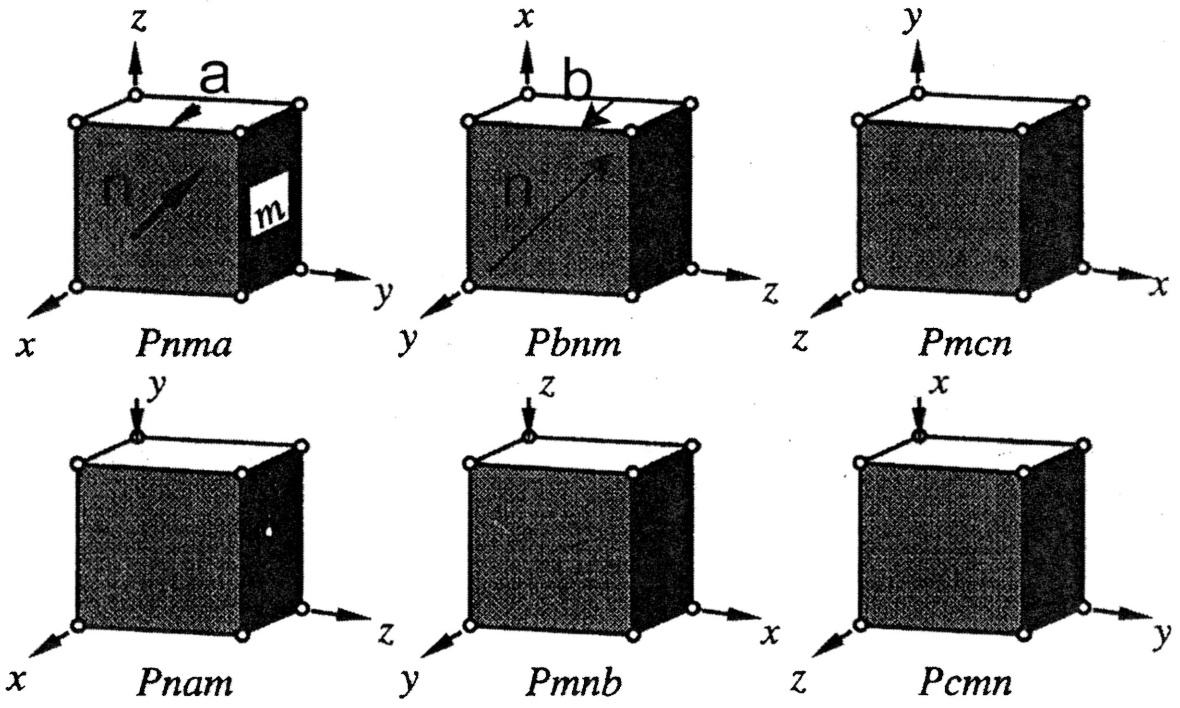

Figure 2.2.1
Various settings of space group no.62 illustrating the relative positioning of symmetry elements with respect to the cell axes. ***Pbnm*** is preferred by solid state scientists for orthorhombic perovskite structures.

2.2.2 X-Ray Diffraction Data

X-ray diffraction data were collected and processed by methods outlined in section 1.3.1 and 1.3.2. Figure 2.2.2.1 illustrates good agreement between the calculated and observed patterns for neighborite in a ***Pbnm*** setting.

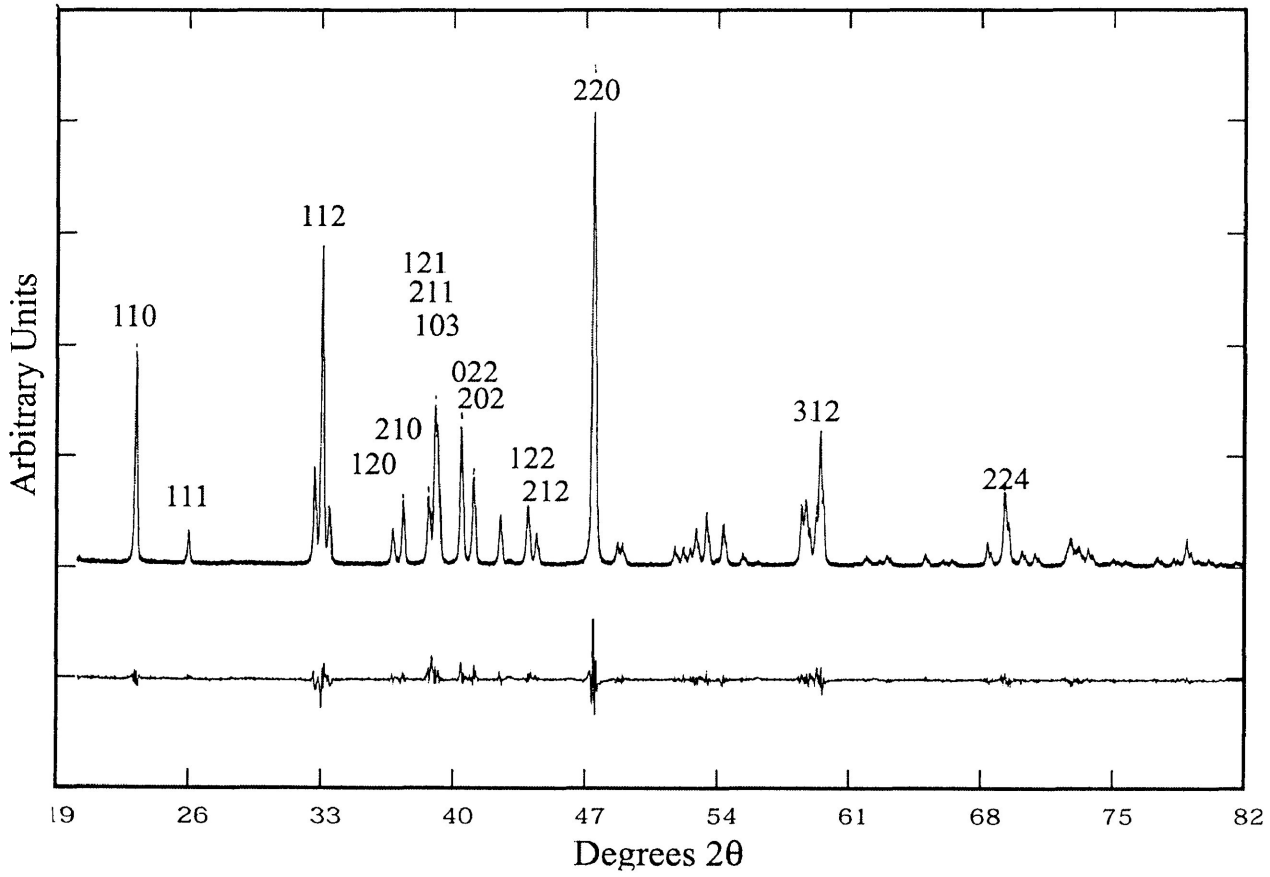

Figure 2.2.2.1
XRD Rietveld difference plot for neighborite, Cu Kα radiation 20 – 80^0 2θ

The superlattice diffraction peaks of the distorted perovskite structure can be related directly to octahedral tilting. The two types of octahedral tilting, namely ϕ^- and ϕ^+, will result in two distinct types of superlattice diffraction peaks. When indexed in a doubled pseudocubic cell $2a_p \times 2a_p \times 2a_p$ (Z=8) inphase rotations such as ϕ^+ develop reflections with indices odd-odd-even (*ooe*) whereas antiphase rotations such as ϕ^- develop indices of the type odd-odd-odd (*ooo*). Specifically, in the orthorhombic ***Pbnm*** phase with a tilt system of $\phi_x^- \phi_y^- \phi_z^+$, *ooo* indicies such as $(113)_{2p}$, $(131)_{2p}$, $(311)_{2p}$ indicate tilts of $\phi_x^- \phi_y^-$. Indices of the type ooe such as $(130)_{2p}$, $(310)_{2p}$, $(132)_{2p}$, $(312)_{2p}$ indicate the ϕ_z^+ tilt (Zhao *et al.*1993b).

Zhao has also shown that reflections of the type *eeo, i.e.* $(023)_{2p}$, $(223)_{2p}$, indicate antiparallel displacement of the ***A***-site cation (Na) perpendicular to the $[001]_p$ axis.

Transformation of *hkl* indices given for the multiple pseudocubic unit cell $2a_p \times 2a_p \times 2a_p$ (Z=8) to orthorhombic $\sqrt{2}a_p$ x $\sqrt{2}a_p$ x $2a_p$ (***Pbnm*** Z=4) indices is given by equation (7):

(7) $(h,k,l)\mathbf{Pbnm} = (h,k,l)_{2ap}$

$$\begin{bmatrix} 1/2 & -1/2 & 0 \\ 1/2 & 1/2 & 0 \\ 0 & 0 & 1 \end{bmatrix}$$

The inverse transformation: ***Pbnm*** $\rightarrow$ doubled pseudocubic unit cell, is given by equation (8):

(8) $(h,k,l)_{2ap} = (h,k,l)\mathbf{Pbnm}$

$$\begin{bmatrix} 1 & 1 & 0 \\ -1 & 1 & 0 \\ 0 & 0 & 1 \end{bmatrix}$$

Thus, neighborite peaks with indices $\{121, 103, 211\}_{Pbnm}$ indicate antiphase tilting $\theta = \phi^{-}_{x+y}$, whereas peaks with indices $(120, 210)_{Pbnm}$ and $(122, 212)_{Pbnm}$ indicate in-phase tilting $\phi = \phi^{+}_{z}$ about [001]. Finally, peaks with indices (113) $_{Pbnm}$ (023) $_{Pbnm}$ indicate the displacement of the *A*-cation. (Zhao *et al.* 1993b). Superlattice diffraction peaks indicative of octahedral rotation and *A* – site cationic displacement are illustrated in figure 2.2.2.2.

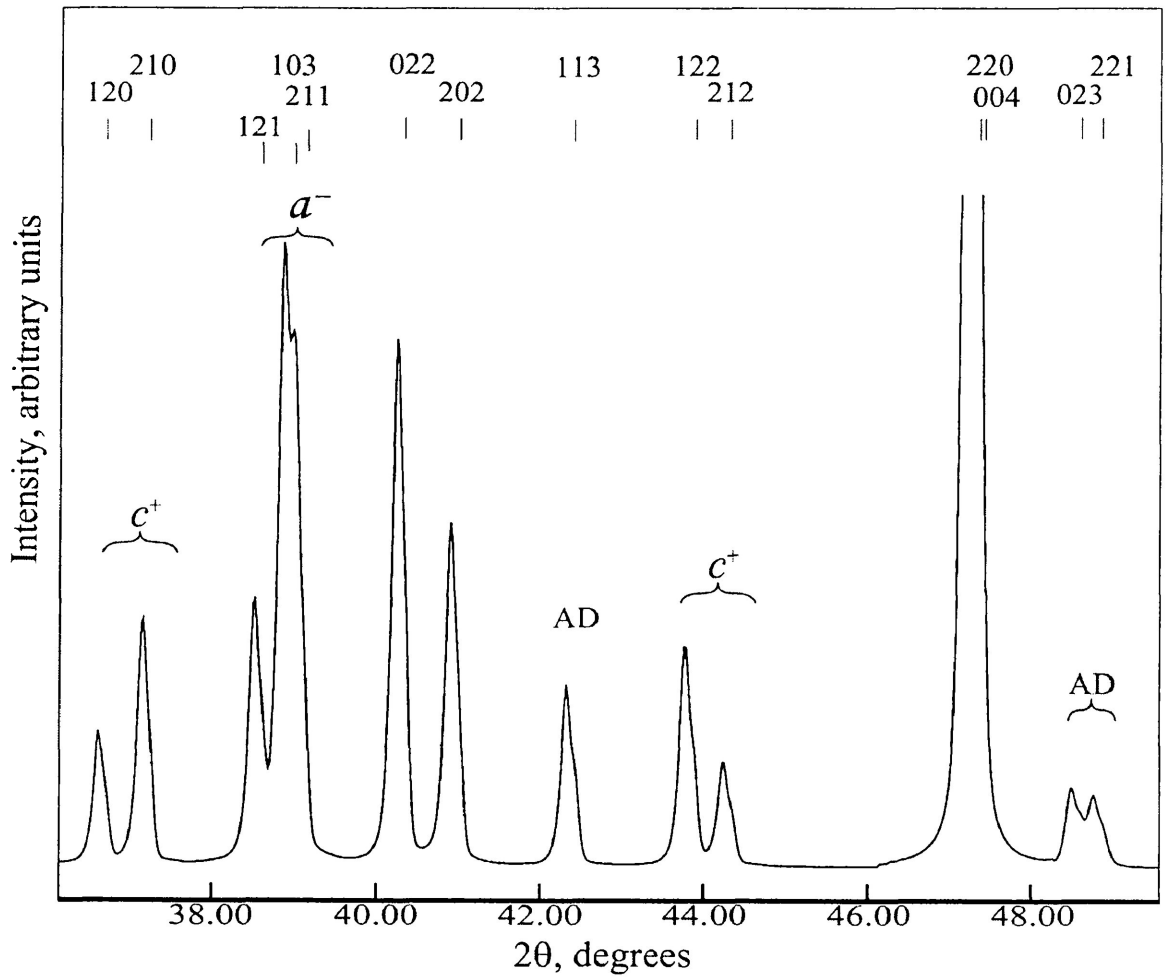

Figure 2.2.2.2

X – Ray powder diffraction pattern of neighborite (x = 0, Cu Kα radiation) for 2θ range 36 – 50^0. Diffraction lines are indexed on a ***Pbnm*** cell; for refinement results see appendix A - 1. The pattern incorporates "lattice" peaks and superlattice peaks indicative of anti phase rotation (a^-), in – phase rotation (c^+) and *A* – site cationic displacement (AD).

2.2.3 Structure of Neighborite

The primary mechanism for the reduction of symmetry from the ideal cubic setting to the pseudocubic, distorted orthorhombic neighborite structure is octahedral rotation. The octahedral tilt system in neighborite consists of two equal antiphase tilts along the a_1 and a_2 pseudo-cubic axes, and a third, inphase tilt, of differing magnitude about the pseudo-cubic a_3 axis. Using the notation described by Glazer (1977), neighborite has an $a^-a^-c^+$ tilt scheme. Figure 2.2.3.1 illustrates the neighborite structure viewed along the c-axis. Successive layers of octahedra lying in parallel planes perpendicular to the c-axis display the inphase c^+ tilting indicated by arrows 1 and 2.

The two antiphase a^-a^- tilts are also shown in figure 2.2.3.1 (arrows 3,4,5 and 6) however these tilts are better observed in figure 2.2.3.2, where the neighbourite structure is viewed close to the $[100]_{ap}$ direction.

Zhao *et al.* (1993b), also describe the octahedral tilt scheme of the perovskite structure. Their approach utilizes three tilts (ϕ, θ, Φ) which are coincident with the $[100]_{ap}$, $[110]_{ap}$, $[111]_{ap}$ pseudocubic axes respectively. The two equal antiphase tilts, $[100]_{ap}$ and $[010]_{ap}$, ($\phi_x^-\phi_y^-$), can be combined into a single $[110]_{ap}$ tilt (θ_{x+y}) tilt. When three tilts are present, they can be combined and described as a single $[111]_{ap}$ tilt. Figure 2.2.3.3 displays the orientation of the three tilt axes. Note that the $[100]_{ap}$ tilt axis corresponds to the same pseudocubic axis used in Glazers notation. Similarly, the $a^-a^-c^+$ tilts described above can be described here as $\phi_x^-\phi_y^-\phi_z^+$. For neighborite $\phi = 8.52^0$, $\theta = 12.26^0$ and $\Phi = 14.90^0$ (this work)[1].

[1] Derived from cell parameters, see section 3.3 method A.

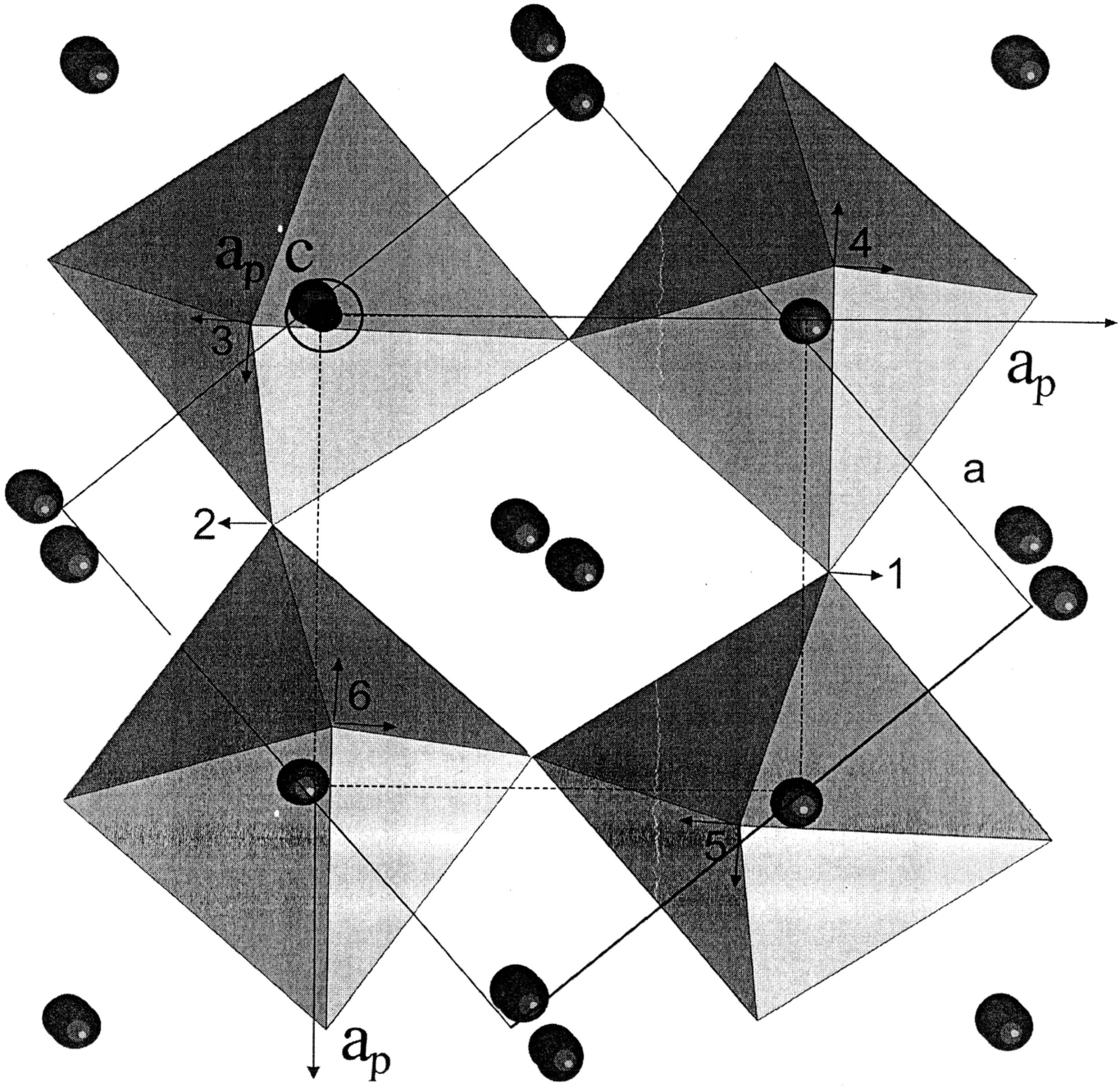

Figure 2.2.3.1

Neighborite perovskite structure viewed along the *c*-axis. Arrows 1 and 2 represent the in phase c^+ tilt. Arrows 3 through 6 indicate two antiphase a^-a^- (equal magnitude) tilts. The relationship between the cubic (dashed black line) and orthorhombic (solid) unit cells is illustrated.

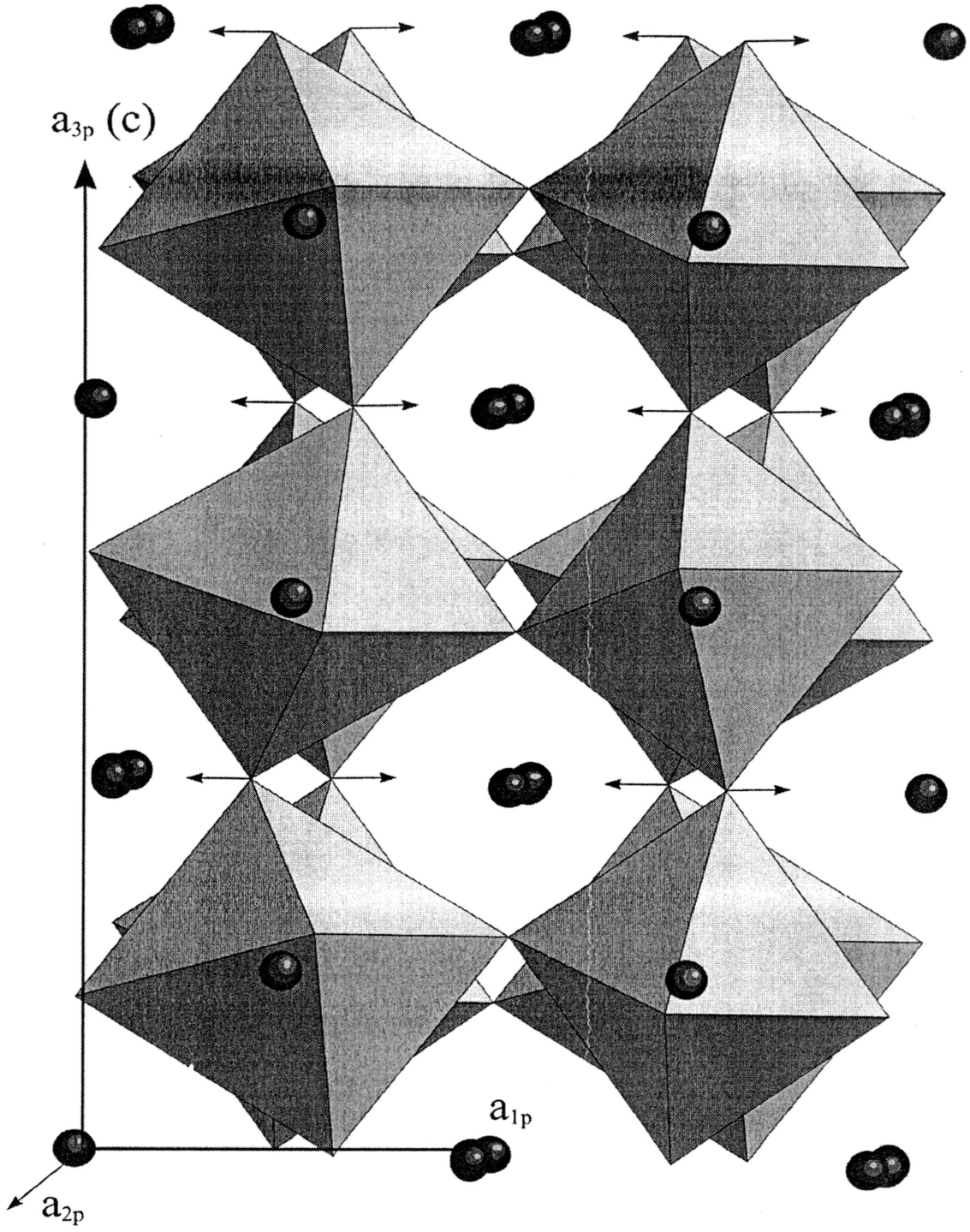

Figure 2.2.3.2

Neighborite perovskite structure. Note the antiphase tilting into the page along the a_2 pseudo-cubic direction. There is an identical tilt scheme about the a_1 pseudo-cubic direction (arrows not shown).

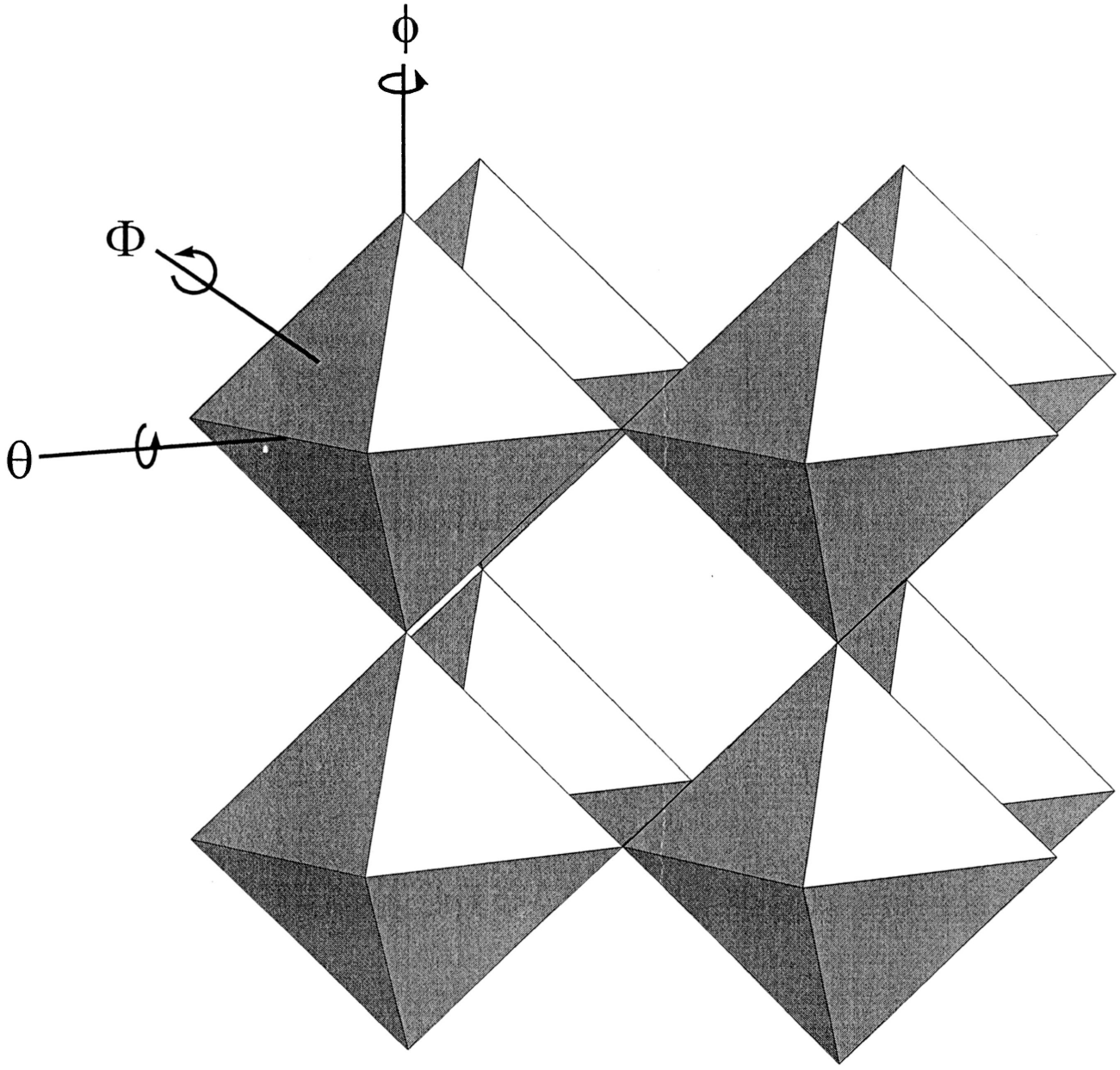

Figure 2.2.3.3
Octahedral diad, triad and tetrad rotational axes (tilts θ, Φ and ϕ respectively)

2.2.4 Coordination Analysis

A coordination analysis was completed for neighborite utilizing the software package **IVTON** and procedures described in section 1.3.2.

Coordination of both cationic sites is in good agreement with the bond valence parameters calculated for each site by **IVTON**: Na, 1.009; Mg, 2.019; F, -1.007.

The ratio of the ***A*** – site polyhedral volume / ***B*** – site polyhedral volume (V_A/V_B) is an effective measure of structural distortion in perovskites. V_A/V_B values less than 5 indicate structural distortions resulting from octahedral rotation, whereas values greater than 5 indicate structural distortions caused by cationic displacements, resulting in hexagonal symmetry (Thomas 1989).

In neighborite, coordination of the ***A***-site cation by ***X***-anions is reduced from 12 in the ideal cubic structure to 9 in the distorted orthorhombic structure. This decrease in coordination results in "uncoordinated space" in the orthorhombic unit cell. To acquire meaningful values of polyhedral volume ratios, the volume of the "uncoordinated" space must be considered as part of the ***A***-polyhedron. Calculation of the total ***A*** - polyhedral volume is given by the expression

$$V_A = (V_{cell} / Z) - V_B \qquad (1)$$

Where; V_A is the volume of the ***A***-polyhedra including the uncoordinated space, V_B is the ***B***-polyhedral volume and V_{cell} is the unit cell volume

Deviation from the holosymmetric arrangement is given by variation in the ***B-X*** bond lengths in table 2.2.4.1. ***X-B-X*** bond angles are not given as they do not deviate significantly from the ideal values of 90^0 and 180^0 (section 3.8).

Given the cell parameters from table 2.2.4.1 and the ***B***-polyhedral volume given by **IVTON** as 10.41Å^3, the ***A***- polyhedral volume calculated by equation (1) is 45.98Å^3 producing a polyhedral volume ratio of 4.416 for neighborite.

Variables for fractional atomic coordinates chosen for neighborite are given in column 1 of table 2.2.4.1 where ***u,v,w*** are fractional atomic displacements from special positions in the unit cell. Values of atomic displacements (***u,v,w***) from special positions in the ideal perovskite structure (column 3) are given in column 4.

Table 2.2.4.1 Atomic Displacements for $NaMgF_3$ (Å).

Atom	General (1)	Neighborite (2)	Ideal Cubic (3)	Difference (4)
A (Na)				
x	1-*u*	0.9903	1	0.0097
y	*v*	0.0433	0	0.0433
z	0.25	0.25	0.25	0
B (Mg)				
x	0	0	0	0
y	0.5	0.5	0.5	0
z	0	0	0	0
X(1) (F-Apical)				
x	*u*	0.089	0	0.089
y	0.5-*v*	0.4736	0.5	0.0264
z	0.25	0.25	0.25	0
X(2) (F-Equatorial)				
x	0.75-*u*	0.7034	0.75	0.0466
y	0.25+*v*	0.2964	0.25	0.0464
z	*w*	0.0483	0	0.0483

Displacements of the *F*(1) atom in the ***u*** and ***v*** directions coupled with displacement of the *F*(2) atom in the ***w*** direction results in the antiphase tilting among the $\boldsymbol{BX_6}$ octahedra about the $[100]_{ap}$, $[010]_{ap}$ directions (ϕ^-_{x+y}) and are therefore directly related to the $\{121, 103, 211\}_{Pbnm}$ triplet. ***u*** and ***v*** displacements of the equatorial *F*(2)

atoms are related to inphase octahedral rotation about the $[001]_{ap}$ axis (ϕ^{+}_{z}). These displacements therefore develop the $(120, 210)_{Pbnm}$ and $(122, 212)_{Pbnm}$ doublets.

The (ϕ^{-}_{x+y}) rotation results in an oscillatory distribution of fluorine atoms about the rotational axes, developing axial glide parallel to ***b*** through a plane perpendicular to ***x*** in addition to the ***n***-glide perpendicular to ***y***. Successive layers of octahedra perpendicular to the $[001]_{ap}$ axis have an inphase tilt (ϕ^{+}_{z}) and are related symmetrically by mirror symmetry through a plane perpendicular to $[001]_{ap}$.

Antiphase rotation of the $\boldsymbol{BX_6}$ octahedra results in doubled periodicity along the $[100]_{ap}$ $[010]_{ap}$ $[001]_{ap}$ directions, which necessitates reorientation of the unit cell ***a*** and ***b*** directions, illustrated in figure 2.2.3.1. Assuming rigid octahedra, deviation of the *F*(2) *z* coordinate from the cubic setting results in doubled periodicity along the $[001]_{ap}$ direction. This results in reorientation of the unit cell such that the cell parameters for an orthorhombic ***Pbnm*** setting are related to the cubic setting by the following expressions;

$$\boldsymbol{a_o} = \boldsymbol{a_p}\sqrt{2} \qquad (2)$$

$$\boldsymbol{b_o} = \boldsymbol{a_p}\sqrt{2} \qquad (3)$$

$$\boldsymbol{c_o} = 2\,\boldsymbol{a_p} \qquad (4)$$

Where $\boldsymbol{a_o}$ $\boldsymbol{b_o}$ and $\boldsymbol{c_o}$ are the orthorhombic cell dimensions and $\boldsymbol{a_p}$ is the pseudocubic cell dimension. In addition, the pseudocubic subcell dimensions may also be related to the orthorhombic structure by:

$$\boldsymbol{a_p} = \sqrt[3]{(V_{cell} / \boldsymbol{Z})} \qquad (5)$$

Where V_{cell} represents the orthorhombic unit cell volume, ***Z*** is the number of formula units in the cell and $\boldsymbol{a_p}$ represents the pseudocubic cell dimension. A summary of the pseudocubic cell dimensions calculated by each method above is given in table

2.2.4.2. The mean pseudocubic cell dimension is based on the average value derived by formulae 2, 3 and 4 whereas the pseudocubic cell dimension based on the unit cell volume is derived by equation 5.

In addition to distortion of the octahedral framework, octahedral rotation causes bending of the $\boldsymbol{B - X - B}$ bond angle, which, in turn results in shortening of the pseudocubic cell dimension relative to the ideal cubic setting. Table 2.2.4.2 gives selected bond angles and interatomic distances. Internal octahedral angles and ligand – ligand distances do not deviate significantly from the ideal cubic setting and indicate relatively low octahedral distortion. A detailed description of polyhedral distortion, bond angle and bond length distortion is given in section 3.

Table 2.2.4.2 Selected Interatomic distances and bond angles for neighborite

Selected Internal Octahedral Angles				Mg - F Bond Lengths	
F1 -	Mg -	F1	180	Mg - F1	1.9818
F1 -	Mg -	F2	88.50	Mg - F1	1.9818
F1 -	Mg -	F2	88.90	Mg - F2	1.9777
F1 -	Mg -	F2	91.50	Mg - F2	1.9898
F1 -	Mg -	F2	91.10	Mg - F2	1.9777
F1 -	Mg -	F2	91.50	Mg - F2	1.9898
F1 -	Mg -	F2	91.10		
F1 -	Mg -	F2	88.50		
F1 -	Mg -	F2	88.90		

B - X - B Bond Angles				Mg -Mg	
Mg -	F1 -	Mg	150.51	Mg - Mg	3.8353
Mg -	F2 -	Mg	150.34		

Pseudocubic Cell Dimension	
ap (mean)	3.8344(1)
ap (volume)	3.8342(1)

Selected Interatomic distances and bond angles for neighborite indicate relatively low octahedral distortion. This assumption is required for meaningful values of *f*, polyhedral volume ratios. For final agreement parameters see appendix A-1.

Chapter 3 Solid Solution Series $Na_{1-x}K_xMgF_3$

3.1 Introduction

Investigation of synthetic $Na_{1-x}K_xMgF_3$ compounds revealed a complete solid solution between neighborite and its potassium analogue. The series has two structural phase transitions, which are, in order of increasing potassium content: from orthorhombic ***Pbnm*** (Z = 4) to tetragonal ***P4/mbm*** (Z = 2) at x = 0.35 – 0.40, and from tetragonal ***P4/mbm*** to cubic $Pm\bar{3}m$ (Z = 1) at x = 0.4 – 0.5.

3.2 XRD Data

Orthorhombic superlattice diffraction peaks that directly reflect differences in ***a, b, c*** axes such as the triplet $\{020, 112, 200\}_{Pbnm}$ and doublet $\{022, 202\}_{Pbnm}$ gradually coalesce with increasing potassium content becoming irresolvable at x = 0.35 (figure 3.2.1). The intensity of peaks indicative of A – site cationic displacement such as $\{113, 023\}_{Pbnm}$ decrease gradually with increasing potassium and are not observed in members containing greater than 30 mol% potassium. Orthorhombic reflections related to the antiphase ϕ^-_{x+y} tilts, namely the $\{121, 103, 211\}_{Pbnm}$ peaks, decrease rapidly in the x = 0.10 – 0.20 range, and are not observed in the x = 0.40 member of the solid solution series. Finally, the orthorhombic $\{120, 210\}_{Pbnm}$ and $\{122, 212\}_{Pbnm}$ peaks coalesce to form the $(210)_{P4/mbm}$ and $(211)_{P4/mbm}$ primitive tetragonal peaks respectively. These peaks, indicative of the inphase ϕ^+_z tilt, gradually decrease in intensity with increasing potassium content. The $(210)_{P4/mbm}$ peak is the only remaining superlattice diffraction peak in the x = 0.40 member of the series. The coalescent peaks are indicative of inphase tilting and overall tetragonal symmetry (space group ***P4/mbm***). The significance of these changes with respect to polyhedral rotation, polyhedral distortion and ionic displacement is discussed further in sections 3.4 – 3.9.

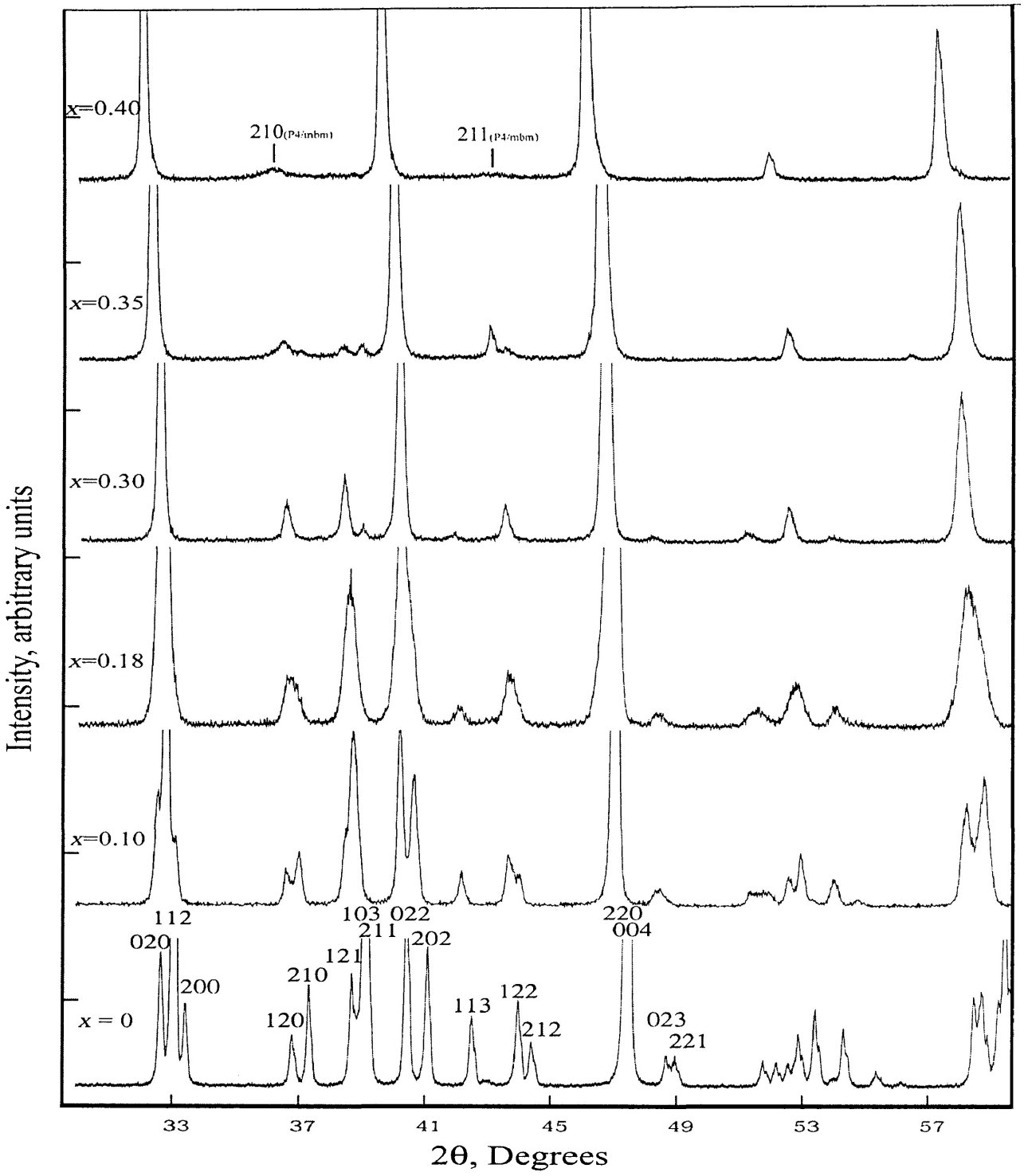

Figure 3.2.1

Illustrates stacked XRD spectra from members in the $x = 0.00 - 0.40$ compositional range Cu Kα radiation. Peaks indicative of symmetry changes are indexed.

Figure 3.2.2 gives the probable sequences of successive structural phase transitions from orthorhombic ***Pbnm*** to the cubic ***Pm$\bar{3}$ m*** symmetry (Aleksandrov 1976).

The distinction between ***P4/mbm*** and ***I4/mcm*** in the range $x \cong 0.40 - 0.46$ was based on the emergence or disappearance of peaks characteristic of these space groups (figure 3.2.3). The development of the primitive tetragonal $(120)_{P4/mbm}$ peak from the coalescence of the orthorhombic {120, 210} is clearly resolvable in the $x = 0.40$ member of the series. The $(121)_{P4/mbm}$ forms from the coalescence of the $\{122, 212\}_{Pbnm}$ peaks and is also an indication of primitive tetragonal symmetry. The $(121)_{P4/mbm}$ peak cannot be seen in the XRD powder pattern for the 40 mol% member however, the intensity of this peak is in good agreement with calculated pattern derived from the Rietveld refinement.

I4/mcm symmetry in the perovskite structure is characterized by the development of the $(211)_{I4/mcm}$ from the coalescence of the $\{121, 103, 211\}_{Pbnm}$ peaks. The difference between theses two tetragonal space groups in this context is whether the single remaining tilt is an inphase (***P4/mbm,*** $a^0a^0c^+$) or antiphase (***I4/mcm,*** $a^0a^0c^-$) rotation of the BX_6 octahedra about a pseudocubic tetrad axis. Thus, the presence of the $(120)_{P4/mbm}$ and the $(121)_{P4/mbm}$ in addition to the absence of the $(211)_{I4/mcm}$ is good indication of overall tetragonal symmetry. A detailed assessment of octahedral rotations is given in section 3.4.

Members containing greater than 50 mol% potassium are cubic ***Pm$\bar{3}$ m*** and do not display significant changes in XRD patterns. Patterns for members in the compositional range $x = 0.6 - 1.0$ are illustrated in figure 3.2.4. Cubic diffraction lines in this range shift to lower 2θ with increasing potassium content, indicating progressively increasing cell dimensions.

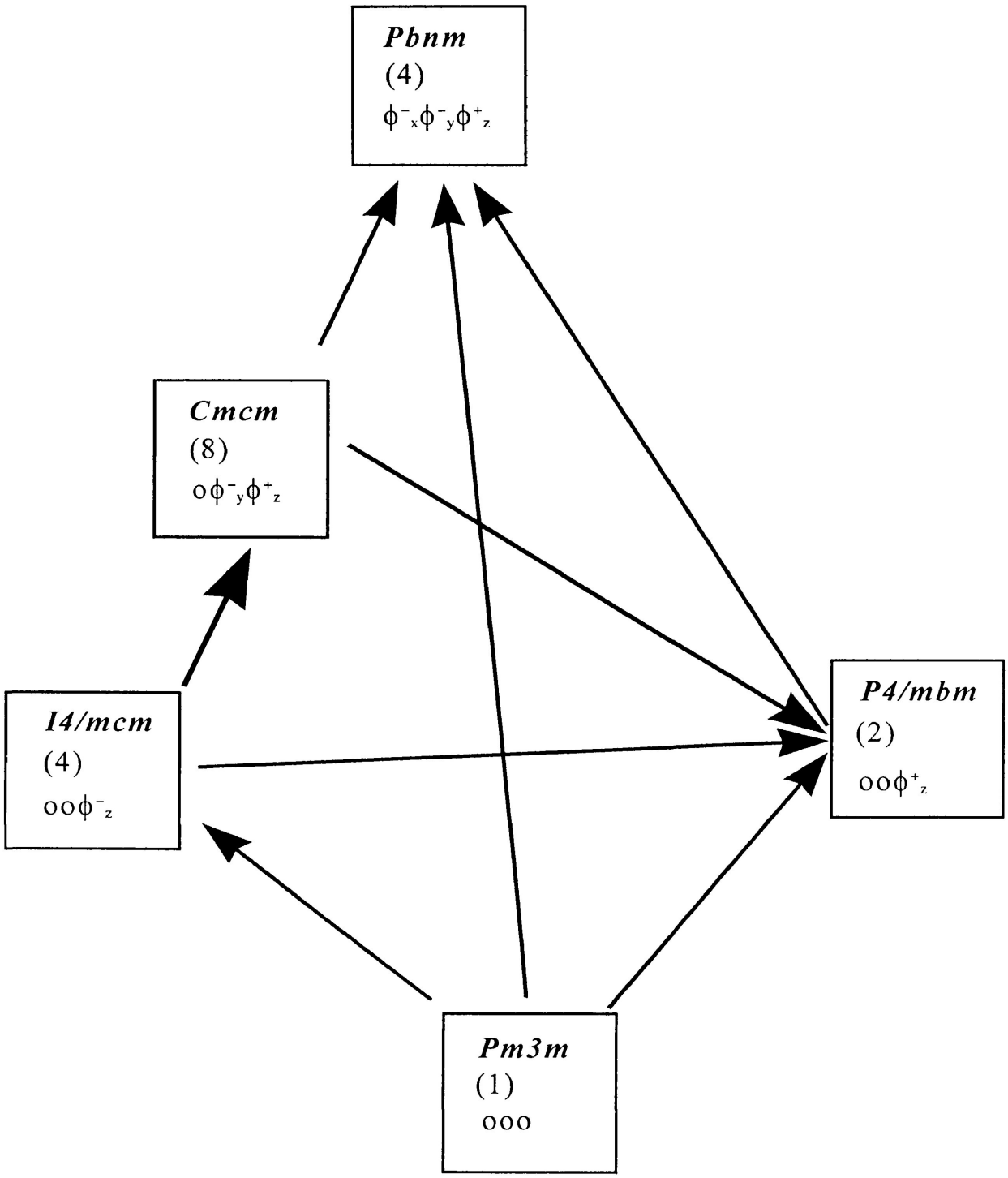

Figure 3.2.2

Probable sequences of structural phase transitions in the $Na_{1-x}K_xF_3$ solid solution series. **Z** and associated tilt systems are also indicated (after Aleksandrov 1976).

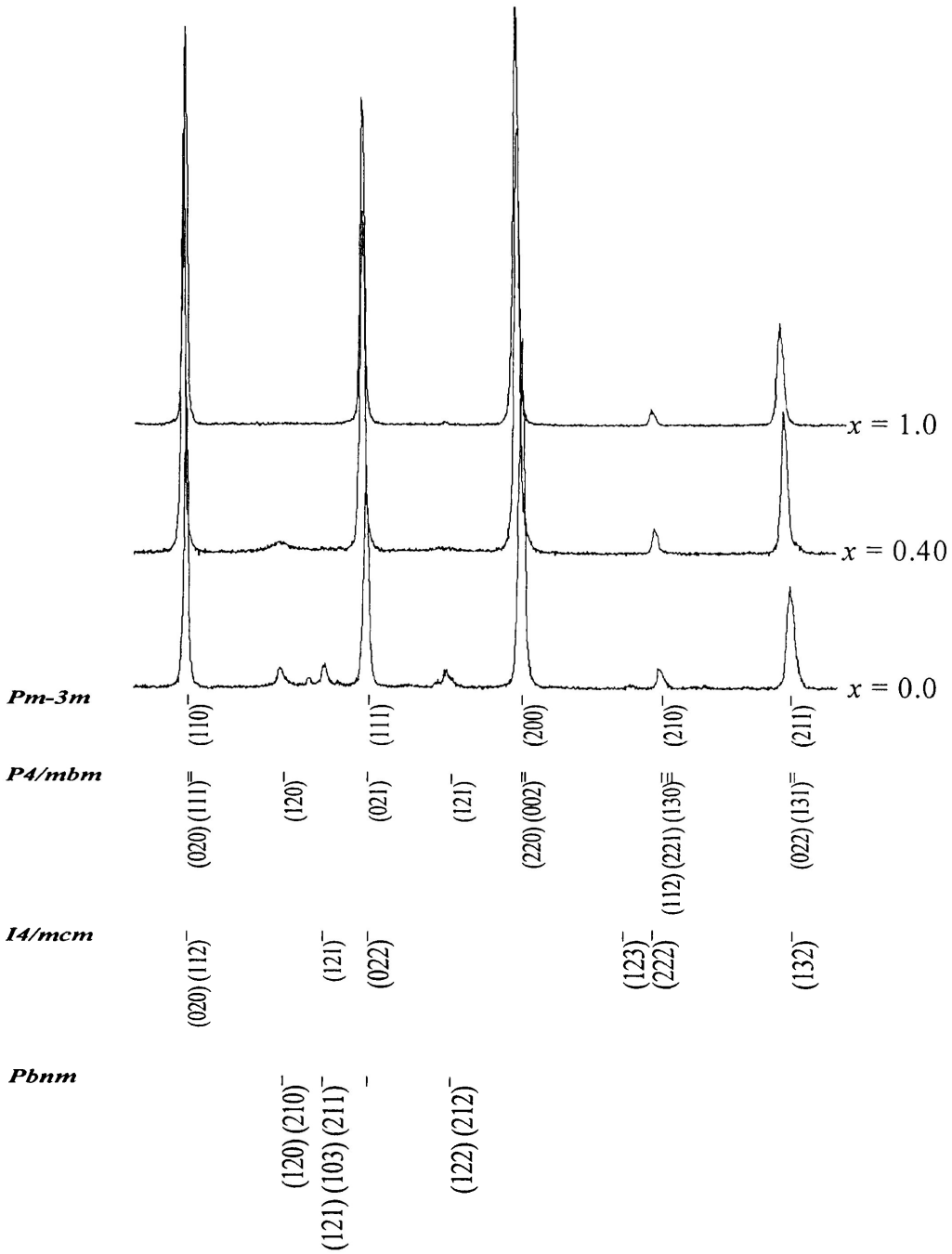

Figure 3.2.3

Progressive change in symmetry through the solid solution series $Na_{1-x}K_xMgF_3$. Development of a primitive tetragonal phase is indicated by the presence of a tetragonal (120) peak. Cu Kα radiation.

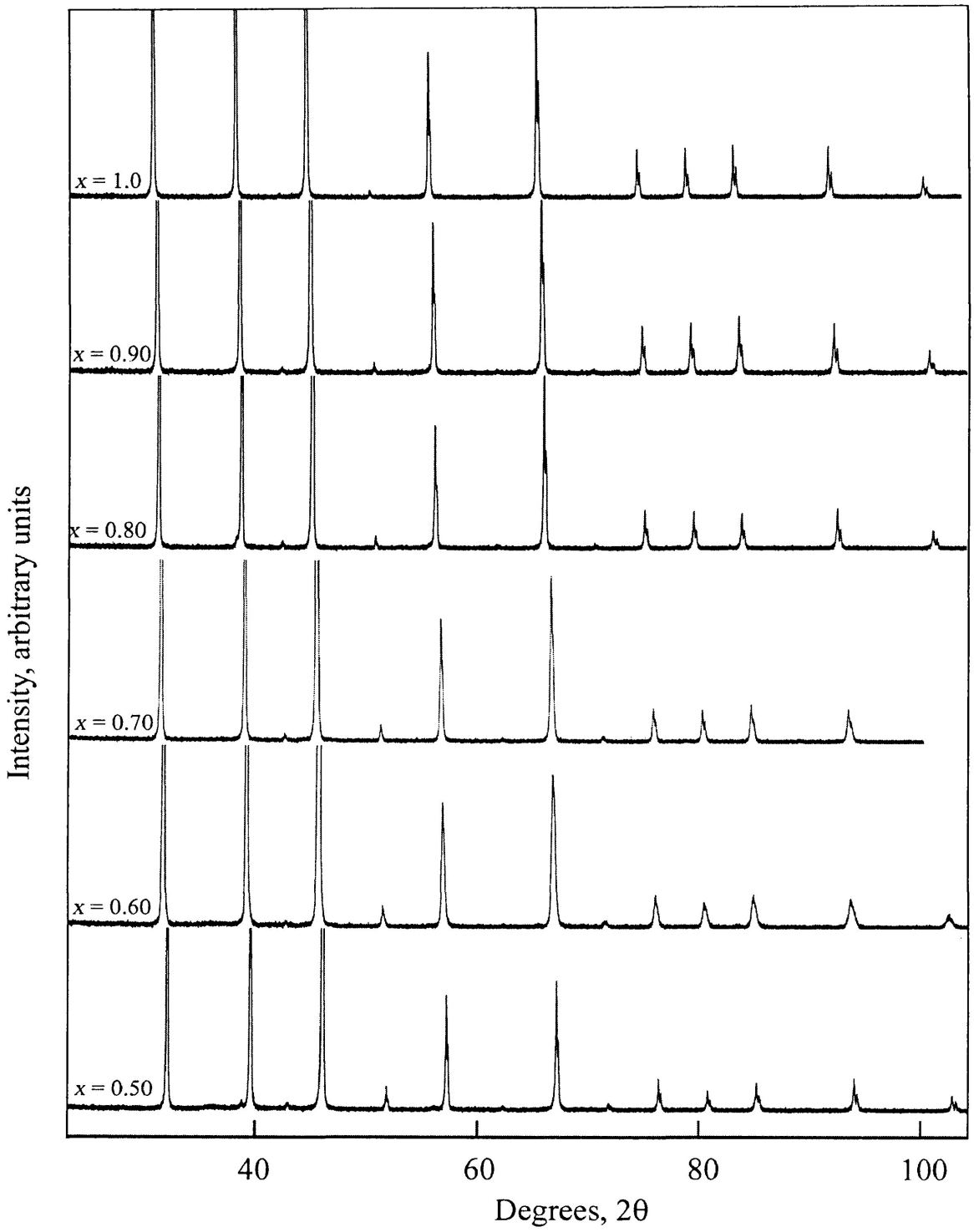

Figure 3.2.4

Cubic X-ray diffraction patterns for members in the $x = 0.5 - 1.0$ range. Some patterns contain a minor amount of MgO not visible in this illustration. Final agreement factors for all XRD patterns are given in appendix A-1. Cu Kα radiation

3.3 Neutron Diffraction

Neutron diffraction data were collected using a **DUALSPEC C2** high-resolution constant – wavelength powder diffractometer located at Chalk River Laboratories, (Atomic Energy Canada Limited) Chalk River, Ontario, Canada. In general, the diffraction data were collected from $35^0 - 115^0$ 2θ using a wavelength of 1.32856 Å. The neutron beam was monochromated by Si (3 3 1 plane), with a take – off angle of $73.9(9)^0$ 2θ. The samples were packed into vanadium sample cylinders with a volume of approximately $1.5cm^3$. The neutron and X-ray diffraction data were similar for those compositions which were investigated. Unfortunately only members with compositions of $x = 0.0, 0.3, 0.4, 0.5, 1.0$. could be analyzed with neutron diffraction.

Table 3.3.1 compares the refined results acquired from each data source. Column 3 in table 3.3.1 contains differences between values derived from the refinement of the two different types of analyses. The Rietveld refinement of the neutron diffraction data gave higher R_{Bragg} values than that for the X – ray diffraction data as a result of a poor neutron background fit. However, peaks indicative of structural phase transitions were observed at the calculated angles and intensities. Figure 3.3.1 is taken from the Rietveld difference plot of the neutron diffraction pattern of the $x = 0.4$ member of the series in which peaks indicative of tetragonal ***P4/mbm*** symmetry ((210) and (211)) are observed. Crystallographic parameters such as cell dimensions and atomic coordinates derived from the Rietveld refinement of the neutron diffraction data are in good agreement with those derived from the X – ray diffraction data (Table 3.3.1).

To improve peak resolution for intermediate member $x = 0.50$, long wavelength (2.3548 Å) neutron diffraction data were collected. Unfortunately, these data did not improve the resolution of the $(210)_{P4/mbm}$ reflection. A Rietveld difference plot for this analysis is given in figure 3.3.2. All analyses of the $x = 0.50$ member (X – ray and neutron) gave similar results for

the $(210)_{P4/mbm}$ peak. There is evidence of a peak in the 56.0^0 – 59.0^0 2θ range, however this reflection is sufficiently broadened to prevent an unequivocal refinement in either cubic (***Pm $\bar{3}$ m***) or tetragonal (***P4/mbm***) symmetry. The broadening effect may be attributed to the presence of a mixture of cubic and tetragonal domains (further discussed in 3.10).

Table 3.3.1 Comparison of X – ray and neutron diffraction data for x = 0.30, 0.40 and 0.50

		x = 0.30		***Pbnm***	x = 0.40		***P4/mbm***	x = 0.50		***Pm $\bar{3}$ m***
		Neutron	X-ray	Difference	Neutron	X-ray	Difference	Neutron	X-ray	Difference
	a	5.501(1)	5.4947(0)	0.006257	5.5434(4)	5.5459(0)	-0.00128	3.9354(2)	3.9403(1)	-0.004874
	b	5.521(1)	5.5199(0)	0.001152	5.5434(4)	5.5459(0)	-0.00128	3.9354(2)	3.9403(1)	-0.004874
	c	7.804(2)	7.8057(0)	-0.001376	3.9221(0)	3.9232(0)	-0.001189	3.9354(2)	3.9403(1)	-0.004874
Na	*x*	0.9873(2)	0.9954(8)	-0.00806	1	1		0	0	
	y	0.009(4)	0.0153(8)	-0.00601	0	0		0.5	0.5	
	z	0.25	0.25		0	0		0	0	
K	*x*	0.9873(2)	0.9954(8)	-0.00806	1	1		0	0	
	y	0.0093(4)	0.0153(8)	-0.00601	0	0		0.5	0.5	
	z	0.25	0.25		0	0		0	0	
Mg	*x*	0	0		0	0		0	0	
	y	0.5	0.5		0	0		0	0	
	z	0	0		0	0		0	0	
F(1)	*x*	0.048(3)	0.0561(1)	-0.00841	0	0		0	0	
	y	0.493(3)	0.4941(10)	-0.00091	0	0		0	0	
	z	0.25	0.25		0.5	0.5		0.5	0.5	
F(2)	*x*	0.718(1)	0.7157(6)	0.0024	0.2699(8)	0.2711(6)	-0.00119			
	y	0.271(1)	0.2843(7)	-0.01252	0.7699(8)	0.7711(6)	-0.00119			
	z	0.011(1)	0.0213(6)	-0.01022	0	0				

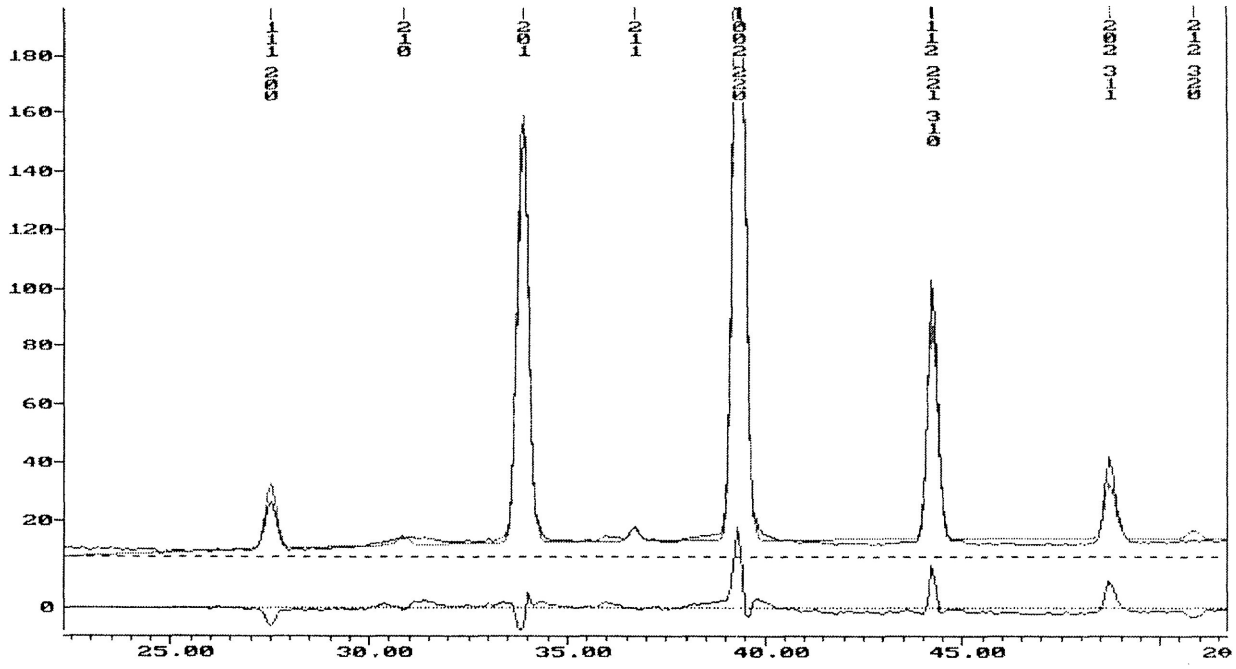

Figure 3.3.1

Calculated and observed neutron diffraction patterns for $x = 0.40$. The lower line represents a difference plot from the two above patterns. For final agreement parameters see section A -1

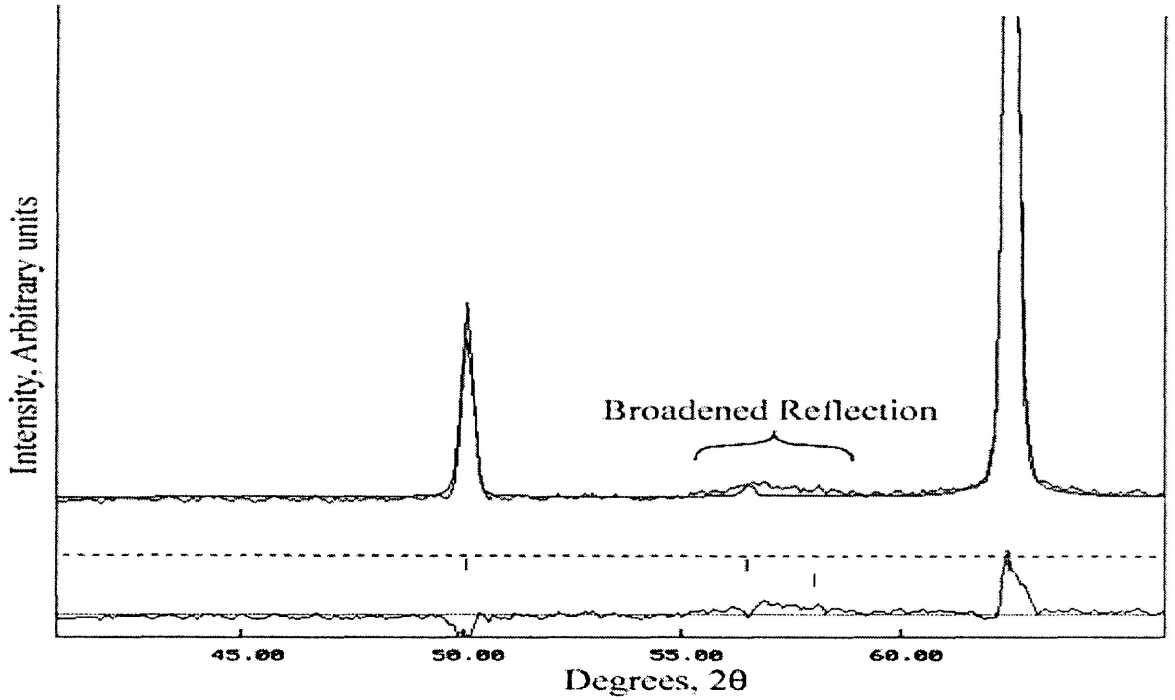

Figure 3.3.2

Illustration of the peak broadening effect observed in the neutron diffraction pattern from 56^0 – 59^0 2θ in the $x = 0.50$ intermediate member.

3.4 Octahedral tilts

Description of the octahedral tilts in the $(Na_{1-x}K_x)MgF_3$ solid solution series using the notation developed by Glazer (1977) gives $a^-a^-c^+$ for the orthorhombic ***Pbnm*** members (x = 0 - 0.40). This method requires deconvolution of octahedral rotations into three component rotations about the three cubic tetrad axes. Deduction of the tilt system will indicate the symmetry of the octahedral framework but may not be indicative of the crystal symmetry. Octahedral distortion and cationic displacement may result in a further decrease of overall crystal symmetry.

A – site cationic displacements in orthorhombic members of the $(Na_{1-x}K_x)MgF_3$ solid solution series are restricted to the $x - y$ plane and are concordant with the glide symmetry present in the ***Pbnm*** space group. For non – cubic members of the series investigated there is no ***B*** – site cationic displacement and BX_6 octahedral distortion is low ($\delta < 0.02$, section 3.4.3). In the x = 0.35 member of the series (fig 3.4.1) reflections indicative of ***A*** – site cationic displacement are indistinguishable from the background, the observed (113) diffraction line is <1% relative intensity. However, reflections indicative of both the inphase (ϕ_z^+) and antiphase (ϕ_{x+y}^-) tilts are present (indicated in figure 3.4.1). Table 3.4.1 gives the crystallographic characteristics of the x = 0.35 member of the series, note that the ***A*** – site cation is not displaced from the ideal position. These observations indicate that the overall crystal symmetry is only influenced by octahedral rotation, and not by cationic displacement. The refinement for this member converged with an unusually high R_{Bragg} of 10.80 %; which is attributed to low relative intensity and overlap of reflections indicative of fluorine displacements.

The tetragonal (***P4/mbm,*** Z = 2) members of the series have a single inphase tilt about the c – axis and belong to the $a^0a^0c^+$ tilt system. This tilt system is present only in the x = 0.40 member of the series.

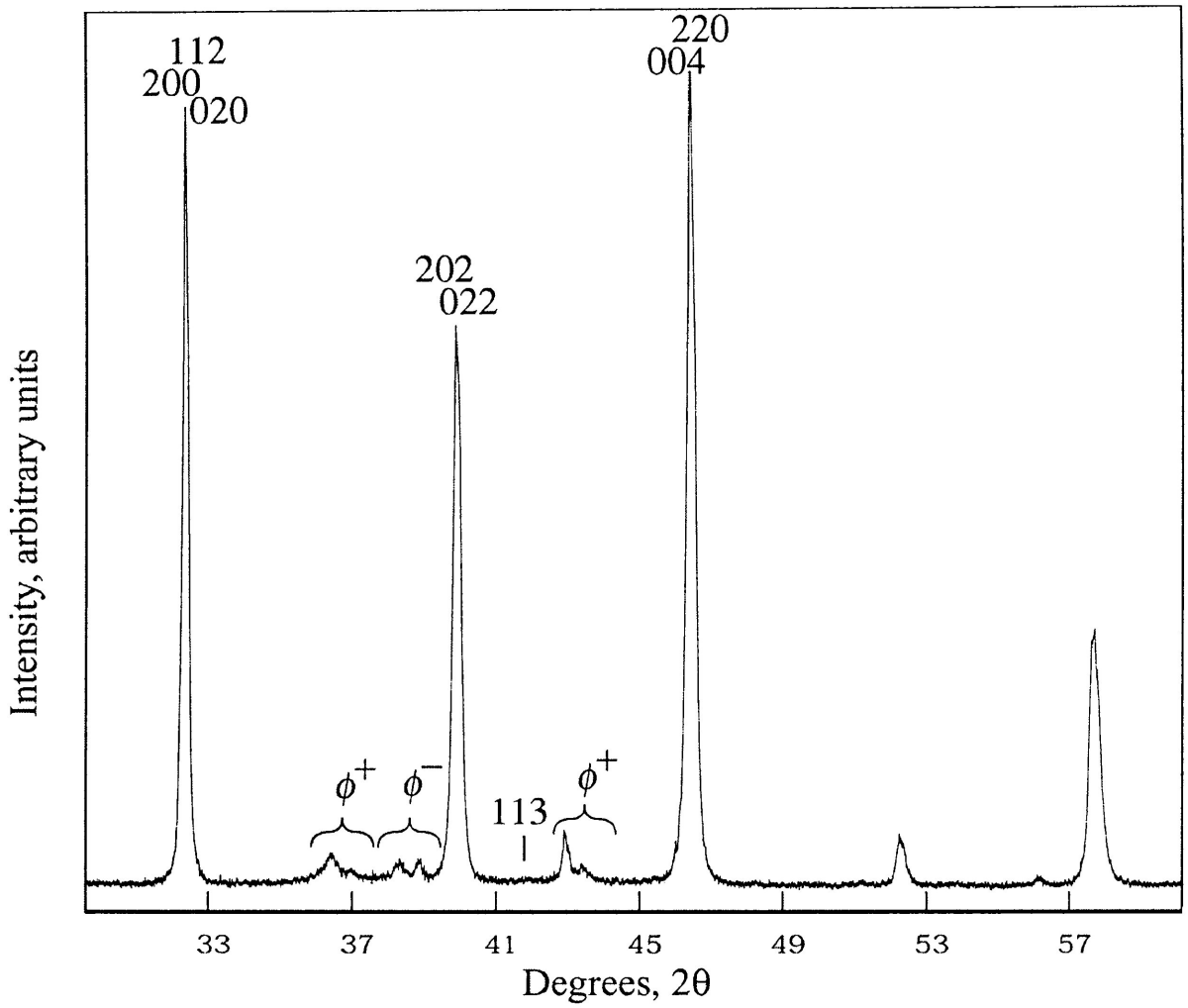

Figure 3.4.1
XRD Pattern of $x = 0.35$ showing no resolvable (113) reflection indicative of A – site cationic displacement. Cu Kα radiation

Table 3.4.1 Crystallographic Characteristics of $x = 0.35$

			Na	K	Mg	F(1)	F(2)
a	5.5218(4)	*x*	0	0	0	0.0587(1)	0.7168(6)
b	5.5387(4)	*y*	0	0	0.5	0.4920(10)	0.2843(7)
c	7.8319(5)	*z*	0.25	0.25	0	0.25	0.0206(6)
ap	3.9123	*B*	2.46(5)	2.46(5)	0.82(4)	2.3(2)	1.7 (1)

Members of the solid solution series with $x = 0.5 - 1.0$ are cubic and all tilts are absent, *i.e.* tilt system $a^0a^0a^0$.

Glazer (1972) does not give a method for determining the magnitude of any given tilt, restricting this scheme to a *qualitative* description of the relative magnitude and nature (inphase *vs.* antiphase) of the tilt system.

Zhao *et al.* (1993b) recognize and resolve this problem by giving several different methods of calculating octahedral tilts. The magnitude of the tilts may be derived from: cell dimensions (Method A); ***B–X–B*** bond angles (Method B); or a combination of cell dimensions and anionic displacements from special positions in the unit cell (Method C). Equations for the derivation of the magnitude of these tilts are given below.

Method A

$\theta = \cos^{-1}(\boldsymbol{a} / \boldsymbol{c})$

$\phi = \cos^{-1}(\sqrt{2}\,\boldsymbol{a} / \boldsymbol{c})$

$\Phi = \cos^{-1}(\sqrt{2}\,\boldsymbol{a}^2 / \boldsymbol{bc})$

Method B

$\theta = ((180^0 - <\boldsymbol{B} - \boldsymbol{X}(1) - \boldsymbol{B}>)/2)$

$\cos\theta = \cos\bar{\phi}_x \cdot \cos\bar{\phi}_y$

$= \cos^2\bar{\phi}_x$

$\phi_{x+y}^- = \text{acos}\sqrt{\cos\theta}$

$\phi_z^+ = (180^0 - <\boldsymbol{B} - \boldsymbol{X}(2) - \boldsymbol{B}>)/\cos\bar{\phi}_x$

$\Phi = \text{acos}(\cos\phi \cdot \cos\theta)$

Method C

$\theta = \tan^{-1}(4 \cdot (\sqrt{x^2}\,\text{F}(1) + \sqrt{y^2}\,\text{F}(1))/\boldsymbol{c})$

$\phi = \tan^{-1}(4 \cdot (\sqrt{x^2}\,\text{F}(2) + \sqrt{y^2}\,\text{F}(2))/\sqrt{(\boldsymbol{a}^2 + \boldsymbol{b}^2)}$

$\Phi = \text{acos}(\cos\phi \cdot \cos\theta)$

*x and y represent atomic displacements in angstroms from special positions for Method C, *i.e.*($u \cdot a$),($v \cdot b$), ($w \cdot c$).

Figures 3.4.2, 3.4.3 and 3.4.4 illustrate trends in octahedral tilts calculated by methods A, B and C respectively. Discrepancies among tilts calculated by the three methods arise from octahedral distortion and the insensitivity of the X-ray diffraction method to the position of the fluorine atoms in this structure. Interestingly, complimentary neutron diffraction data did not yield data that are more accurate (section 3.3). For the purposes of this study, Method B is considered to be most accurate as a result of relatively low BX_6 octahedral distortion, (section 3.5.2). A common feature of all three methods is a decrease in octahedral rotation with increasing potassium content.

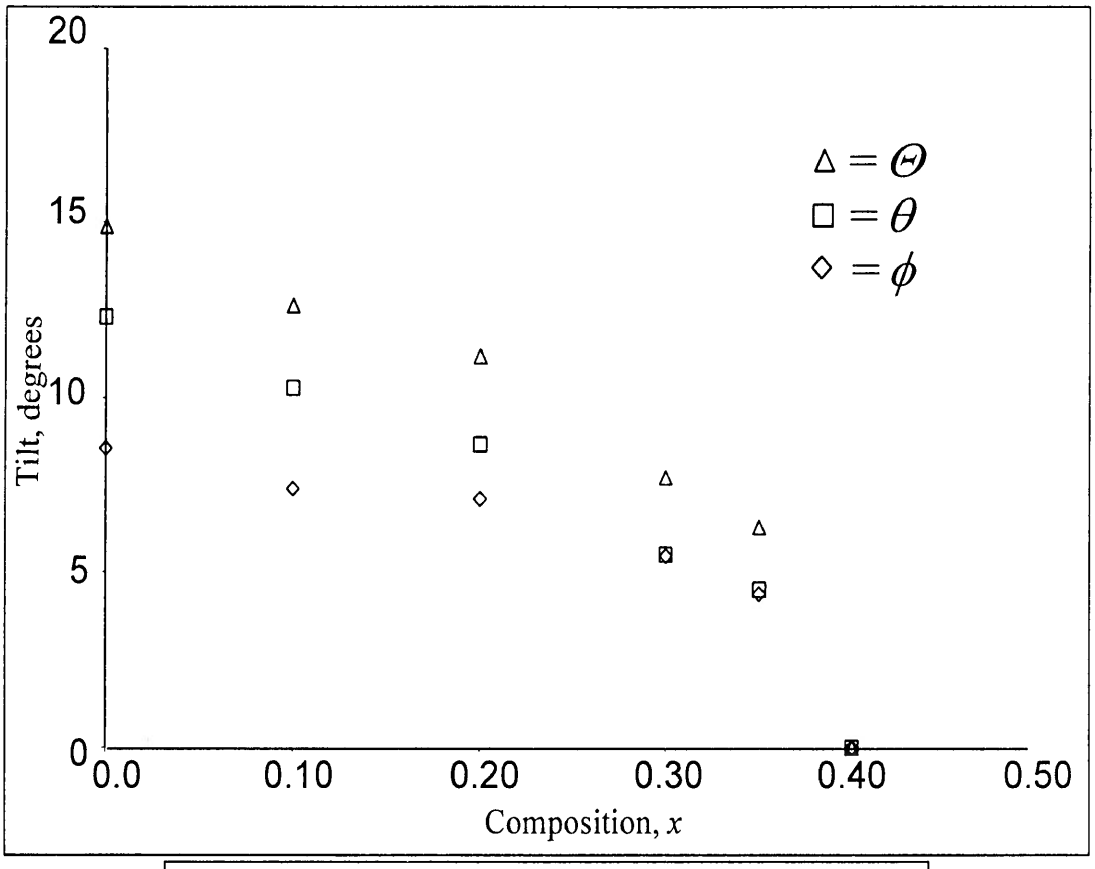

Figure 3.4.2
Octahedral tilts from Cell Dimensions, Method A.

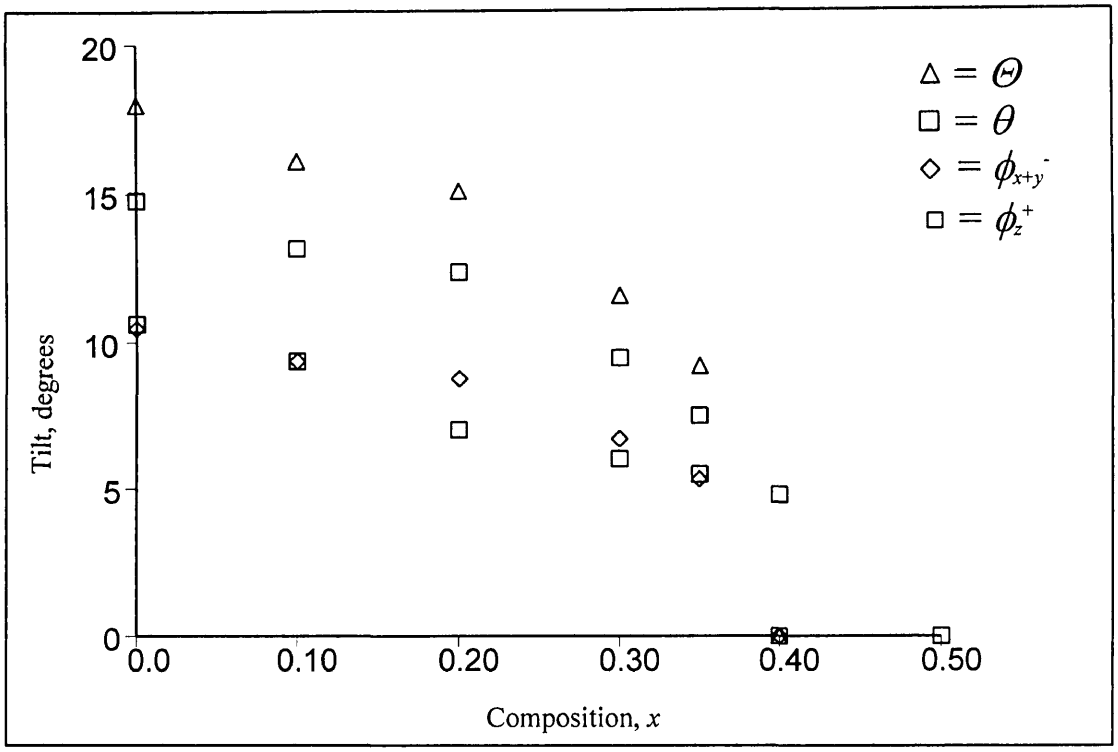

Figure 3.4.3
Octahedral tilts from ***B*** – ***X*** – ***B*** Bond Angles Method B

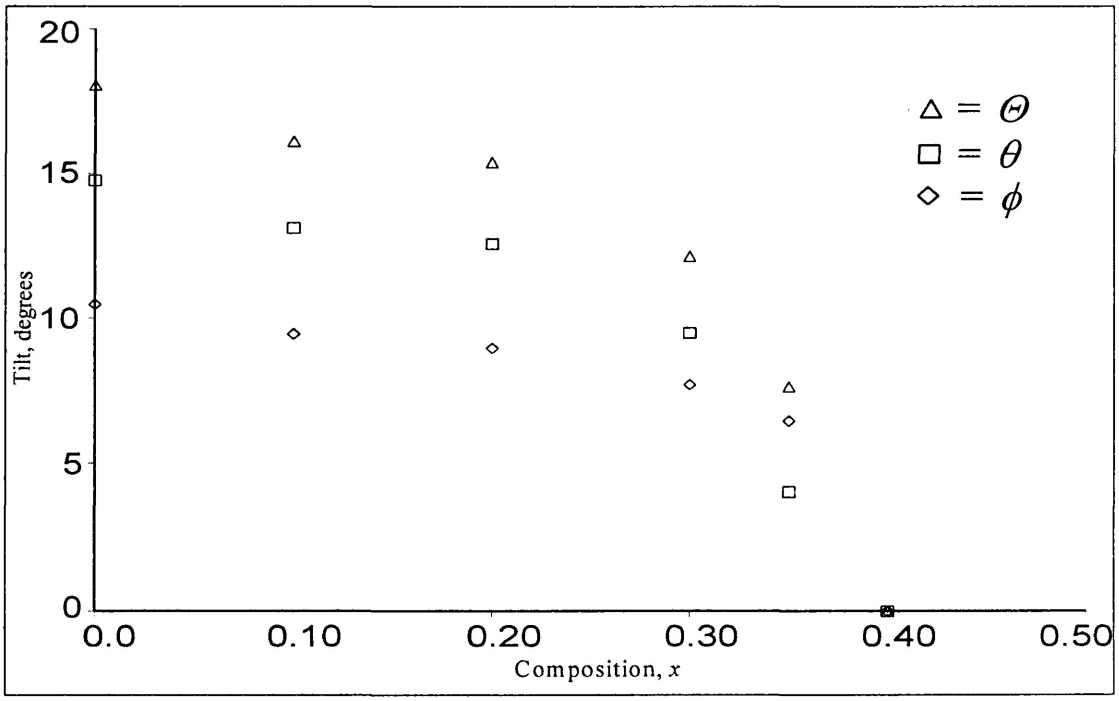

Figure 3.4.4
Octahedral tilts from Atomic Displacements, Method C.

Table 3.4.2 Comparison of octahedral tilts derived from methods A, B and C

Space group	***Pbnm***	***Pbnm***	***Pbnm***	***Pbnm***	***Pbnm***	***P4/mbm***
Composition (x)	0.00	0.10	0.20	0.30	0.35	0.40
Tilts (degrees)						
Method A						
ϕ	8.52	7.38	7.08	5.43	4.39	
θ	12.27	10.27	8.67	5.48	4.48	
Φ	14.90	12.62	11.17	7.71	6.27	
Method B						
ϕ	10.46	9.32	8.75	6.69	5.31	
ϕz	10.60	9.32	7.02	6.03	5.47	4.80
θ	14.75	13.15	12.35	9.45	7.50	
Φ	18.01	16.07	15.10	11.56	9.18	
Method C						
ϕ	10.49	9.44	8.93	7.67	6.42	4.82
θ	14.75	13.14	12.59	9.47	4.04	
Φ	18.03	16.13	15.40	12.17	7.58	

Note: The ϕ tilt given by method C indicates the ϕ^+ tilt only.

Table 3.4.2 compares tilt angles calculated by the three methods. Methods B and C give an additional individual calculation for the $(001)_p$ ϕ^+_z tilt, the only tilt present in tetragonal members. Figure 3.2.1 illustrates the gradual disappearance of reflections associated with octahedral rotations characteristic of the neighborite perovskite structure. The {121, 103, 211} triplet (ϕ_{x+y} tilt) coalesce from $x = 0$ to $x = 0.20$, then, decreases rapidly towards $x = 0.30$. Reflections indicative of inphase rotation {120, 210} and {122, 212} also coalesce, but do not decrease as rapidly as their antiphase counterparts, showing no significant change in intensity among members that contain less than 30 mol% potassium. They exhibit significant decrease in the $x = 0.30 - 0.40$ compositional range but remain after the disappearance of the "antiphase peaks", indicating primitive tetragonal symmetry (section 3.2)

3.5 Cell Dimensions

The relationship of the pseudocubic subcell to the orthorhombic cell is illustrated in figure 2.4.1. Equations 2 – 5 are from section 2.5 and show two methods by which the pseudocubic cell dimension may be calculated from the orthorhombic cell dimensions.

$$a' = a_p \sqrt{2} \qquad (2)$$

$$b' = a_p \sqrt{2} \qquad (3)$$

$$c' = 2\, a_p \qquad (4)$$

$$a_p = \sqrt[3]{(V_{cell} / Z)} \qquad (5)$$

Equations 2 – 4 give derivations of subcell dimensions based on each crystallographically distinct axis. Figure 3.5.1 illustrates subcell dimensions calculated for each member of the series. The orthorhombic members show the greatest variance in subcell dimension which nearly converge for the $x = 0.40$ member of the series.

For comparison, figure 3.5.2 shows data from each of the above methods, where the arithmetic mean is taken from values derived by equations 2 – 4. Inspection of figure 3.5.2 shows excellent agreement between the two methods and an overall linear increase in the pseudocubic subcell dimension.

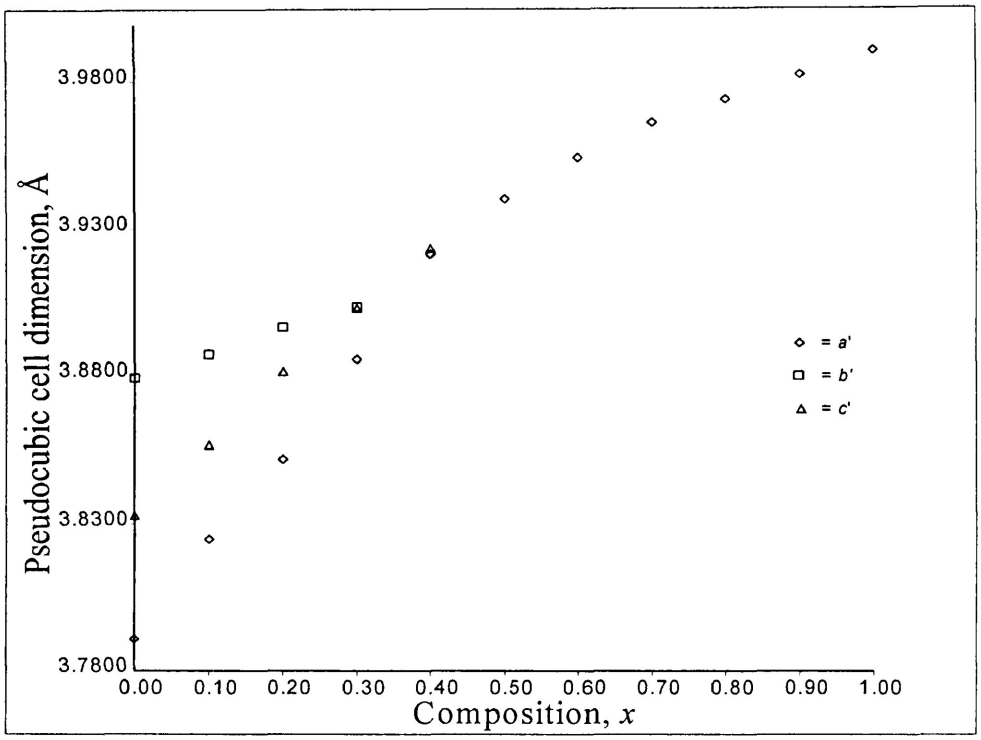

Figure 3.5.1
Pseudocubic subcell dimensions where *a'*,*b'*,*c'*, are subcell dimensions derived from the *a*,*b*,*c* orthorhombic axes respectively.

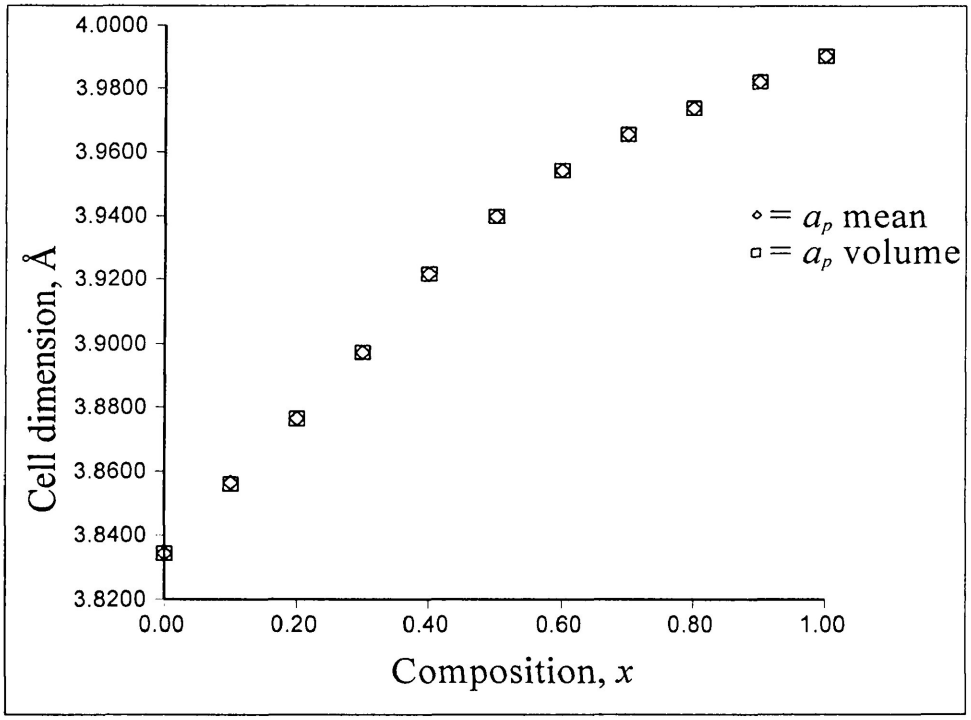

Figure 3.5.2
Pseudocubic subcell dimensions derived by taking the arithmetic mean of values derived by equations 2 – 4 and plotting with subcell values derived by equation 5.

3.6 Polyhedral Volume Ratio

For members of the $(Na_{1-x}K_x)MgF_3$ solid solution series the coordination of the ***A***-site cation changes with potassium content. The ***A*** – site polyhedron in neighborite contains 9 fluorine atoms, representing the smallest ***A*** – site cationic coordination number of all members of the series. In the $x = 0.10$ intermediate member of the series, the ***A*** – site polyhedron includes 10 F atoms. In this member, there are 4 magnesium atoms closer to the sodium (Na – Mg 3.2105Å •2 and 3.2924Å •2) than the remaining two fluorine atoms (Na – F 3.2936Å). For these members, ($x = 0$, 0.10, 0.20) where the ***A*** – site cation has fewer than 12 anions in the first coordination sphere, there remains "uncoordinated" space, given as:

$$\Delta V = (V_{cell} / Z) - (V_A + V_B) \quad \text{(modified version of eq. 1)}$$

The ratio of the ***A*** – site / ***B*** – site polyhedral volume introduced in section 2.5 is described quantitatively as f, and is equal to 5 for ideal cubic perovskite structures (Andrault *et al.* 1991):

$$f = V_A / V_B$$

Where V_A and V_B are the polyhedral volumes.

When deriving f, the uncoordinated volume must be added to the ***A*** – site polyhedral volume such that the entire volume of the ***A*** – site in the structure is considered in the calculation, *i.e.* V_A for AX_{12}. Figure 3.6.1 illustrates f values gradually approaching 5 with increasing potassium content, *i.e.* decreasing octahedral rotation. f = 5 for all cubic members. In neighborite the ***A*** – site cation is coordinated by 9 fluorine anions giving a ΔV value of 15.83 $Å^3$ comprising 28.06% of the unit cell volume.

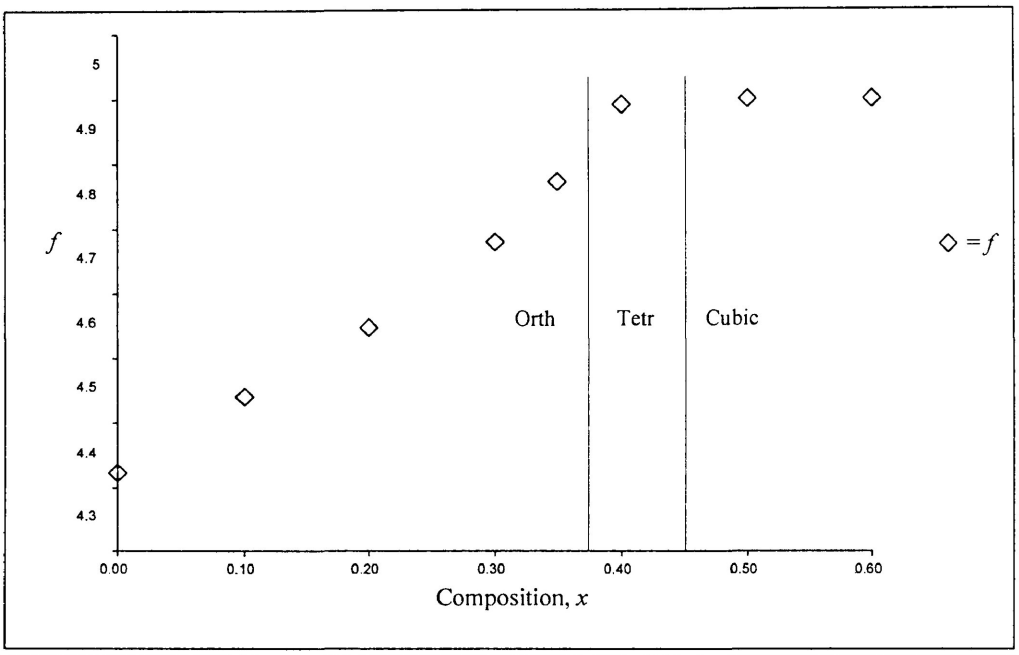

Figure 3.6.1
Increasing polyhedral volume ratio (*f*) with increasing potassium content. (This work)

Table 3.6.1 Comparison of polyhedral data for selected members of the $Na_{1-x}K_xMgF_3$ Solid Solution Series

Space group		***Pbnm***	***Pbnm***	***Pbnm***	***Pbnm***	***Pbnm***	***P4/mbm***	***Pm $\bar{3}$ m***	***Pm $\bar{3}$ m***	***Pm $\bar{3}$ m***
Composition (x)		0.00	0.10	0.20	0.30	0.35	0.40	0.50	0.60	0.70
a		5.3609	5.4092	5.4473	5.4947	5.5218	5.5459	3.9403	3.9545	3.9659
b		5.4862	5.4973	5.5102	5.5199	5.5387	5.5459	3.9403	3.9545	3.9659
c		7.6661	7.7135	7.7628	7.8057	7.8320	3.9232	3.9403	3.9545	3.9659
V_{cell}		225.47	229.37	233.01	236.75	239.53	120.67	61.18	61.84	62.38
V_{cell}/Z (Vap)		56.37	57.34	58.25	59.19	59.88	60.33	61.18	61.84	62.38
V_A Ivton	30.14		38.66	49.54	50.29	51.05	51.05	50.98	51.53	51.98
$V\Delta$		15.83	8.34							
V_A calc		45.97	46.99	47.94	48.95	49.69	50.11			
V_B		10.39	10.35	10.31	10.24	10.20	10.23	10.20	10.31	10.40
f		4.42	4.54	4.65	4.78	4.87	4.99	5.00	5.00	5.00

Where: Vcell is the unit cell volume, Vcell/Z is the pseudocubic cell volume, V_A Ivton is the calculated volume of the ***A*** – site first coordination sphere given by **IVTON**, V_Δ is the "uncoordinated space" given above by equation 5, V_A calc Is the calculated volume of the ***A*** – site polyhedron derived from the addition of V_Δ and V_A Ivton, and V_B is the ***B*** – site polyhedral volume given by **IVTON**

3.7 Bond Length Variance (Δ)

In most perovskite structures the $\boldsymbol{BX_6}$ polyhedra are considered not to undergo significant distortion during tilting. Experimentally determined $\boldsymbol{B-X}$ bond lengths demonstrate that in most perovskite – type compounds this assumption is correct (Sasaki *et al.* 1987). The octahedra may exhibit small distortions which result in an increase or decrease of $\boldsymbol{B-X}$ bond lengths and/or angular distortion of the $\boldsymbol{B-X}$ bond angles from 90^0 or 180^0.

Polyhedral bond length distortion is defined as:

$\Delta = 1/n \times \sum\{(r_i - r)/r\}^2 \times 10^3$ (Shannon 1976)

Where r_i and r are individual and average bond lengths respectively and n is the number of bonds. For the neighborite end member $\Delta = 0.0030$. For comparison $\Delta = 0.0017$ for TiO_6 in $CaTiO_3$ (Buttner & Maslen 1992). It should be noted that these distortions are quite small relative to those observed for Jahn – Teller distorted octahedra e.g. $\Delta = 8.799$ for CuF_6 in $KCuF_3$ (Burns *et al.* 1997).

Figure 3.7.1 shows variation in MgF_6 octahedral bond lengths. Note that the bond length variance is sensitive to the positions of the fluorine atoms in this structure, which are not sensitive to the X – ray techniques used here. Thus, the purpose of figure 3.7.1 is merely to illustrate the relatively low variance of bond lengths in the $\boldsymbol{BX_6}$ octahedra. The relatively high values for $x = 0.20$ and $x = 0.30$ members may be considered to be the result of poor refinements. However, the refinement of the $x = 0.20$ member converged with an R_{Bragg} of 4.66 indicative of good agreement between the calculated and observed patterns. Therefore bond lengths in the $\boldsymbol{BX_6}$ octahedra exhibit maximum variance in the $x = 0.20 - x = 0.30$ compositional range followed by a rapid decrease in variance from $x = 0.30 - x = 0.50$

A – site cations in the ***Pbnm*** perovskite may be regarded as being coordinated by 8, 9 or 10 anions (Park and Parise 1997) thus forming a distorted square anti – prism. In this study it was determined by bond valence analysis that the coordination number for orthorhombic phases was 9 for neighborite; 10 for $x = 0.10$ and 12 for the remaining members of the series (section 3.6). Data in figure 3.7.2 represent all 12 F atoms about the *A* – site cation, which, for the $x = 0$ and $x = 0.10$ members, includes F atoms outside of the first coordination sphere.

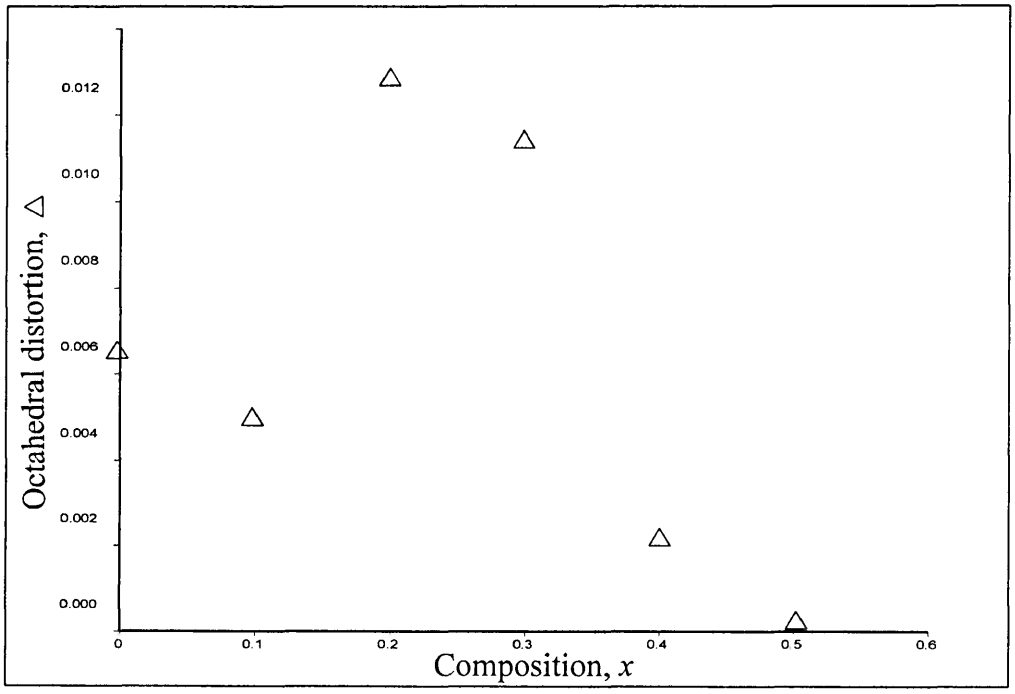

Figure 3.7.1
Bond length variance of the MgF_6 octahedra for members of the $(Na_{1-x})K_xMgF_3$ solid solution series.

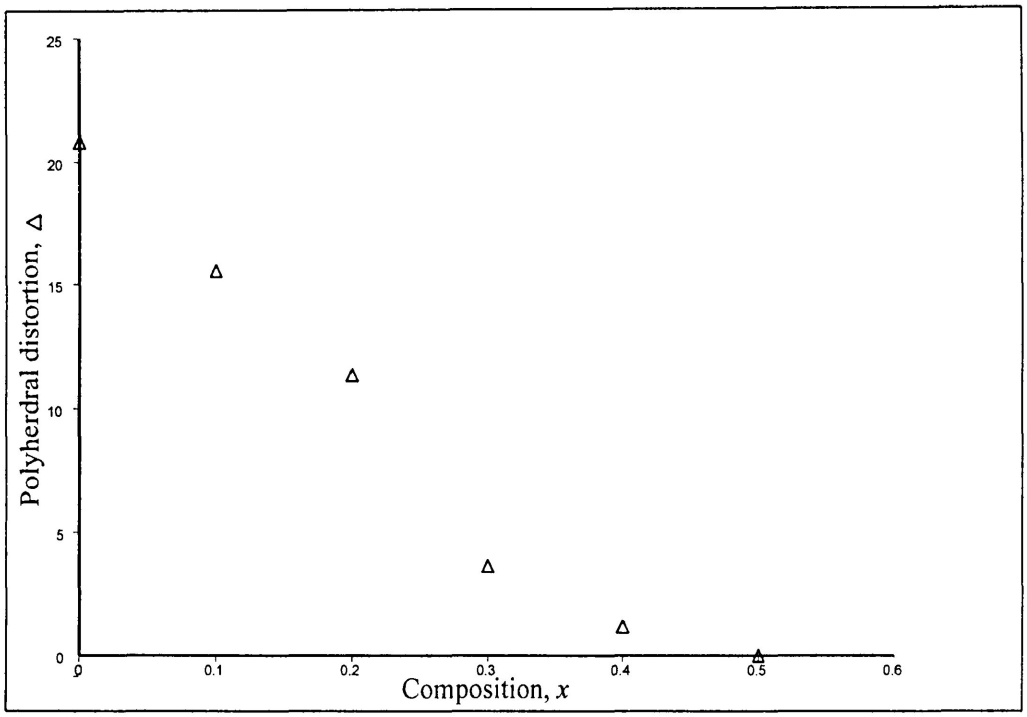

Figure 3.7.2
Bond length variance of the AX_{12} polyhedra for members of the $(Na_{1-x}K_x)MgF_3$ solid solution series.

3.8 Bond Angle variance (δ)

Distortion of the MgF_6 octahedra may also be described in terms of deviation of $\boldsymbol{B} - \boldsymbol{X}$ bond angles from the ideal values of 90 or 180^0. Such distortion is defined by Park and Parise (1997) as:

$$\delta = \Sigma[(\theta_i - 90)^2 / n - 1]$$

Where; δ = the bond angle variance
$\theta_i = \boldsymbol{B} - \boldsymbol{X}$ bond angle (ideally 90^0) for each observation
n = number of observations

Figure 3.8.1 illustrates the bond angle variance for members in the x = 0 – 0.4 compositional range. Again it should be stated that the bond angle variance is greatly affected by

the positions of fluorine in this structure, hence these data should be taken only as an indication of the order of magnitude of the bond angle variation *i.e.* < 2 degrees. Typically the bond angle variance ranges from $0 - 2^0$ but may be as much as 4^0 in some highly distorted octahedra. For comparison, $\delta = 0.61^0$ for $GdCrO_3$ and $\delta = 6.99^0$ for $ScCrO_3$.

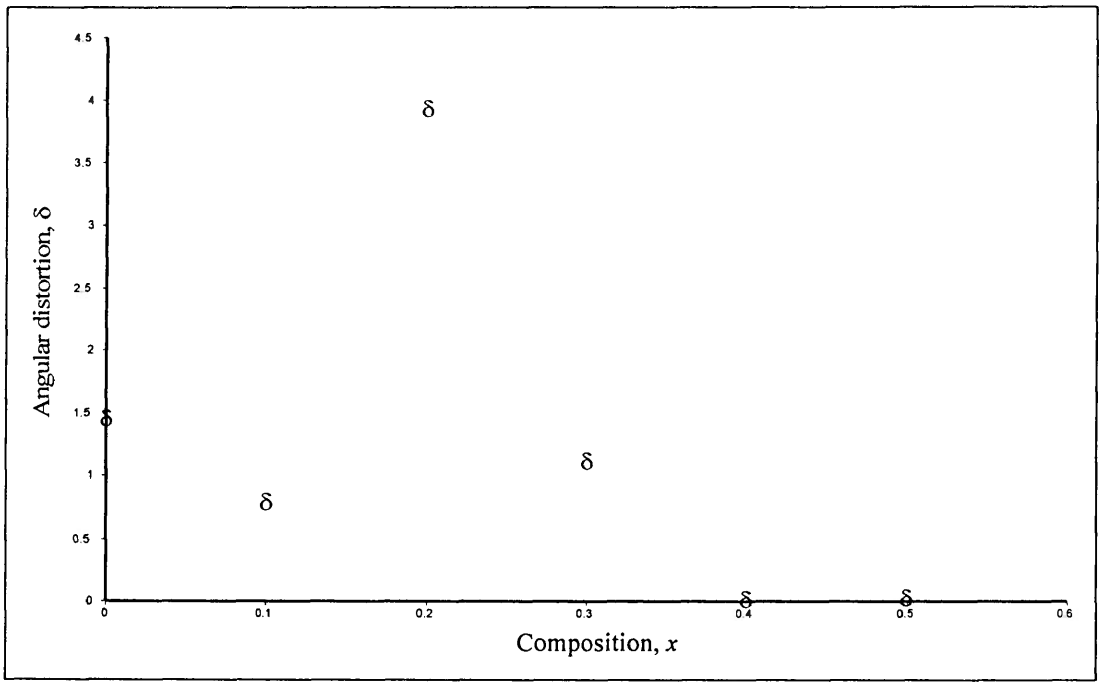

Figure 3.8.1
Bond angle variance of the MgF_6 octahedra. See text for definition.

3.9 Atomic Displacements

As stated in section 3.4 ***Pbnm*** symmetry can accommodate both displaced and non – displaced A – site cations. The u and v A – site displacements are at a maximum in the neighborite end – member and decrease linearly to $x = 0.30$. From $x = 0.30 - x = 0.35$ they diminish rapidly to 0.

A – site cationic displacements calculated from Rietveld refinement are illustrated below in figure 3.9.1. These displacements are low relative to those of fluorine but are accentuated

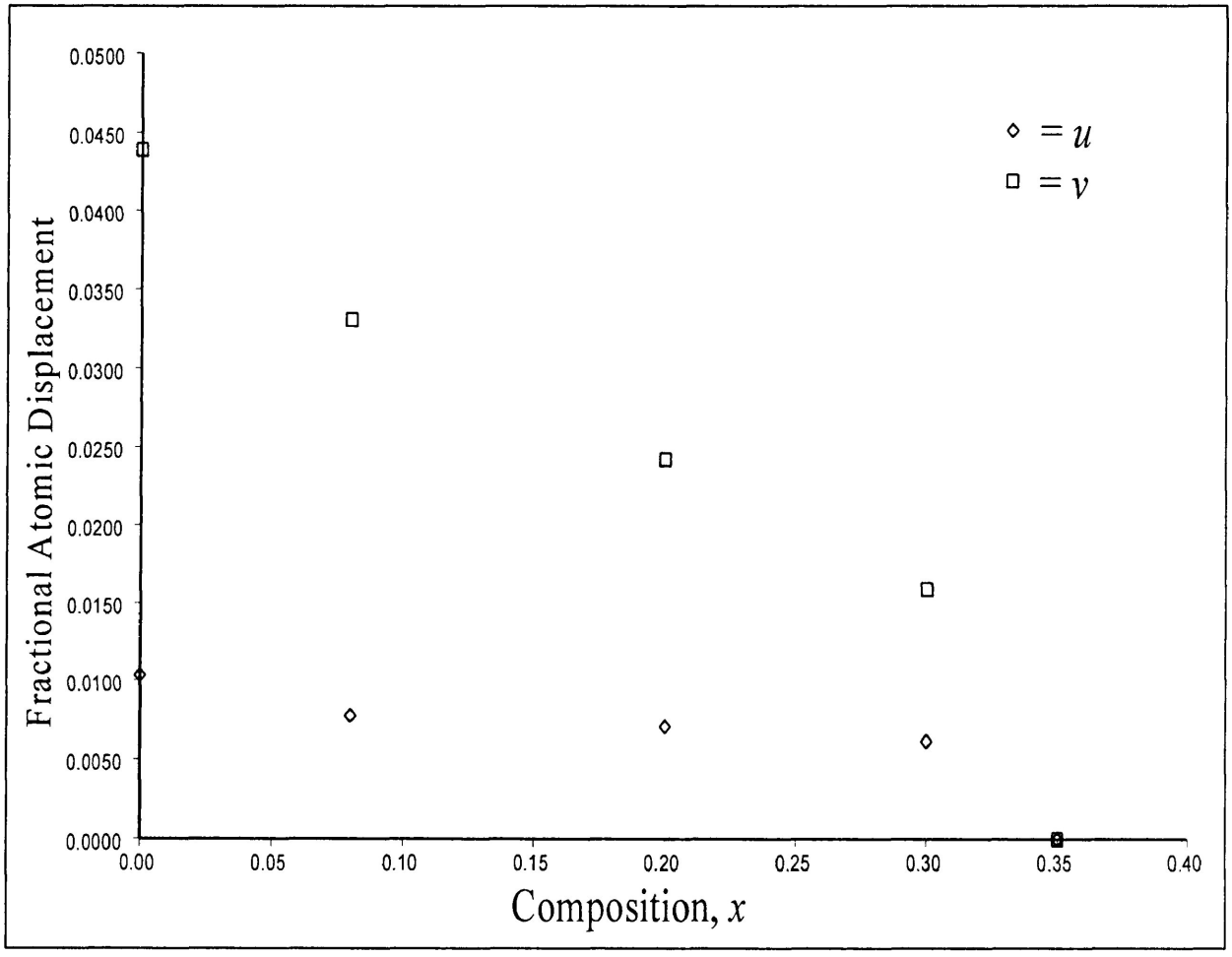

Figure 3.9.1
Fractional atomic coordinates of the A – site cation approach unity with increasing potassium content

graphically (fig 2.4.1) because of glide planes present in the crystal symmetry.

The ***Pbnm*** perovskite symmetry requires the ***w*** coordinate of the F(1) anion to remain fixed at a fractional atomic coordinate of 1/4 whereas the ***u*** and ***v*** coordinates may vary. The deviation of the F(1) ***u*** coordinate from the special position decreases in a linear manner with increasing potassium in the $x = 0$ to $x = 0.3$ compositional range (figure 3.9.2). It subsequently decreases rapidly from $u = 0.0897$ to the special position $u = 0$ from $x = 0.3$ to $x = 0.4$. Conversely the F(1) ***v*** coordinate approaches the special position ($v = 0$) in a linearly from $v = 0.0277$

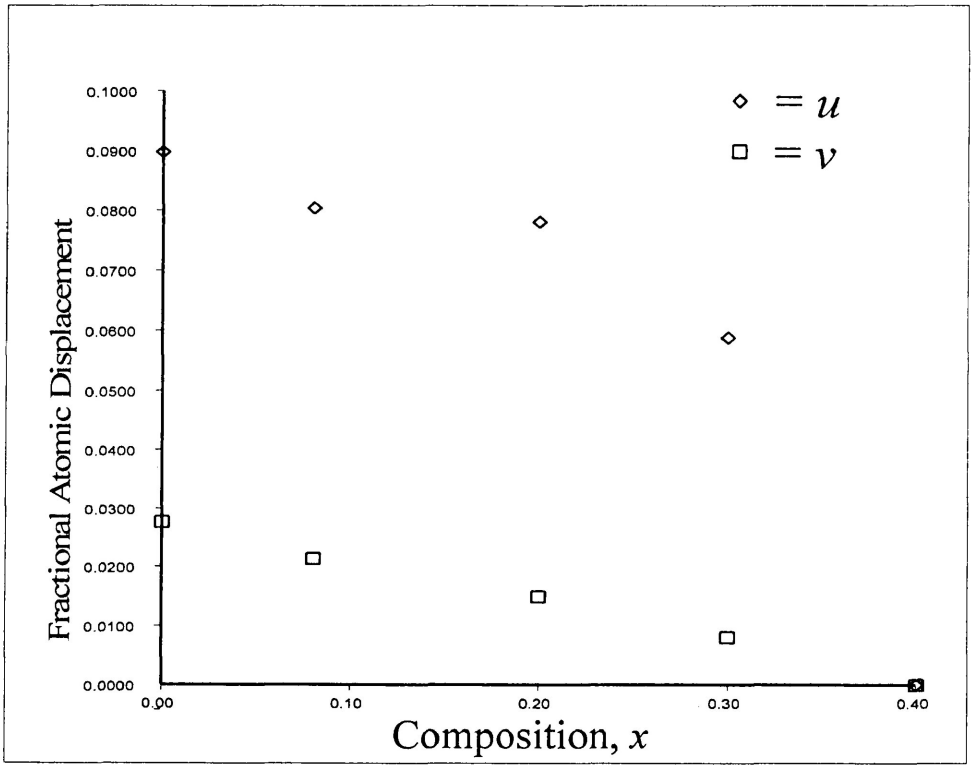

Figure 3.9.2
Fractional atomic displacements of the F(1) anion.

Displacement of the F(2) anion in the ***u*** and ***v*** crystallographic directions exhibits characteristics similar to the F(1) ***x*** displacements in that it decreases steadily in a linear manner.

Notable characteristics of the F(2) displacements (fig. 3.9.3)include the divergence and reemergence of the u v w atomic displacements. In the $x = 0$ and $x = 0.10$ members they are equal and decrease gradually. In the $x = 0.20$ member the w coordinate has decreased by 0.094Å and continues to decrease to 0 in $x = 0.40$. The u and v displacements diverge in $x = 0.20$ and reconverge in $x = 0.40$, finally diminishing to 0 in $x = 0.50$.

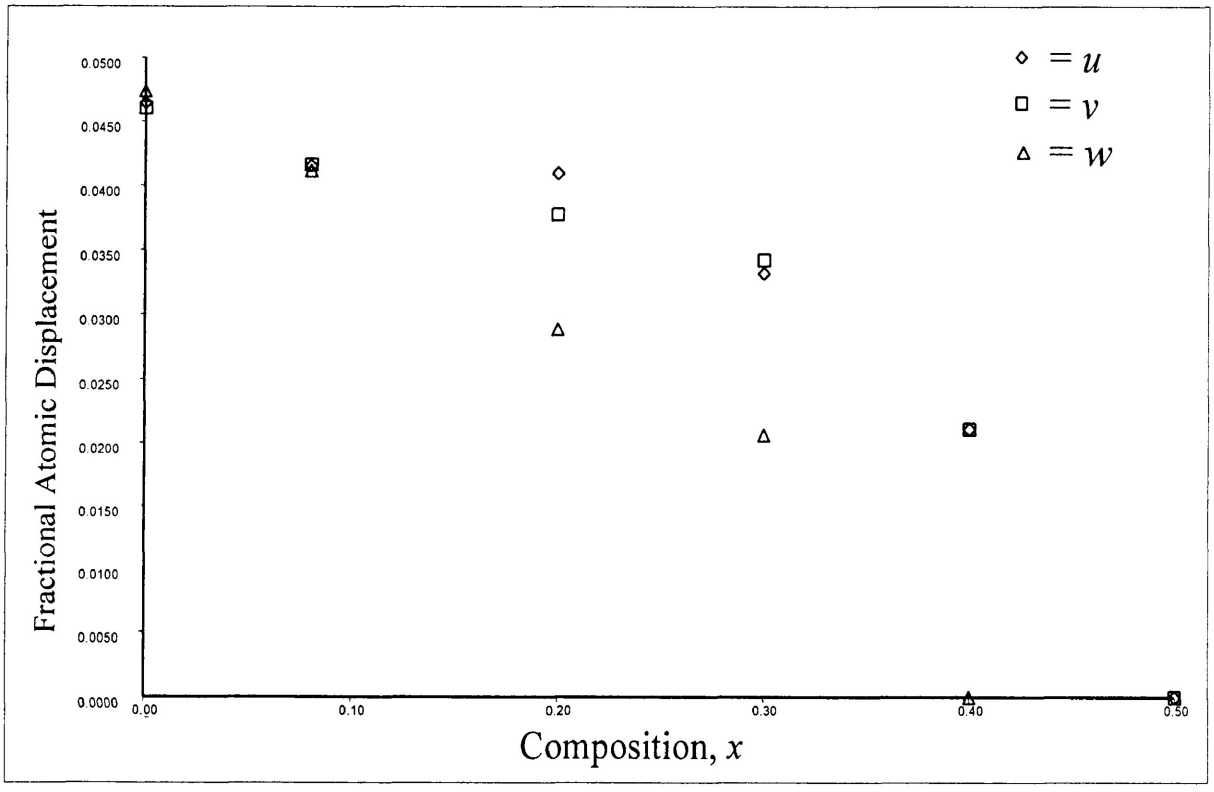

Figure 3.9.3
Fractional atomic displacements of the F(2) anion.

3.10 Discussion

Data from this study show that there is complete solubility between orthorhombic (***Pbmn***) neighborite and cubic (***Pm$\bar{3}$m***) "potassium neighborite". Two structural phase transitions exist in the $(Na_{1-x}K_x)MgF_3$ solid solution. The first is from orthorhombic (***Pbmn***) to tetragonal (***P4/mbm***) at x = 0.30 – 0.40, the second is from tetragonal (***P4/mbm***) to cubic (***Pm$\bar{3}$m***) at x = 0.40 – 0.50.These structural phase transitions are a direct result of a decrease of octahedral rotation with increasing potassium content (section 3.3 – 3.5).

The tilts exhibited by the orthorhombic $NaMgF_3$ end – member can be described as three independent tilts ϕ^-_x, ϕ^-_y and ϕ^+_z which correspond to rotations about the [100], [010] and the [001] pseudocubic axes respectively. For neighborite $\phi^-_x \approx \phi^-_y \approx 10.4^{\,0}$ and $\phi^+_z \approx 15.6^{\,0}$. Introduction of the relatively large potassium cation (ionic radius 1.33Å vs. 0.98Å for Na) into the orthorhombic neighborite perovskite structure causes fluorine displacements that result in decreased rotation of the relatively undistorted MgF_6 octahedra. To accommodate the potassium substitution the octahedra rotate towards the ideal cubic setting, gradually increasing the volume of the ***A*** – site polyhedron and coordination of the ***A*** – site cation.

The fluorine displacements are towards special positions in the unit cell, which subsequently develop structures of higher symmetry such as ***P4/mbm*** and ***Pm$\bar{3}$m***. The ***x*** and ***y*** coordinates of the F(1) site, associated with orthorhombic reflections {121, 103, 211}, are not restricted by ***Pbnm*** symmetry (Wyckoff position 4*c*, (***x, y,*** 1/4)) however, tetragonal symmetry confines the F(1) anion to a special position (2*b*) in the cell where all coordinates are fixed. This fluorine movement combined with the displacement of the F(2) anion from a general position in the orthorhombic cell (8*d*) to a position with a fixed ***z*** coordinate in the tetragonal cell (4*g*) reduces the antiphase tilts (ϕ^-_x, ϕ^-_y) to 0^0. The ***x*** and ***y*** coordinates of the F(2) anion, associated

with indices {120, 210}, are not restricted to special coordinates in ***P4/mbm*** symmetry and are therefore entirely responsible for the inphase octahedral rotation about the ***c*** – axis (ϕ^+_z) in tetragonal members of the series. The relative magnitude of the inphase tilt is greater than that for the antiphase tilt, therefore, it is not surprising that this tilt remains after the antiphase tilts have disappeared.

A – site cationic displacement does not affect the overall symmetry of the orthorhombic unit cell and is not associated with structural phase transitions. The (113) and (023) peaks observed in the X – ray diffraction data indicate that the ***A*** – site cation moves from the 4*c* (***Pbnm***) where the ***x*** and ***y*** coordinates are not fixed to the 2*c* (***P4/mbm***) special position in the $0.40 < x < 0.50$ compositional range.

Zhao (1998) has previously investigated the $(Na_{1-x}K_x)MgF_3$ solid solution series where he determined that a pure tetragonal phase was present in the $x = 0.3 - 0.4$ compositional range and that above $x = 0.4$ all members were cubic. Below $x = 0.4$, Zhao reported a mixture of tetragonal and orthorhombic phases. This study does not concur with Zhao's conclusions.

Differences between results from this study and Zhao (1998) may be attributed to the difference in temperature used to synthesize the members of the series. For this study $(Na_{1-x}K_x)MgF_3$ compounds were synthesized at 1023^0 K for 8 hrs. while members in Zhao's study were synthesized at 1073^0K (50^0K difference) for 8 hrs. This duration may have been insufficient to anneal completely intermediate members with compositions near the structural phase transitions. In addition, he interpreted semi – coalescent peaks as an indication of the presence of an additional phase. Visual inspection of the published data does not show significant differences in his X – ray data versus data from this work. Zhao did not give atomic positions and cell dimensions for all members of his series and therefore a complete comparison was not possible.

A final note on these data should be acknowledged. Localized concentrations of potassium may result in domain phenomena that cause diffuse spectra or peak broadening. Zhao noted similar effects in his investigation. The resultant F(2) atomic displacements shown in figure 3.9.2 and 3.9.3 are intended as an approximate representation of the displacement trends present in the $(Na_{1-x}K_x)MgF_3$ solid solution series.

In conclusion, the structural phase transitions in the $(Na_{1-x}K_x)MgF_3$ solid solution series are a direct result of octahedral rotation, *i.e.* fluorine migration. ***A*** – site cationic displacement and octahedral distortion do not have a significant effect on symmetry changes and structural phase transitions in this solid solution series. Interestingly, the $(Na_{1-x}K_x)MgF_3$ solid solution series does not exhibit cationic ordering common in perovskite structures (Woodward 1993).

Chapter 4, Alumino - Fluoroperovskites

4.1.1 Introduction

Naturally occurring examples of alumino – fluoroperovskites include elpasolite (K_2NaAlF_6), cryolite (Na_2NaAlF_6) and simmonsite (Na_2LiAlF_6). Of these only cryolite and simmonsite were investigated in this study. Natural and synthetic cryolite were first analyzed to test the validity of Rietveld structural refinement of X – ray powder diffraction data from alumino – fluoroperovskites. After successful cryolite refinements, synthetic simmonsite was investigated (section 4.3). Foord *et al.* (1999) were unable to determine the crystal structure of natural simmonsite due to the complexly-twinned character of the material. This study of the synthetic analogue was initiated as data on this compound are relevant to the structure of the naturally – occurring material. Based on compositional similarities to cryolite it is expected that simmonsite will crystallize in space group $P2_1/n$ (Anderson *et al.* 1993).

4.1.2 Ordering in Alumino – fluoroperovskites

Alumino – fluoroperovskite compounds are characterized by the presence of Al in the ***B*** – octahedral site. These compounds have the general formula $A_2BB'X_6$, where ***A*** is ideally in 12 – fold coordination, ***B*** and ***B'*** are different cations in octahedral coordination situated at crystallographically distinct sites, and ***X*** is anionic. If the ***B*** and ***B***' cations are situated such that they alternate along the pseudocubic axes a 1:1 ***B*** – site ordered perovskite develops, such compounds are termed double perovskites (Mitchell 2000).

The overall reduction in symmetry from the disordered ideal cubic (***Pm-3m***) to the ordered monoclinic (***$P2_1/n$***) structure is related to both octahedral rotation and ***B*** – site cationic ordering. In the ideal setting, the presence of ordered ***B*** – site cations causes a reduction in symmetry from a primitive to a face centered unit cell (***Pm-3m*** → ***Fm-3m***). Octahedral rotations further reduce the symmetry to ***$P2_1/n$*** (Anderson *et al.* 1993). **N.B**: removal of ordering from B – site cations increases the symmetry to orthorhombic, making a ***Pbnm*** structure as the disordered analogue of ***$P2_1/n$*** ordered perovskites (Mitchell, 2000).

Mitchell (2000) shows that the distinction between disordered orthorhombic ***Pbnm*** and ordered monoclinic ***$P2_1/n$*** symmetry may be difficult based on X – ray diffraction data because of similar systematic absences in both settings. Fortunately ***Pbnm*** symmetry does not permit reflections where *0kl*; $k = 2n+1$, whereas ***B*** – site ordered monoclinic perovskite structures develop peaks specifically of this type, *i.e.* 011. In structures where the ordering is incomplete or where the ordered ***B*** and ***B'*** cations do not differ significantly in atomic number, the relative intensity of the 011 reflection may be very low although cationic ordering may be present. In this instance, monoclinic symmetry may also be recognized on the basis of splitting of the 200 cubic peak into the 110 and 002 monoclinic peaks.

4.2 Cryolite

Natural cryolite from the type locality, Ivigtut, Greenland, was analyzed by powder X – ray diffraction using the initial parameters given from a single crystal refinement of cryolite by Hawthorne and Ferguson (1975). Table 4.2.1 shows reasonable agreement of data from this study and that of Hawthorne and Ferguson (1975). Figure

4.2.1 shows a difference plot for the Rietveld structural refinement (R_{Bragg} = 6.41%), for final agreement, parameters see appendix A-2.

Table 4.2.1, Crystallographic Parameters of from this study and Hawthorne and Ferguson (1975)

Cryolite $Na_2(NaAl)F_6$

Hawthorne and Ferguson (1975)										This Study									
a	5.4024	(2)Å								*a*	5.4058	(2)Å							
b	5.5959	(2)Å								*b*	5.5926	(2)Å							
c	7.7564	(3)Å								*c*	7.7699	(3)Å							
β	90.28	(1)Å								*β*	90.195	(1)Å							
	x		*y*		*z*		*B*				*x*		*y*		*z*		*B*		
Al	0		0		0		.67	(1)		Al	0		0		0		0.9	(1)	
Na(1)	0		0		1/2		1.07	(2)		Na(1)	0		0		1/2		1.4	(1)	
Na(2)	0.5133	(2)	-0.0519	(2)	0.2474	(1)	1.55	(2)		Na(2)	0.5119	(5)	0.9489	(0)	0.2488	(7)	2.4	(1)	
F(1)	0.1026	(2)	0.0455	(2)	0.2194	(2)	1.31	(2)		F(1)	0.1036	(6)	0.0442	(6)	0.2196	(7)	1.3	(1)	
F(2)	0.7268	(2)	0.1737	(2)	0.0462	(2)	1.34	(2)		F(2)	0.7257	(7)	0.1741	(7)	0.0425	(6)	1.9	(1)	
F(3)	0.1634	(2)	0.269	(2)	-0.063	(2)	1.39	(2)		F(3)	0.1693	(7)	0.2683	(7)	-0.0609	(6)	1.8	(1)	

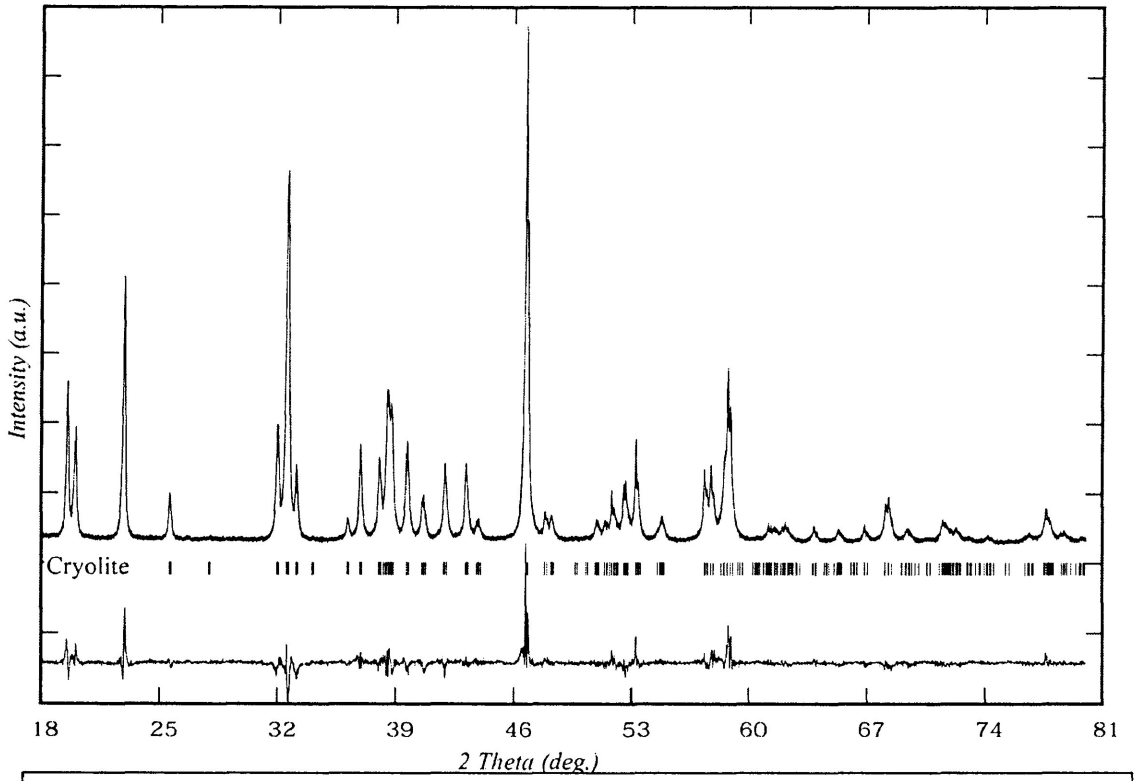

Figure 4.2.1
XRD pattern and Rietveld difference plot of natural cryolite. 20 – 80^0 2θ shown. CuKα radiation.

Cryolite was also synthesized using the method outlined in section 1.4. Figure 4.2.2 shows a Rietveld difference plot for synthetic cryolite, which converged to a final R_{Bragg} of 6.48%. The reasonable agreement between the crystallographic parameters of natural and synthetic cryolite determined in this study and those of Hawthorne and Ferguson (1975) indicate that powder X – ray diffraction data obtained from alumino - fluoroperovskites are adequate for Rietveld structural refinement and determination. Table 4.2.2 gives crystallographic parameters for natural and synthetic cryolite from this study. Note that the orientation of the unit cell has been changed from that shown in Table 4.2.1. This is because the setting shown in Table 4.2.2 is required for the octahedral tilt calculations given in section 4.4.1. All monoclinic structures reported hereafter are given in the setting of table 4.2.2.

Table 4.2.2, Crystallographic Parameters of Synthetic and Natural Cryolite

Synthetic cryolite										Natural cryolite									
This Study										This Study									
a	5.4098	(1)Å								*a*	5.4063	(2)Å							
b	5.5945	(1)Å								*b*	5.5945	(2)Å							
c	7.7723	(1)Å								*c*	7.7669	(3)Å							
β	90.118	(0)Å								*β*	90.185	(1)Å							
	x		*y*		*z*		*B*				*x*		*y*		*z*		*B*		
Al	0.5		0		0		1.5	(1)		Al	0.5		0		0		1.8	(1)	
Na(1)	0.5		0		1/2		1.1	(2)		Na(1)	0.5		0		1/2		0.7	(2)	
Na(2)	0.507	(1)	0.5446	(6)	0.2714	(7)	1.55	(2)		Na(2)	0.514	(5)	0.5475	(0)	0.2730	(7)	2.4	(1)	
F(1)	0.164	(1)	0.1640	(2)	-0.0471	(8)	1.31	(2)		F(1)	0.1585	(6)	0.1791	(6)	-0.0581	(7)	2.0	(1)	
F(2)	0.277	(1)	0.741	(1)	-0.040	(1)	1.34	(2)		F(2)	0.271	(7)	0.7269	(7)	-0.0516	(6)	1.9	(1)	
F(3)	0.388	(1)	0.9562	(9)	0.2742	(9)	1.39	(2)		F(3)	0.397	(7)	0.958	(7)	0.2542	(6)	1.9	(1)	

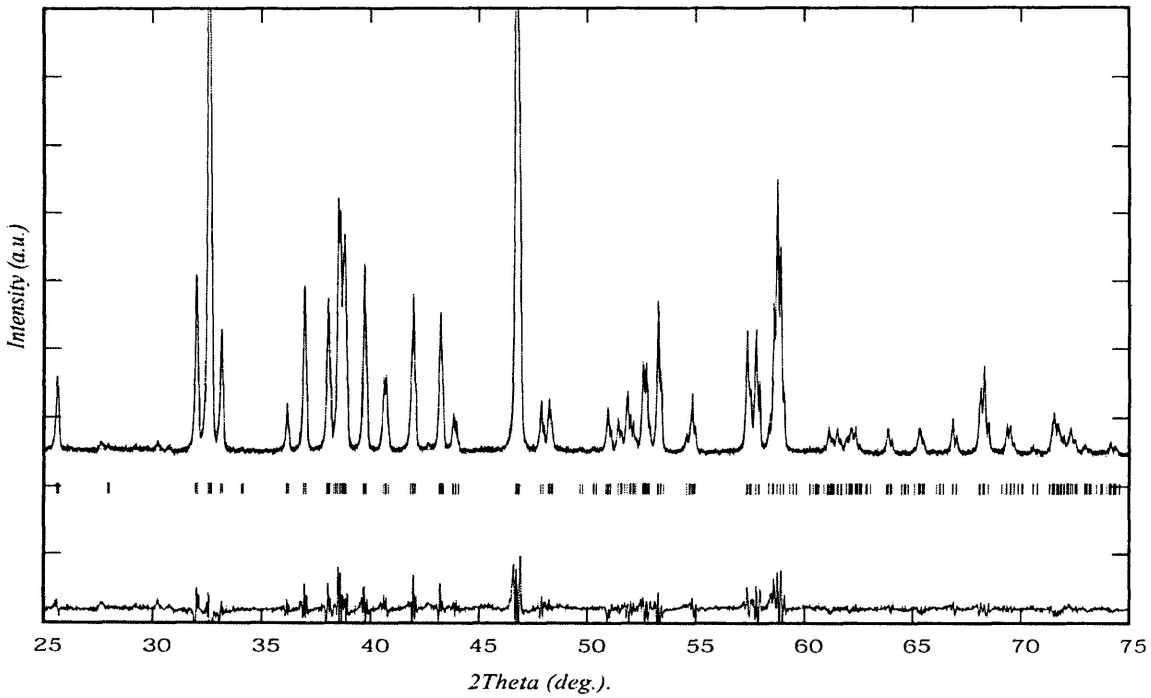

Figure 4.2.2

XRD patter of synthetic cryolite, 25 – 75^0 2θ, CuKα radiation. For final agreement parameters see appendix A-2

4.3.1 Simmonsite

Simmonsite, Na_2LiAlF_6, was discovered in 1992 by Arthur E. Soregaroli while mapping the Zapot pegmatite in the Gilles Range, approximately 25km north of Hawthorne, Mineral Co., Nevada, U.S.A. For details on the geology and mineralogy of this pegmatite, see Foord *et al.* (1998). The mineral was named after William B Simmons (b.1943), professor of mineralogy and petrology, University of New Orleans, New Orleans, Louisiana, U.S.A, in recognition of his contribution to the study of granitic pegmatites and their mineralogy.

The fluoroperovskites simmonsite, cryolite and the garnet-structured cryolithionite ($Na_3Li_3Al_2F_{12}$) occur together as part of an alumino – fluoride assemblage in a late stage breccia pipe structure cutting the Zapot amazonite – topaz – zinwaldite pegmatite. The alumino – fluoride assemblage is of hydrothermal origin and contains approximately equal amounts of the three minerals. This assemblage was subject to subsequent episodes of hydrothermal alteration which produced a secondary assemblage of alumino – fluorides consisting of minerals containing hydroxyl anions or water, including: pachnolite, weberite, thomsenolite, prosopite, ralstonite and a second generation of cryolithionite. Fluorite is intimately intergrown with these secondary alumino- -fluorides. Naturally – occurring simmonsite is pale cream in color with white streak, translucent to transparent with a Mohs hardness of 2.5 – 3. It has no distinct cleavage, subconchoidal fracture and no parting. For more information on the optical and crystallochemical properties of simmonsite, see Foord *et al.* (1999).

4.3.2 Previous Studies

Several previous investigations have addressed the complex mineralogy and crystallography of the system Na_3AlF_6 – Li_3AlF_6. Garton and Wanklyn (1967) reinvestigated the system after widely divergent data had been reported by Rolin and Muhlethaler (1964), Beletskii and Sasksonov (1957), and Drossbach (1936). Garton and Wanklyn used powder X – ray diffraction and Differential Thermal Analysis (DTA) data to show complete solubility between Na_3AlF_6 (Na_2NaAlF_6) and Na_2LiAlF_6 where the later represents complete substitution of Li for Na in the 2*b* octahedral site. At concentrations greater than 33.3 mol % Li cryolithionite precipitates as a Li rich phase. They indexed Na_2LiAlF_6 on a hexagonal cell (a = 5.30(0)Å, c = 13.09(5)Å), regardless of the presence of reflections which violate hexagonal symmetry. Their observed d – values are given with those obtained in this work and other previous studies in Table 4.3.

Holm and Holm (1970) also investigated the Na_3AlF_6 – Li_3AlF_6 system by DTA and X – ray powder diffraction. They suggested a ***B*** – centered monoclinic cell with $\boldsymbol{a}$ = 7.538(3)Å, $\boldsymbol{b}$ = 7.516(3)Å, $\boldsymbol{c}$ = 7.525(4)Å and $\beta = 90.81(0)^0$. However, they also report violations of the proposed symmetry by the presence of 11-2 reflections (***B*** – centering restricts h,k,l to $h+l = 2n$).

Foord *et al.* (1999) collected X – ray diffraction data from natural Na_2LiAlF_6 from the type locality and, assuming that it was isostructural with the synthetic analogues discussed above, suggested that both earlier studies were in error and that simmonsite is in fact monoclinic crystallizing in $\boldsymbol{P2_1}$ or $\boldsymbol{P2_1/m}$ symmetry at room temperature. They indexed their pattern based on a double monoclinic cell $\boldsymbol{a}$ = 7.5006(6)Å, $\boldsymbol{b}$ = 7.474(1)Å, $\boldsymbol{c}$ = 7.503(1)Å, $\beta = 90.847(9)^0$ Z = 4. They maintain that an ***n*** – glide is absent on the basis

of the presence of several very weak reflections in violation of ***n*** – glide conditions (*h0l;* $h + l = 2n$) which they unfortunately did not list. Because their indexed reflections comply with conditions for a [010] 2_1 screw axis (*0k0*; $k = 2n$), they adopted the Holm and Holm (1970) monoclinic cell in space group $\boldsymbol{P2_1}$ or $\boldsymbol{P2_1/m}$.

Data from this work suggest that all of the above are in error and that simmonsite crystallizes in $\boldsymbol{P2_1/n}$ symmetry at room temperature. Assuming that synthetic and natural phases are isostructural, simmonsite exhibits structural characteristics similar to those of cryolite.

Table 4.3.2 Comparison of experimental *d* - values from this and other structural investigations

This study					Holm and Holm					Garton and Wanklyn					Foord *et al.*				
Monoclinic					Doubled monoclinic					Hexagonal					Doubled monoclinic				
a	5.2860		(1)		*a*	7.538		(3)		*a*	5.30		(0)		*a*	7.5006		(6)	
b	5.3731		(1)		*b*	7.516		(3)							*b*	7.474		(1)	
c	7.5101		(1)		*c*	7.525		(4)		*c*	13.09		(5)		*c*	7.503		(1)	
β	90.029		(1)		*β*	90.81									*β*	90.847		(9)	
H	K	L	Dobs	Int	H	K	L	Dobs	Int	H	K	L	Dobs	Int	H	K	L	Dobs	Int
0	1	1	4.366	52.1	1	1	-1	4.366	vs	0	0	3	4.34	vs	0	1	1	4.33	100
-1	0	1	4.320	27.5	1	1	1	4.325	vs										
1	0	1	4.318	28.2	2	0	0	3.796	m										
1	1	0	3.764	15.3	0	0	-2	3.762	m	1	0	2	3.76	w					
0	0	2	3.754	7.3	0	2	0	3.758	w						0	0	2	3.78	10
					0	1	-2	3.369	m				3.37	vw	-1	1	1	3.36	5
0	2	0	2.634	13.4	2	0	-2	2.681	s						0	2	0	2.65	60
-1	1	2	2.658	25.3	2	0	2	2.656	m										
1	1	2	2.657	20.7						1	1	0	2.66	vs					
2	0	0	2.640	8.3															
1	2	0	2.392	9.6	1	0	-3	2.39	m						1	2	0	2.37	15
2	1	0	2.369	17.7	1	0	3	2.37	m				2.37	w					
-1	2	1	2.280	25.9	1	1	-2	2.28	vs										
-1	0	3	2.2620	7.7															
1	0	3	2.2610	33.2															
-2	1	1	2.259	28.9						1	1	3	2.26	s	1	0	3	2.25	70
0	2	2	2.183	70.6	2	2	-3	2.183	vs	0	0	6	2.187	s					
-2	0	2	2.160	27.0	2	2	2	2.162	m	2	0	2	2.158	s	-2	0	2	2.18	50
2	0	2	2.1589	27.8											0	2	2	2.158	40
1	1	3	2.0835	6.0	2	3	0	2.086	m						1	1	3	2.076	5
-1	2	2	2.0177	8.3	1	2	-3	2.017	m				2.015	w	-1	2	2	2.008	10
					1	3	2	2.006	w										
2	2	0	1.8820	100						2	0	4	1.881	vs					
0	0	4	1.877	54.0											0	0	4	1.877	90
					1	0	-4	1.831	w										
					2	3	-2	1.831	w				1.83	vw					
															0	2	3	1.824	5
															3	0	1	1.711	5
-1	3	1	1.6529												-2	2	2	1.646	5
															-3	1	2	1.536	5
															1	3	2	1.526	25
															3	2	1	1.435	10
															-2	2	4	1.335	5
															0	4	0	1.324	20

4.3.3 X – Ray Diffraction Data

XRD data were collected and refined by the methods outlined in section 1.3.The Rietveld structural refinement of powder X – ray diffraction data from synthetic simmonsite also included cryolite and LiF, of which the latter two were present in minor amounts as impurities (cryolite 4.6vol%, LiF 3.2vol%). Simmonsite reflections were successfully indexed on a primitive monoclinic unit cell whose approximate cell dimensions are related to the pseudocubic subcell by $a \approx \sqrt{2}a_p$, $b \approx \sqrt{2}a_p$, $c \approx 2a_p$. Monoclinic symmetry was chosen on the basis of systematic absences, compositional similarities to cryolite and broadening of the 200 $_{Fm\bar{3}m}$ into the $110_{P2_1/n}$ and $002_{P2_1/n}$ monoclinic peaks. Refinements of the $P2_1$ and $P2_1/m$ settings of Holm and Holm (1970)

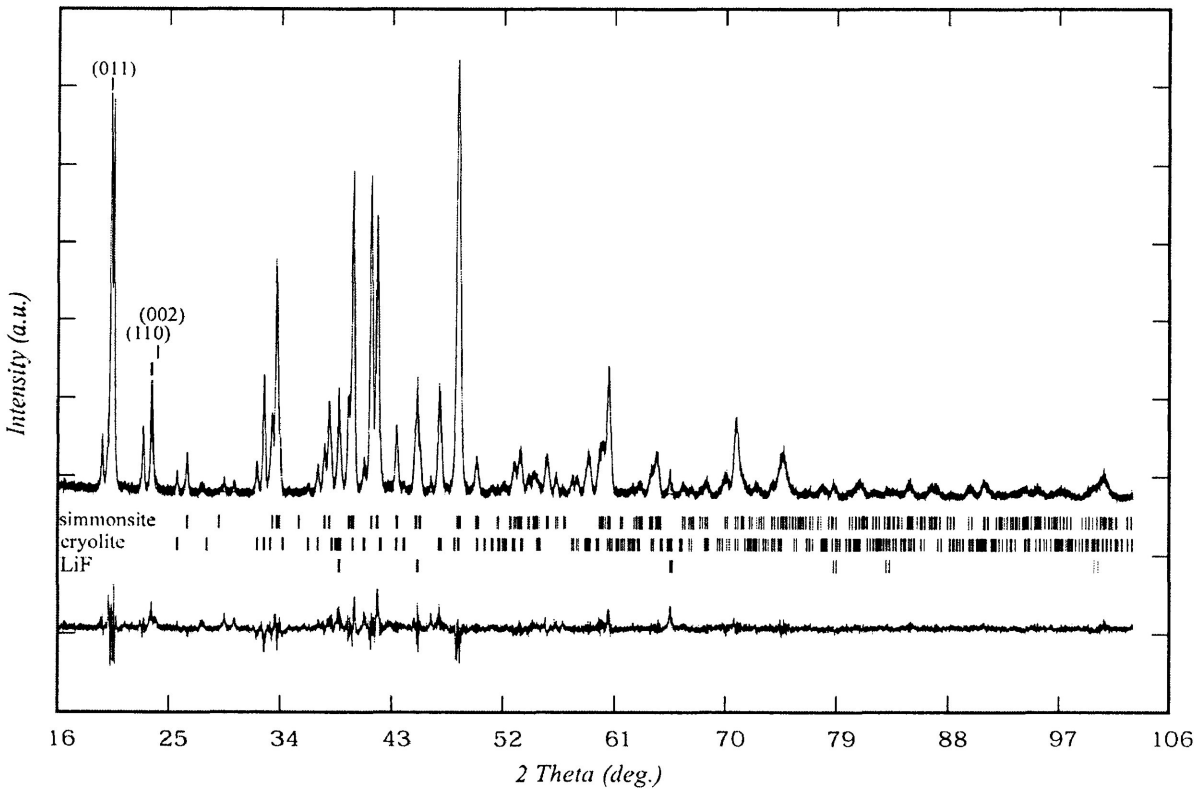

Figure 4.3.3
XRD Rietveld difference plot for synthetic simmonsite. 15 – 105 $^0 2\theta$, Cu radiation.

were conducted. Major discrepancies arose between the calculated and observed data which were attributed to the presence of *h0l; h + l = 2n + 1* type reflections, as these reflections are not present in the observed XRD pattern. The ***P2$_1$*** refinement converged with a final R_{Bragg} of 34.8%. The ***P2$_1$/m*** refinement converged with a final R_{Bragg} of 14.62% and gave crystallographic parameters which resulted in highly distorted octahedra and spurious thermal isotropic parameters.

The Rietveld structural refinement of synthetic simmonsite gave the best agreement parameters in space group ***P2$_1$/n*** (***a*** = 5.2861(1)Å, ***b*** = 5.3732(1)Å, ***c*** = 7.5100(2Å, β = 89.970(9)^0, R_{Bragg} is 4.70%). This is not surprising as reflection indices for simmonsite (Table 4.3) show compliance with reflection limiting conditions for a [010] 2_1 screw axis (*0k0; k = 2n*) and ***n*** – glide (*h0l; h+l = 2n*). Furthermore, the presence of an intense 011 reflection (53% relative intensity to the 220 100% peak) clearly indicates an ordered monoclinic structure where the ***B*** – site cations differ by 10 atomic numbers.

4.3.4 Structure

Simmonsite, a 1:1 ordered ***$A_2BB'X_6$*** perovskite – type compound, is structurally similar to cryolite [$Na_2(NaAl)F_6$] in that the ***B*** and ***B'*** octahedral cations are ordered between the *2c* and *2d* crystallographic sites respectively. Figure 4.3.4 illustrates the simmonsite structure where light octahedra contain Li (*2c*) and dark octahedra contain Al (*2d*). Crystallographic parameters for synthetic simmonsite are given in table 4.3.4. This 1:1 ***B*** – site ordered perovskite is best described as two ***B*** – site sublattices that are comprised of regular isolated octahedra of their respective cations (figure 4.4, light(Li) and dark(Al) octahedra). The octahedra of each sublattice are corner linked to octahedra

of the other to complete the perovskite octahedral framework. ***A*** – site cations occupy the cubo - octahedral site, which in simmonsite, is reduced from 12 – fold coordination in the ideal cubic setting (*i.e.* elpasolite) to 10 – fold coordination as a result of distortion caused by increased octahedral rotation.

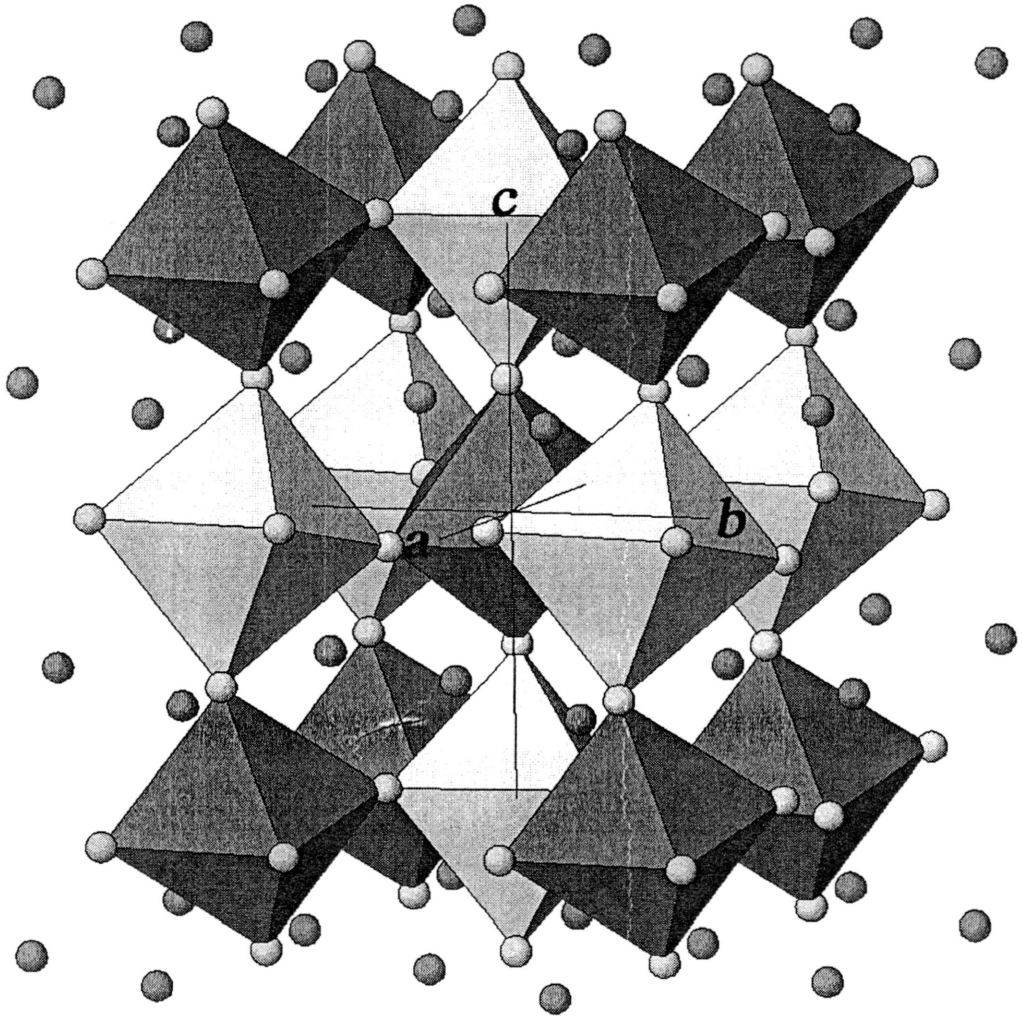

Figure 4.3.4
Illustration of 1:1 ***B*** – cation ordered simmonsite perovskite structure. Aluminum sublattice shown by dark octahedra, lithium sublattice shown by light octahedra.

Table 4.3.4 Crystallographic parameters for synthetic simmonsite

Space Group	*P121/n1*				
Cell Dimensions					
a	5.2860 (1)Å	ap (mean)	3.7641 Å		
b	5.3731 (1)Å	ap (volume)	3.7640 Å		
c	7.5101 (2)Å	Z	4		
B	90.029 $(0)^0$				

	Wyck	*x*		*y*		*z*		*B*		*N*
Li	*2c*	0.5		0		0.5		1.2	(1)	0.5
Na	*4e*	0.5066	(7)	0.5392	(3)	0.2522	(6)	2.6	(1)	1
Al	*2d*	0.5		0		0		1.0	(1)	0.5
F(1)	*4e*	0.2208	(7)	0.1951	(6)	0.9630	(8)	1.9	(1)	1
F(2)	*4e*	0.3097	(7)	0.7219	(6)	0.9560	(7)	1.7	(1)	1
F(3)	*4e*	0.4257	(6)	0.9771	(5)	0.2374	(9)	2.4	(1)	1

Values in parentheses indicate errors. For final agreement factors see appendix A – 2.

4.4 Octahedral Tilts

A feature common to all $P2_1/n$ ordered perovskites is that the BX_6 and $B'X_6$ octahedra have different tilt angles as a result of octahedral distortion and difference in size. Mitchell (2000) indicates that it can be shown by geometrical analysis that the smaller octahedra must always rotate more than the larger, and that tilts for both octahedra must have the same sense, *i.e.* if $\phi B' < \phi B$ then $\theta B' < \theta B$ must also be true.

Mitchell (2000) also gives a method for the derivation of the [001] (ϕ^+) and [110] (θ) octahedral tilts for each crystallographically-distinct octahedra in the 1:1 ***B*** – site ordered (or partially-ordered) monoclinic perovskite structure. These calculations, given below, (after Groen *et al.* (1986), revised by Mitchell (2000)) derive tilt angles in degrees from a combination of cell dimensions and anionic coordinates.

The choice of monoclinic setting is very important for these calculations; for example, attempting to calculate tilt angles for monoclinic perovskites arranged in a setting similar to that of Hawthorne and Ferguson (1975) as in Table 4.2.1, will result in erroneous values on the order of 50 – 60^0. Note that this setting places the ***B*** and ***B'*** cations in the 0,0, ½ (*2b*) and 0,0,0 (*2a*) crystallographic sites respectively, whereas the monoclinic setting chosen by Groen *et al.* (1986) for Nd_2MgTiO_6 or Chakhmouradian *et al.*(1998) for $x = 0.4 - 0.5$ members of the $CaTi_{1-2x}Fe_xNb_xO_3$ solid solution series, places the ***B*** and ***B'*** cations in the ½,0,0 (*2d*) and ½,0, ½ (*2c*) positions.

B' [001] tilt = ½ atan [A·*a*/*b*] + ½ atan [B·*b*/*a*]

B [001] tilt = ½ atan [C·*a*/*b*] + ½ atan [D·*b*/*a*]

B' [110] tilt = atan $[(E^2 + F^2)^{½}]$ / {[½ - z(***X***3)·*c*}

B [110] tilt = atan $[(E^2 + F^2)^{½}]$ / [z(***X***3)·*c*]

Where A = $[x(X2) - x(X1)]/[y(X2) - y(X1)]$; B = $[1 - y(X1) - y(X2)]/[x(X2) + x(X1)]$; C = $[x(X2) - x(X1)]/[1 + y(X1) - y(X2)]$; D = $[1 - y(X2) - y(X1)]/[1 - x(X2) - x(X1)]$; E = $\{[½ - x(X3)]\cdot a\}$; and F = $\{1 - y(X3)]\cdot b]$. ***X*** followed by a number denotes crystallographically distinct anions, in this case fluorine.

4.4.2 Octahedral Tilts in Simmonsite and Cryolite

The reduction of symmetry from cubic $Fm\bar{3}m$ to monoclinic $P2_1/n$ is a direct result of octahedral rotation. The octahedral rotation schemes in simmonsite and cryolite are similar to that of neighborite ($a^-a^-c^+$) and are described in Glazer's (1972) notation as $a^+b^-b^-$. Although labeled differently, these two octahedral tilt schemes are identical in nature, *i.e.* two antiphase tilts and one inphase tilt. The tilt angles derived by equations in section 4.4.1 for simmonsite and cryolite are given in Table 4.4.2. The octahedral tilts are greater in cryolite than in simmonsite, consequently, cryolite will exhibit the greater overall structural distortion. In both structures, the AlF_6 octahedron has the greatest rotation and therefore is expected to be the smaller of the two octahedra.

Table 4.4.2 Octahedral Tilts for simmonsite and cryolite

		Simmonsite	Cryolite
ϕ	B' [001] =	9.10	10.41
ϕ	B [001] =	10.33	12.97
θ	B' [110] =	11.93	15.52
θ	B 110] =	12.79	19.73
Φ	B' [111] =	14.96	18.61
Φ	B [111] =	16.38	23.46

Note, in both structures the ***B*** cation is Al. In simmonsite ***B'*** is Li and in cryolite ***B'*** is Na.
Data for cryolite above and hereafter are from the natural phase.

4.5 Coordination Analysis

Interatomic distances and angles were derived by **IVTON** as outlined in section 1.3. Table 4.5 gives a summary of coordination parameters for cryolite and synthetic simmonsite. As expected, cryolite exhibits greater structural distortion due to greater octahedral rotation.

Section 4.4.2 showed that the octahedra in cryolite were rotated more than those of simmonsite. This results in greater overall structural distortion as shown by the difference in values of f (simmonsite $f = 4.51$, cryolite $f = 4.01$). Structural distortion caused by octahedral rotation is also related to the reduction in coordination of the ***A*** – site cation from 10 anions in simmonsite to 8 in cryolite. This leads to an increase in "uncoordinated space" which, in total comprises ≈ 37% of the unit cell volume.

The comparatively greater distortion of the cryolite structure may also be recognized on the basis of ***B***(Al) and ***B'*** octahedral distortion. Strong anion affinity for the trivalent Al cation results in relatively small, regular octahedra as compared to octahedra coordinating the ***B'*** cation. This is consistent with earlier observations in that the Al octahedra posses the greatest rotations and therefore must be the smallest of the octahedra (Mitchell 2000). Variation in Al – F bond lengths is low in both phases, however, angular distortion increases from $\delta = 0.2458$ in simmonsite to $\delta = 1.10$ in cryolite. The mean Al – F bond length and bond length distortion (Δ) in simmonsite is 1.8306(4) and 0.0001 and for cryolite they are 1.812(5) and 0.0430 indicating that distortion of the ***B*** – site octahedra does not greatly increase as a result of substitution of Na for Li in the ***B'*** – crystallographic site.

In contrast the ***B'*** octahedra show dramatically different degrees of octahedral distortion. Table 4.5 shows that the cryolite NaF_6 octahedron exhibits significant angular distortion (δ = 14.40(2)) with respect to simmonsite (LiF_6 δ = 2.74(2)) in addition to an increase in mean bond length of 0.2Å This, in turn, increases the B' octahedral volume from 11.175Å^3 in simmonsite to 15.146Å^3 in cryolite resulting in lower values of *f*.

The ***B'*** octahedral distortion in cryolite is attributed to low anion affinity for the weakly charged monovalent cation in addition to the larger ionic radii of Na as compared to Li.

Table 4.5 Coordination Parameters for simmonsite and cryolite

Na_3AlF_6	(natural)			**Simmonsite**			
ap (mean)	3.8866(3)	V_{cell}	234.760(1)Å^3	*ap* (mean)	3.7641(5)	V_{cell}	213.309(1)Å^3
ap (volume)	3.8862(3)	***V/Z (Vap)***	58.690(1)Å^3	*ap* (volume)	3.7640(5)	***V/Z (Vap)***	53.327(1)Å^3
Z	4			*Z*	4		
	A - Site cation				**A - Site cation**		
Na Cn = 8		V_A Ivton	25.241 (1)Å^3	Na Cn = 10		V_A Ivton	35.824(1)Å^3
m1	2.5018	$V\Delta$	21.882 (1)Å^3	m1	2.5804	$V\Delta$	7.826(1)Å^3
m2	3.4098	V_A calc	47.123 (1)Å^3	m2	3.2344	V_A calc	43.650(1)Å^3
m3	2.8044			m3	2.6894		
	B and B' cations				**B and B' cations**		
	Al (***B***)	Na (***B'***)			Al (***B***)	Li (***B'***)	
mean	1.8123(1)	2.2460(2)		mean	1.8306	2.032	
Δ	0.0430	0.1066		Δ	0.0001	0.0555	
δ	1.0997	14.0440		δ	0.2458	2.0321	
V_BAl	7.987 Å^3	V_BNa 15.146 Å^3		V_BAl	8.179 Å^3	V_BLi 11.175 Å^3	
	f=4.074				f=4.511		

Note; m1 is the mean Interatomic distance within the first coordination sphere, m2 is the mean bond length of the remaining anions and m3 is the mean of all 12 anions surrounding the ***A*** – site Na cation

Summary

This work shows that fluoroperovskite – type compounds are amenable to powder X – ray diffraction analysis and Rietveld structural refinement. For many fluoroperovskite – type compounds powder XRD techniques have proven effective, however, as indicated in section 3.9 exact structural refinements of compounds whose compositions are near compositionally derived phase transitions may be difficult to achieve due to peak broadening and domain effects.

Further studies should include the investigation of possible solid solution between cryolite and simmonsite as solubility between these two minerals may be expected on the basis of structural similarities. Furthermore, the introduction of a cation which might cause Jahn – Teller distortion into the fluoroperovskite structure may result in some interesting perovskite modifications. Jahn – Teller distorted perovskites are characterized by octahedra that exhibit elongation of the two apical bonds and contraction of the four equatorial bonds.

Perovskite – type compounds have a multitude of uses even though their structures are poorly understood. Clearly, there is a need for additional, detailed, systematic investigations of perovskite – type compounds.

References

Aleksandrov K.S. (1976). The sequence of structural phase transitions in perovskites. Ferroelectrics 16, 801.

Balic – Zunic, T. and Vickovic, I. (1996) IVTON crystal chemical structure software

Beletskii M.S. and Saksonov Y.G. (1957). "Phases in the system Na_3AlF_6 – Li_3AlF_6". Zh. Neorgan. Khim. 2, 2, 414 – 416.

Bodias, C. and Monceau, D. (1997) *Carine Crystallography Software*

Burns P. (1996) A structural phase transition in $K(Mg_{1-x}Cu_x)F_3$ perovskite. Physical Chemistry of Minerals 23, 141-150.

Buttner, R.H. and Maslen, E.N. (1992). Electrodensity and structural parameters of $CaTiO_3$. Acta Crystallographica B48, 644-649.

Chao, E.C.T., Evans, H.T.Jr., Skinner, B.J. and Milton, C. (1961). Neighborite, $NaMgF_3$, A new mineral from the Green River Formation. South Ouray, Utah. American Mineralogist 46, 370 – 393.

Dawson J.B., Pinkerton, H., Norton, G.E., Pyle, D.M., Browning, P., Jackson, D. and Fallick, A.E. (1995). Petrology and geochemistry of Oldoinyo Lengai lavas extruded November 1988: magma source, ascent and crystallization. Carbonatite Volcanism Springer – Verlag, Berlin, 47 – 54.

Dowty, E. *ATOMS* V4.0 (1997)

Drossbach P. (1936). Electrometallurgy of aluminum. Elektochemica, 42, 1, 65 – 70.

Foord, E.E., O'Connor, J.T., Hughes, J.M., Sutley, S.J., Falster, A.U., Soregaroli, A.E., Lichte, F.E. and Kile, D. (1999). Simmonsite, Na_2LiAlF_6, a new mineral from the Zapot amazonite – topaz – zinwaldite pegmatite, Hawthorne, Nevada, U.S.A. American Mineralogist, 84, 769.

Foord, E.E., Soregaroli, A.E. and Gordon, H.M. (1999) The Zapot amazonite – topaz – zinwaldite pegmatite. Mineral Record in press.

Garton, G. and Wanklyn, B. M. (1967). Reinvestigation of the system Na_3AlF_6 – Li_3AlF_6. Journal of the American Ceramic society 50, 395.

Glazer, A. M. (1972). The classification of tilted octahedra in perovskites. Acta Crystallographica, B28, 3384.

Glazer, A. M. (1975). Simple ways of determining perovskite structure. Acta Crystallographica A31, 756.

Hawthorne F.C. and Ferguson R.B. (1975). Refinement of the crystal structure of cryolite. Canadian Mineralogist 13, 377-382.

Holm J.L. and Holm B.J. (1970). Phase investigations in the system $Na_3AlF_6 - Li_3AlF_6$. Acta Scandinavica 24, 2535.

Mitchell R.H. (2000). Perovskites: Ancient and Modern; Structure and Composition. In preparation, Almaz Publishing.

Mitchell, R. H. (1997). Carbonate – Carbonate Immiscibility, Neighborite and Potassium Iron Sulphide in Oldoinyo Lengai natro carbonatite. Mineralogical Magazine, 61, 779 – 789.

Mitchell, R. H. and Chakhmouradian, Anton, R. (1998). A structural study of the perovskite series $CaTi_{1-2x}Fe_xNb_xO_3$. Journal of Solid State Chemistry, 138, 272 – 277,.

Mitchell, R. H., Chakhmouradian, Anton, R. A (1998). A structural study of the perovskite series $Na_{1/2+x}La_{1/2-3x}Th_{2x}TiO_3$. Journal of Solid State Chemistry, 138, 307 – 312.

O'Keefe M. and Hyde B.G. (1996). Crystal Structures. Mineralogical society of America monograph.

O'Keeffe, M. and Hyde, B. G. (1977). Some structure topologically related to cubic perovskite ($E2_1$), ReO_3 ($D0_9$) and Cu_3Au ($L1_2$). Acta Crystallographica, B33, 3802 – 3813.

Park J.H. and Parise, J.B. (1997). High-pressure synthesis of a new chromite $ScCrO_3$. Materials Research Bulletin 32, 1617 – 1624.

Robin M. and Mulethaler R. (1964). Study of the system $Na_3AlF_6 - Li_3AlF_6$ and the dissolution of Al_2O_3 in it. Bulliten Soc. Chim. France 10 2593-2599.

Rodriguez and Caraval *Fullprof Program* Journal of Applied Crystallography 14, 149, 1981.

Ross, K.R. An X – Ray Diffraction Analysis and Rietveld Refinement of $Na_{1-x}K_xMgF_3$. HBSc. Thesis Lakehead University.

Sasaki, S., Prewitt, C.T., Bass, J.D. and Schulze, W.A.(1987). Orthorhombic perovskite $CaTiO_3$: structure and space group. Acta Crystallographica C48, 1668, 1987.

Shannon R.D. (1976) Revised effective ionic radii and systematic studies of Interatomic distances in halides and chalcogenides. Acta Crystallographica A32, 751-767.

Thomas Noel W. (1996) The compositional dependence of octahedral tilting in orthorhombic and tetragonal perovskites. Acta Crystallographica B52, 16-31.

Woodward, P. M. Octahedral tilting in perovskites. I. Geometrical considerations. Acta Crystallographica B53, 32-43.

Young R.A. (1995) The Rietveld Method. IUCr Monograph on crystallography #5. Oxford Science Publications

Zhao, Yusheng, Weider, D.J., Parise, J.B. and Cox D.E. (1993). Thermal expansion and structural distortion of perovskite – Data for $NaMgF_3$ perovskite. Part I. Physics of the Earth and Planetary Interiors, 76, 1 – 16.

Zhao, Yusheng, Weider, D.J., Parise, J.B. and Cox D.E. (1993). Critical Phenomena and Phase Transition of Perovskite – Data for $NaMgF_3$ Perovskite. Part II. Physics of the Earth and Planetary Interiors, 76, 17 – 34.

Zhao, Yusheng, Weinder, D.J., Ko, J., Leinenweber, K., Liu, X., Li, B., Meng, Y., Pacalo, R.E.G., Vaughan, M.T., Wang, Y. and Yeganeh – Haeri, A. (1994). Perovskite at High P – T Conditions: An in situ Synchrotron X-ray diffraction study of $NaMgF_3$ perovskite. Journal of Geophysical Research, 99, B2, 2871 – 2875.

Zhao, Yeusheng, (1998). Crystal chemistry and phase transitions of perovskite in P – T – X space: data for $(K_xNa_{1-x})MgF_3$ perovskites. Journal of Solid State Chemistry I41, 121 132.

Appendix A - 1

This appendix contains crystallographic information on the $Na_{1-x}K_xMgF_3$ solid solution series. For the A – site cations m1 is the mean interatomic distance for anions in the first coordination sphere, m2 is the mean interatomic distance between the A – site cation and the remaining anions that are not included in the first coordination sphere but would be in the ideal cubic setting. m3 is the mean interatomic distance of all 12 anions.

The $x = 0.35$ member was not included in this appendix nor were data from it included in any of the diagrams showing tends in the solid solution. It was excluded because the Rietveld refinement for this member would not converge with a reasonable error value. This is attributed to peak broadening due to the proximity of the structural phase transition and micro – domain phenomena.

Some members were refined in multiple phase refinements. Additional phases are indicated on the Rietveld difference plots.

$x =$ 0

Composition Na1.0K0.0MgF3

Space Group ***Pbnm***

Cell Dimensions

a	5.3609	(1)	ap (mean)	3.8344	
b	5.4862	(1)	ap (volume)	3.8342	Na
c	7.6661	(1)	*Z*	4	K
a'	3.7907				Mg
b'	3.8793				F(1)
c'	3.8330				F(2)

Crystallographic Parameters

Wyck	*x*		*y*		*z*		*B*		*N*
4*c*	0.9897	(3)	0.0439	(2)	0.25		2.0	(3)	0.5000
4*c*	0.9897	(3)	0.0439	(2)	0.25		2.0	(3)	0
4*b*	0		0.5		0		1.0	(2)	0.5
4*c*	0.0897	(3)	0.4723	(3)	0.25		1.4	(4)	0.5
8*d*	0.7035	(2)	0.2961	(2)	0.0474	(1)	1.2	(3)	1

Polyhedral Data

V	V/Z (Vap)	*VA* Ivton	*V*D	*VA* calc	*VB*	*f*
225.466	56.367	30.142	15.833	45.975	10.392	4.42

Interatomic Distances

Na		Mg	
1st C.S.		F1	1.9818
F1	2.4101	F1	1.9818
F1	3.1309	F2	1.9777
F1	2.2889	F2	1.9898
F2	2.5844	F2	1.9777
F2	2.3097	F2	1.9898
F2	2.6987	mean	1.9831
F2	2.6987		
F2	2.5844		
F2	2.3097		
m1	2.5573		
F2	3.3735		
F1	3.1819		
F2	3.3735		
m2	3.3096		
m3	2.7454		

Bond Angles

B-X1-B	151
B-X2-B	150

Octahedral Tilts

Method 1 (Cell Param)

ϕ	8.52
θ	12.27
Φ	14.90

Method 2 (*B* - *X* - *B*)

ϕ	10.46
ϕz	10.60
θ	14.75
Φ	18.01

Method 3 (*X*, *Y*, *Z*)

ϕ	10.49
θ	14.75
Φ	18.03

Agreement Parameters

Rp:	12.3
Rwp:	15.0
Rexp:	10.0
Chi2:	2.3
R-Bragg	**4.9**
DW-Stat.:	1.1

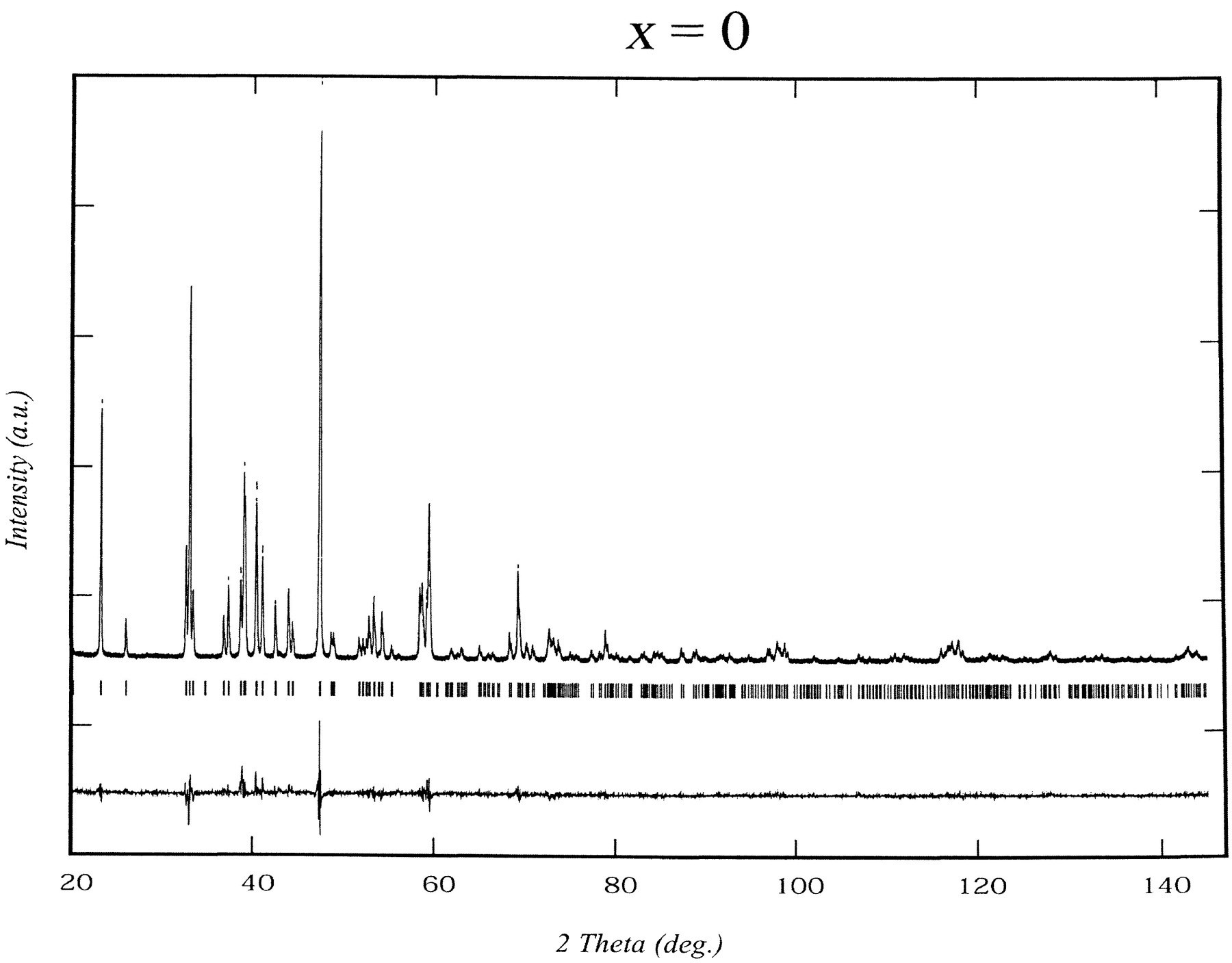
x = 0
Intensity (a.u.)
20
40
60
80
100
120
140
2 Theta (deg.)

Phase $x = 0$ NaMgF3 endmember

h	*k*	*l*	*D(A)*	*2T*	*HW*	*Iobs*	*Icalc*	*io-ic*
1	0	1	4.3933	20.197	0.125	11.6	6.3	5.2
1	0	1	4.3933	20.246	0.125	6.5	3.3	3.3
1	1	0	3.8343	23.179	0.127	299	290.1	8.9
0	0	2	3.833	23.187	0.127	129.4	125.9	3.4
1	1	0	3.8343	23.236	0.127	144.1	144.3	-0.3
0	0	2	3.833	23.243	0.127	62.5	62.7	-0.1
1	1	1	3.4292	25.962	0.128	61	60.7	0.3
1	1	1	3.4292	26.025	0.128	31.5	30.2	1.3
0	2	0	2.7431	32.618	0.132	200.6	211.3	-10.7
0	2	0	2.7431	32.698	0.132	93.6	105.1	-11.5
1	1	2	2.7108	33.017	0.132	687	723.1	-36.1
1	1	2	2.7108	33.099	0.132	364.4	359.7	4.6
2	0	0	2.6805	33.402	0.133	119.2	123.5	-4.3
2	0	0	2.6805	33.485	0.133	51.6	61.4	-9.8
1	2	0	2.442	36.775	0.135	80.6	78.5	2.1
1	2	0	2.442	36.866	0.135	42.4	39	3.4
2	1	0	2.4084	37.307	0.135	156.7	150.1	6.6
2	1	0	2.4084	37.4	0.135	74.6	74.7	0
1	2	1	2.3268	38.666	0.136	176.4	158.5	17.9
1	2	1	2.3268	38.763	0.136	96.4	78.8	17.6
1	0	3	2.3067	39.016	0.136	387.5	356.9	30.7
1	0	3	2.3067	39.114	0.136	183.6	177.5	6.1
2	1	1	2.2977	39.176	0.136	245.1	237	8
2	1	1	2.2977	39.274	0.136	119.2	117.9	1.3
0	2	2	2.2307	40.402	0.137	362.7	336.7	26
0	2	2	2.2307	40.503	0.137	176.1	167.5	8.6
2	0	2	2.1966	41.057	0.138	229.2	218.6	10.6
2	0	2	2.1966	41.16	0.138	120.9	108.7	12.1
1	1	3	2.1264	42.478	0.139	130.8	116.6	14.2
1	1	3	2.1264	42.585	0.139	63.4	58	5.4
1	2	2	2.0595	43.927	0.14	158.9	147.6	11.3
1	2	2	2.0595	44.038	0.14	85.1	73.4	11.7
2	1	2	2.0392	44.387	0.14	80.1	69.8	10.4
2	1	2	2.0392	44.5	0.14	39.2	34.7	4.5
2	2	0	1.9171	47.381	0.142	865	863.2	1.9
0	0	4	1.9165	47.397	0.142	459.1	457.7	1.5
2	2	0	1.9171	47.502	0.142	417.4	429.3	-11.9
0	0	4	1.9165	47.518	0.142	220.4	227.6	-7.2
0	2	3	1.8698	48.658	0.143	57.1	58.7	-1.6
0	2	3	1.8698	48.783	0.143	28.4	29.2	-0.8
2	2	1	1.8599	48.934	0.144	50.2	50.4	-0.2
2	2	1	1.8599	49.06	0.144	26.9	25.1	1.8
1	2	3	1.7655	51.738	0.146	48.2	45.2	3
1	2	3	1.7655	51.872	0.146	23.9	22.5	1.4
2	1	3	1.7526	52.145	0.146	41.7	40.6	1.2
2	1	3	1.7526	52.28	0.146	21.3	20.2	1.2
3	0	1	1.7403	52.543	0.147	40.5	38.7	1.8
3	0	1	1.7403	52.678	0.147	19.9	19.3	0.6
1	3	0	1.7308	52.854	0.147	100.5	98.5	2
1	3	0	1.7308	52.99	0.147	53	49	4
2	2	2	1.7146	53.392	0.147	83.1	81.6	1.5
1	1	4	1.7143	53.403	0.147	63.6	62.7	0.9
2	2	2	1.7146	53.53	0.148	39.3	40.6	-1.3

$x = 0$

h	*k*	*l*	*D(A)*	*2T*	*HW*	*Iobs*	*Icalc*	*io-ic*
1	1	4	1.7143	53.541	0.148	30.3	31.2	-0.9
3	1	0	1.6991	53.918	0.148	10	10.8	-0.8
3	1	0	1.6991	54.058	0.148	5.7	5.4	0.4
1	3	1	1.6883	54.292	0.148	111.3	118	-6.7
1	3	1	1.6883	54.433	0.148	57.7	58.7	-1
3	1	1	1.6589	55.337	0.149	37.1	29	8.1
3	1	1	1.6589	55.482	0.149	21.4	14.4	7
1	3	2	1.5774	58.461	0.152	183.7	172.8	10.9
1	3	2	1.5774	58.615	0.152	87.7	86	1.8
0	2	4	1.5711	58.722	0.152	176.7	174.5	2.3
0	2	4	1.5711	58.877	0.152	88.6	86.8	1.9
2	0	4	1.559	59.22	0.153	144.3	134.4	9.9
2	0	4	1.559	59.377	0.153	69.3	66.9	2.4
3	1	2	1.5533	59.458	0.153	400	402.6	-2.6
3	1	2	1.5533	59.616	0.153	187.8	200.3	-12.5
2	1	4	1.4996	61.816	0.155	10.4	8.1	2.4
3	2	0	1.4973	61.923	0.155	24.8	21.7	3.1
3	2	0	1.4973	62.089	0.156	14.5	10.8	3.7
2	3	1	1.4821	62.627	0.156	15.6	12.4	3.2
2	3	1	1.4821	62.794	0.156	6.7	6.2	0.5
1	0	5	1.4741	63.007	0.157	30.8	32.1	-1.3
1	0	5	1.4741	63.176	0.157	14.5	16	-1.5
1	3	3	1.433	65.032	0.159	34.6	30.3	4.3
1	3	3	1.433	65.207	0.159	15.6	15.1	0.6
3	1	3	1.4149	65.971	0.16	15.5	16.6	-1.1
3	1	3	1.4149	66.15	0.16	7.5	8.3	-0.7
2	3	2	1.4054	66.472	0.16	17.1	19.7	-2.5
2	3	2	1.4054	66.652	0.16	8	9.8	-1.8
0	4	0	1.3715	68.337	0.162	75.7	76.2	-0.5
0	4	0	1.3715	68.524	0.163	36.8	37.9	-1.1
2	2	4	1.3554	69.266	0.163	280	269.7	10.3
2	2	4	1.3554	69.457	0.164	129.2	134.2	-5
0	4	1	1.3501	69.577	0.164	10.5	11.3	-0.7
0	4	1	1.3501	69.768	0.164	5.6	5.6	0
4	0	0	1.3402	70.165	0.164	46	45.3	0.7
0	2	5	1.3383	70.278	0.165	5.3	5.2	0.1
4	0	0	1.3402	70.358	0.165	22.3	22.5	-0.3
1	4	0	1.3288	70.861	0.165	43.6	42.8	0.8
1	4	0	1.3288	71.057	0.166	22	21.3	0.7
4	1	0	1.3019	72.549	0.167	26.1	24.6	1.5
2	3	3	1.3004	72.648	0.167	38.6	38.9	-0.3
4	1	0	1.3019	72.751	0.168	11.6	12.3	-0.7
1	2	5	1.2985	72.773	0.168	62.5	66.7	-4.2
2	3	3	1.3004	72.851	0.168	17.9	19.4	-1.4
1	2	5	1.2985	72.976	0.168	31.7	33.2	-1.5
2	1	5	1.2934	73.108	0.168	27.8	29.1	-1.3
3	2	3	1.2919	73.207	0.168	35.4	37.7	-2.3
0	4	2	1.2914	73.239	0.168	7.7	8.3	-0.6
2	1	5	1.2934	73.312	0.168	13.2	14.5	-1.3
3	2	3	1.2919	73.412	0.168	17.4	18.8	-1.4
1	3	4	1.2845	73.694	0.169	45.1	44.7	0.4
4	1	1	1.2836	73.758	0.169	12.6	12.9	-0.3
1	3	4	1.2845	73.901	0.169	22.1	22.3	-0.2
4	1	1	1.2836	73.965	0.169	6.4	6.4	0

x = 0

h	*k*	*l*	*D(A)*	*2T*	*HW*	*Iobs*	*Icalc*	*io-ic*
3	1	4	1.2714	74.583	0.17	5.2	4	1.2
4	0	2	1.2651	75.016	0.17	21.3	21.3	0
4	0	2	1.2651	75.228	0.171	9.7	10.6	-0.9
1	4	2	1.2555	75.695	0.171	14.6	15.2	-0.6
1	4	2	1.2555	75.909	0.172	7.2	7.6	-0.4
4	1	2	1.2328	77.343	0.174	29.6	28.9	0.8
4	1	2	1.2328	77.563	0.174	13.4	14.4	-0.9
2	4	0	1.221	78.23	0.175	22.9	23.5	-0.6
2	4	0	1.221	78.454	0.175	12.4	11.7	0.7
3	3	2	1.2125	78.887	0.176	36.4	35.3	1.1
1	1	6	1.2121	78.912	0.176	58.7	57.5	1.2
3	3	2	1.2125	79.114	0.176	16.2	17.6	-1.4
1	1	6	1.2121	79.138	0.176	26.4	28.6	-2.2
4	2	0	1.2042	79.537	0.177	14.1	14.1	0
4	2	0	1.2042	79.766	0.177	7.2	7	0.2
2	2	5	1.1974	80.079	0.177	20.9	23.2	-2.3
2	2	5	1.1974	80.311	0.178	10.2	11.6	-1.4
4	2	1	1.1896	80.711	0.178	5.6	5.9	-0.3
3	2	4	1.1799	81.514	0.179	5.2	5.4	-0.2
1	4	3	1.1789	81.598	0.18	9.2	9.7	-0.5
3	0	5	1.1636	82.904	0.182	19.2	19.6	-0.3
3	0	5	1.1636	83.147	0.182	9.1	9.8	-0.7
4	1	3	1.1601	83.215	0.182	19.8	20.9	-1.1
4	1	3	1.1601	83.459	0.182	10.4	10.4	-0.1
1	3	5	1.1477	84.317	0.184	25.8	27.6	-1.8
1	3	5	1.1477	84.567	0.184	13.7	13.8	0
3	3	3	1.1431	84.734	0.184	24.7	24.6	0.1
3	3	3	1.1431	84.986	0.185	12.5	12.3	0.2
3	1	5	1.1383	85.175	0.185	24.9	28.6	-3.7
3	1	5	1.1383	85.429	0.185	10.9	14.3	-3.3
0	4	4	1.1154	87.36	0.189	46.2	47.6	-1.3
0	4	4	1.1154	87.623	0.189	23.3	23.7	-0.4
2	4	3	1.1017	88.726	0.191	31.7	32.9	-1.2
2	4	3	1.1017	88.995	0.191	16.2	16.4	-0.2
4	0	4	1.0983	89.07	0.191	28.1	28.3	-0.1
4	0	4	1.0983	89.341	0.192	14	14.1	-0.1
1	4	4	1.092	89.727	0.193	8.4	8.3	0.1
4	2	3	1.0893	90.008	0.193	9	10.5	-1.5
4	3	0	1.081	90.89	0.195	5.7	6.3	-0.6
1	5	0	1.075	91.547	0.196	8.3	8.2	0.1
1	0	7	1.073	91.763	0.196	15	15.5	-0.4
1	0	7	1.073	92.047	0.197	7.1	7.7	-0.6
4	3	1	1.0704	92.048	0.197	10.4	11.4	-0.9
4	3	1	1.0704	92.333	0.197	5.5	5.7	-0.2
1	5	1	1.0645	92.705	0.198	23.5	23.1	0.4
1	5	1	1.0645	92.994	0.199	11.1	11.6	-0.5
1	1	7	1.053	94.025	0.201	7.4	6.1	1.3
3	4	2	1.0467	94.776	0.202	21	20.7	0.3
3	4	2	1.0467	95.076	0.203	10.5	10.3	0.2
1	5	2	1.035	96.187	0.205	8.8	7.1	1.7
2	4	4	1.0298	96.841	0.206	40.3	36.6	3.7
1	3	6	1.0279	97.071	0.207	23.2	21.3	1.9
2	4	4	1.0298	97.152	0.207	19.2	18.3	0.9
1	3	6	1.0279	97.383	0.207	11.5	10.6	0.9

$x = 0$

h	*k*	*l*	*D(A)*	*2T*	*HW*	*Iobs*	*Icalc*	*io-ic*
0	4	5	1.0222	97.798	0.208	17.8	15.9	1.9
3	1	6	1.0212	97.933	0.208	59.7	54.2	5.4
0	4	5	1.0222	98.114	0.209	8.2	8	0.2
4	2	4	1.0196	98.134	0.209	25.2	24.6	0.5
3	1	6	1.0212	98.25	0.209	27.8	27.1	0.6
4	2	4	1.0196	98.452	0.21	13.1	12.3	0.8
5	1	2	1.0147	98.773	0.21	67.7	66.9	0.8
5	1	2	1.0147	99.094	0.211	32	33.5	-1.5
1	5	3	0.9909	102.048	0.218	18.9	19.1	-0.2
1	5	3	0.9909	102.389	0.218	8.7	9.6	-0.9
5	1	3	0.973	104.684	0.224	13.3	13.7	-0.4
5	1	3	0.973	105.041	0.225	6.2	6.9	-0.7
4	4	0	0.9586	106.95	0.23	16.6	12.4	4.2
0	0	8	0.9583	107	0.23	10.8	8.3	2.5
4	4	0	0.9586	107.322	0.231	7.2	6.2	1
4	4	1	0.9512	108.163	0.233	14	13.1	0.8
4	4	1	0.9512	108.544	0.234	7.4	6.6	0.8
1	5	4	0.9375	110.493	0.24	18.9	17.9	1
1	5	4	0.9375	110.89	0.241	9.2	9	0.1
3	5	0	0.935	110.937	0.241	22.7	22.4	0.3
3	5	0	0.935	111.338	0.242	11.7	11.3	0.4
4	4	2	0.9299	111.858	0.244	21.7	20	1.7
1	1	8	0.9297	111.906	0.244	13.3	12.3	1
3	5	1	0.9282	112.181	0.245	6.3	5.9	0.4
4	4	2	0.9299	112.266	0.245	10.7	10	0.6
1	1	8	0.9297	112.314	0.245	6.7	6.2	0.5
5	3	0	0.9249	112.779	0.247	8.1	7.7	0.3
0	6	0	0.9144	114.798	0.253	8.4	7.6	0.8
3	5	2	0.9084	115.984	0.257	56.6	53.1	3.5
3	5	2	0.9084	116.425	0.259	28.2	26.7	1.5
0	2	8	0.9046	116.749	0.26	58.2	56.1	2.2
3	3	6	0.9036	116.965	0.261	42.4	40.9	1.5
0	2	8	0.9046	117.197	0.262	28.6	28.2	0.4
2	0	8	0.9023	117.228	0.262	49.3	48.9	0.4
3	3	6	0.9036	117.415	0.262	20.4	20.6	-0.3
2	0	8	0.9023	117.681	0.263	25.2	24.6	0.6
5	3	2	0.8991	117.901	0.264	101.5	97.7	3.8
5	3	2	0.8991	118.36	0.266	47.9	49.2	-1.3
6	0	0	0.8935	119.113	0.269	7.4	6.5	0.9
0	6	2	0.8894	120.013	0.272	8.5	7	1.4
3	4	5	0.8873	120.485	0.274	6.9	5.7	1.2
2	3	7	0.8867	120.63	0.275	12.8	11	1.8
2	3	7	0.8867	121.115	0.277	6	5.6	0.5
3	2	7	0.8839	121.253	0.277	12.4	11.7	0.7
4	3	5	0.8835	121.357	0.278	23.5	22.1	1.3
2	4	6	0.8827	121.532	0.278	6.6	6.4	0.3
6	1	0	0.8819	121.733	0.279	6.4	6.5	-0.2
3	2	7	0.8839	121.744	0.279	5.7	5.9	-0.2
4	3	5	0.8835	121.849	0.28	11.1	11.2	0
1	5	5	0.8802	122.129	0.281	13.3	12.6	0.6
1	5	5	0.8802	122.629	0.283	6.9	6.4	0.5
1	6	2	0.8774	122.785	0.284	19.9	19	0.9
4	2	6	0.8763	123.049	0.285	12.3	11.8	0.4
1	6	2	0.8774	123.291	0.286	10.1	9.6	0.4

x = 0

h	*k*	*l*	*D(A)*	*2T*	*HW*	*Iobs*	*Icalc*	*io-ic*
4	2	6	0.8763	123.558	0.287	6.5	6	0.5
6	0	2	0.8702	124.563	0.292	10.2	9.2	1
5	1	5	0.8676	125.21	0.295	13.7	13.6	0.1
5	1	5	0.8676	125.744	0.297	7.4	6.9	0.5
2	6	0	0.8654	125.774	0.297	7.3	6.7	0.6
0	6	3	0.8609	126.953	0.303	9	7.8	1.2
2	6	1	0.8599	127.213	0.305	8.2	7.3	0.9
6	1	2	0.8594	127.354	0.305	14.8	13.2	1.6
6	1	2	0.8594	127.913	0.308	8.1	6.7	1.4
4	4	4	0.8573	127.925	0.308	23	19	4
2	2	8	0.8571	127.97	0.309	27.5	22.6	4.9
4	4	4	0.8573	128.491	0.311	11.2	9.6	1.5
2	2	8	0.8571	128.537	0.312	13.4	11.5	2
6	2	0	0.8496	130.11	0.32	7.4	6.1	1.2
2	5	5	0.8466	130.973	0.325	11.7	12.8	-1.1
2	5	5	0.8466	131.58	0.329	6.8	6.5	0.4
2	6	2	0.8442	131.71	0.33	12.3	11.3	1
2	6	2	0.8442	132.328	0.333	6.4	5.7	0.6
3	5	4	0.8404	132.877	0.337	26.2	22.2	4
1	3	8	0.8383	133.512	0.341	12.5	10.7	1.8
3	5	4	0.8404	133.513	0.341	13.2	11.3	1.9
4	1	7	0.8381	133.597	0.342	11.6	10	1.6
1	3	8	0.8383	134.157	0.345	6.5	5.4	1.1
4	1	7	0.8381	134.243	0.346	6.1	5.1	1
3	3	7	0.8316	135.722	0.356	12.2	12.7	-0.5
3	3	7	0.8316	136.403	0.361	6	6.5	-0.5
6	2	2	0.8294	136.471	0.362	12.1	12.9	-0.8
6	2	2	0.8294	137.165	0.367	5.2	6.5	-1.3
0	6	4	0.8253	137.945	0.373	12.5	14.3	-1.9
0	6	4	0.8253	138.667	0.379	6.6	7.3	-0.7
1	5	6	0.8226	138.934	0.381	14.4	14.9	-0.6
1	5	6	0.8226	139.675	0.388	6.8	7.6	-0.8
2	4	7	0.8153	141.766	0.407	20.8	22.3	-1.5
3	6	0	0.814	142.284	0.412	13.3	13.9	-0.6
2	4	7	0.8153	142.568	0.415	11.2	11.4	-0.1
4	4	5	0.8128	142.784	0.417	22.6	22.5	0.1
5	1	6	0.8123	143.006	0.419	83.7	81.9	1.8
3	6	0	0.814	143.098	0.42	7.2	7	0.2
4	4	5	0.8128	143.611	0.426	11.4	11.4	0
5	1	6	0.8123	143.838	0.428	42.3	41	1.3
4	2	7	0.8102	143.888	0.429	7.2	6.8	0.3
6	0	4	0.8098	144.06	0.431	13	12.1	0.9
6	0	4	0.8098	144.918	0.44	5.3	4.6	0.6

$x =$ 0.10

Composition Na0.9K0.1MgF3

Space Group ***Pbnm***

Cell Dimensions

a	5.4092	(0)	ap (mean)	3.8563	
b	5.4973	(0)	ap (volume)	3.8562	Na
c	7.7135	(0)	*Z*	4	K
a'	3.8249				Mg
b'	3.8872				F(1)
c'	3.8568				F(2)

Crystallographic Parameters

Wyck	*x*		*y*		*z*		*B*		*N*
4*c*	0.9922	(4)	0.0331	(3)	0.25		2.05	(4)	0.4500
4*c*	0.9922	(4)	0.0331	(3)	0.25		2.05	(4)	0.0500
4*b*	0		0.5		0		1.01	(3)	0.5
4*c*	0.0803	(5)	0.4786	(5)	0.25		1.68	(7)	0.5
8*d*	0.7085	(3)	0.2916	(3)	0.0411	(2)	1.37	(5)	1

Polyhedral Data

V	V/Z (Vap)	*VA* Ivton	*VD*	*VA* calc	*VB*	*f*
229.367	57.342	38.659	8.336	46.995	10.347	4.54

Interatomic Distances

Na		Mg	
1st C.S.		F1	1.9801
F1	3.0851	F1	1.9801
F1	2.4949	F2	1.9746
F1	3.1112	F2	1.9854
F1	2.3318	F2	1.9746
F2	2.6401	F2	1.9854
F2	2.3531	mean	1.9800
F2	2.7090		
F2	2.7090		
F2	2.6401		
F2	2.3531		
m1	2.6428		
F2	3.2937		
F2	3.2937		
m2	3.2937		
m3	2.7512		

Bond Angles

B-X1-B	153.7
B-X2-B	153.7

Octahedral Tilts

Method 1 (Cell Param)

ϕ	7.38
θ	10.27
Φ	12.62

Method 2 (*B* - *X* - *B*)

ϕ	9.32
ϕz	9.32
θ	13.15
Φ	16.07

Method 3 (*X*, *Y*, *Z*)

ϕ	9.44
θ	13.14
Φ	16.13

Agreement Parameters

Rp:	16.5
Rwp:	20.0
Rexp:	15.3
Chi2:	1.7
R-Bragg	**6.1**
DW-Stat.:	1.3

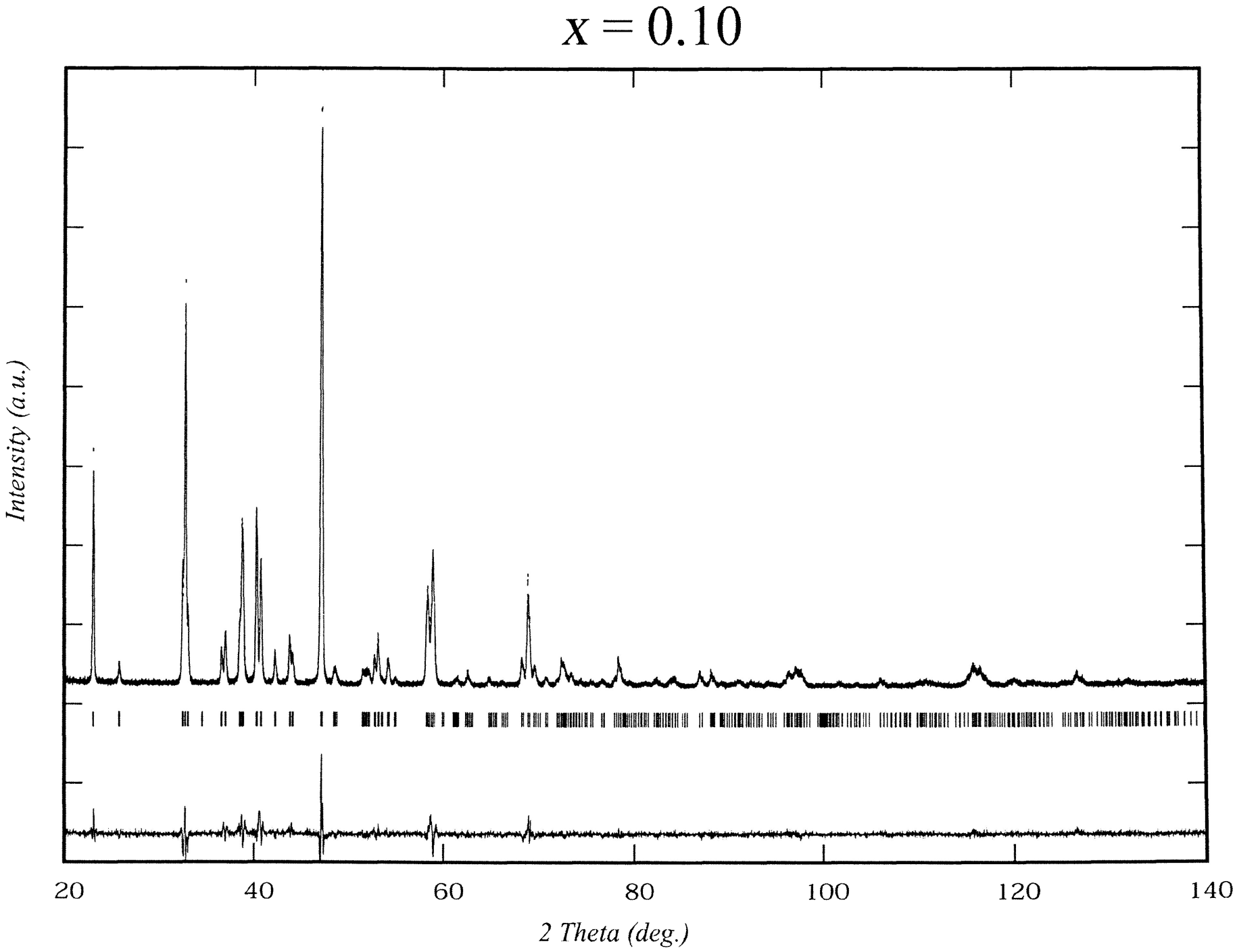
x = 0.10
Intensity (a.u.)
20
40
60
80
100
120
140
2 Theta (deg.)

Phase $x = 0.10$

h	*k*	*l*	*D(A)*	*2T*	*HW*	*Iobs*	*Icalc*	*io-ic*
1	0	1	4.4287	20.082	0.153	1.6	0.5	1.1
0	0	2	3.8566	23.043	0.156	56.3	53.5	2.8
1	1	0	3.8556	23.049	0.156	116.9	110.8	6.1
0	0	2	3.8566	23.099	0.156	28	26.6	1.4
1	1	0	3.8556	23.105	0.156	58	55.1	2.8
1	1	1	3.4487	25.813	0.158	18.1	17.2	0.9
1	1	1	3.4487	25.876	0.159	9.6	8.6	1.1
0	2	0	2.7485	32.551	0.166	92.6	101.3	-8.7
0	2	0	2.7485	32.632	0.166	45.3	50.4	-5.1
1	1	2	2.7267	32.82	0.166	344.2	344.5	-0.3
1	1	2	2.7267	32.901	0.166	166	171.4	-5.3
2	0	0	2.7046	33.095	0.166	55.4	63.5	-8.1
2	0	0	2.7046	33.177	0.166	28.6	31.6	-2.9
1	2	0	2.4503	36.645	0.171	33.1	31.6	1.5
1	2	0	2.4503	36.736	0.171	18.6	15.7	2.9
2	1	0	2.4268	37.014	0.171	54.7	50.8	3.9
2	1	0	2.4268	37.106	0.171	30.2	25.3	4.9
1	2	1	2.3353	38.519	0.173	62.9	55.5	7.3
1	2	1	2.3353	38.615	0.173	30.5	27.6	2.8
1	0	3	2.3221	38.747	0.174	134.4	123.4	11
1	0	3	2.3221	38.844	0.174	63.4	61.4	2.1
2	1	1	2.3149	38.872	0.174	83.8	81.1	2.7
2	1	1	2.3149	38.969	0.174	46.9	40.3	6.6
0	2	2	2.2383	40.26	0.176	186.1	181.2	4.9
0	2	2	2.2383	40.361	0.176	98.4	90.1	8.2
2	0	2	2.2143	40.714	0.176	147.1	128.8	18.3
2	0	2	2.2143	40.816	0.177	71.1	64	7.1
1	1	3	2.1391	42.214	0.179	34.9	31.8	3.1
1	1	3	2.1391	42.32	0.179	18.1	15.8	2.2
1	2	2	2.0682	43.734	0.181	58.9	50.7	8.3
1	2	2	2.0682	43.844	0.181	30.1	25.2	4.9
2	1	2	2.054	44.052	0.181	33.5	28.4	5.1
2	1	2	2.054	44.164	0.182	16.4	14.1	2.2
0	0	4	1.9283	47.091	0.186	224.5	224.2	0.2
2	2	0	1.9278	47.104	0.186	429.9	426.2	3.7
0	0	4	1.9283	47.211	0.187	111.9	111.5	0.3
2	2	0	1.9278	47.224	0.187	210.9	212	-1.1
0	2	3	1.8776	48.442	0.189	16.9	17	-0.1
0	2	3	1.8776	48.565	0.189	8	8.4	-0.4
2	2	1	1.8703	48.645	0.189	12.8	13.5	-0.7
2	2	1	1.8703	48.769	0.189	7.9	6.7	1.2
1	2	3	1.7738	51.477	0.194	16.3	16.7	-0.3
1	2	3	1.7738	51.61	0.194	7.4	8.3	-0.8
2	1	3	1.7648	51.759	0.195	13.8	15.9	-2
2	1	3	1.7648	51.893	0.195	7.4	7.9	-0.5
3	0	1	1.7557	52.046	0.195	15.4	17.1	-1.7
3	0	1	1.7557	52.181	0.195	8.5	8.5	0
1	3	0	1.7355	52.7	0.196	33.3	30.4	2.9
1	3	0	1.7355	52.836	0.197	14.5	15.1	-0.6
1	1	4	1.7246	53.058	0.197	23.9	22.5	1.4
2	2	2	1.7244	53.067	0.197	30.3	28.5	1.8
1	1	4	1.7246	53.195	0.197	11.5	11.2	0.3
2	2	2	1.7244	53.204	0.197	14.5	14.2	0.3
1	3	1	1.6932	54.124	0.199	34.4	33.8	0.5
1	3	1	1.6932	54.264	0.199	17.2	16.8	0.4
3	1	1	1.6725	54.848	0.2	8.2	8.6	-0.4
1	3	2	1.5826	58.251	0.207	82.5	82.6	-0.1
1		2	1.5826	58.405	0.208	43.5	41.1	2.5
0	2	4	1.5785	58.416	0.208	73	68.5	4.5
0	2	4	1.5785	58.57	0.208	40.1	34.1	6.1

$x = 0.10$

h	*k*	*l*	*D(A)*	*2T*	*HW*	*Iobs*	*Icalc*	*io-ic*
2	0	4	1.5701	58.761	0.208	60.4	53.5	7
2	0	4	1.5701	58.916	0.209	26	26.6	-0.6
3	1	2	1.5657	58.942	0.209	156	160.3	-4.3
3	1	2	1.5657	59.097	0.209	85.1	79.7	5.3
3	2	0	1.5076	61.453	0.214	6.6	7.3	-0.7
1	0	5	1.4835	62.564	0.217	12	13.1	-1.1
1	0	5	1.4835	62.731	0.217	5.6	6.5	-1
1	3	3	1.4384	64.757	0.222	11.2	8.4	2.8
1	3	3	1.4384	64.931	0.222	5.5	4.2	1.3
2	3	2	1.4117	66.139	0.225	6	7.1	-1.1
0	4	0	1.3743	68.183	0.23	39.4	42.4	-3
0	4	0	1.3743	68.37	0.23	19	21.1	-2.1
2	2	4	1.3633	68.807	0.232	156.3	146.9	9.4
2	2	4	1.3633	68.995	0.232	75.2	73.1	2.1
4	0	0	1.3523	69.448	0.233	24.2	26.5	-2.4
4	0	0	1.3523	69.638	0.234	12.4	13.2	-0.8
1	4	0	1.3319	70.666	0.236	14.3	14.1	0.1
1	4	0	1.3319	70.861	0.237	6.9	7	-0.1
4	1	0	1.3132	71.833	0.24	8.9	8.9	0
2	3	3	1.3065	72.255	0.241	12.7	12.2	0.5
1	2	5	1.3055	72.322	0.241	27.2	26.5	0.6
2	3	3	1.3065	72.456	0.241	5.9	6.1	-0.2
1	2	5	1.3055	72.523	0.241	12.6	13.2	-0.6
2	1	5	1.3019	72.554	0.241	8.7	9.2	-0.5
3	2	3	1.3005	72.641	0.242	15.7	16.6	-0.9
3	2	3	1.3005	72.844	0.242	8.3	8.3	0
4	1	1	1.2945	73.032	0.243	6.5	6.5	0.1
1	3	4	1.29	73.332	0.244	16.5	15.2	1.3
1	3	4	1.29	73.537	0.244	8.5	7.6	0.9
4	0	2	1.2761	74.26	0.246	7.3	8.2	-0.9
1	4	2	1.259	75.446	0.25	7.9	7.7	0.2
4	1	2	1.2431	76.585	0.253	11.9	12	-0.2
4	1	2	1.2431	76.802	0.254	6.1	6	0.1
2	4	0	1.2252	77.913	0.257	11.8	12.8	-1
2	4	0	1.2252	78.135	0.258	5.9	6.4	-0.5
1	1	6	1.2195	78.342	0.258	25.9	26.1	-0.2
3	3	2	1.2193	78.362	0.258	18.9	19.1	-0.2
1	1	6	1.2195	78.567	0.259	12.6	13	-0.4
3	3	2	1.2193	78.586	0.259	9.2	9.5	-0.3
4	2	0	1.2134	78.815	0.26	6.9	7.4	-0.5
2	2	5	1.2045	79.514	0.262	6.8	7.3	-0.4
1	4	3	1.1827	81.283	0.267	5.2	4.4	0.8
3	0	5	1.1722	82.167	0.27	8.7	8.8	-0.1
4	1	3	1.1694	82.399	0.271	7.4	8	-0.7
1	3	5	1.153	83.84	0.276	9.9	8.3	1.6
3	3	3	1.1496	84.146	0.277	8.9	8.6	0.3
3	1	5	1.1464	84.433	0.278	9.4	9.3	0.1
0	4	4	1.1191	86.992	0.287	29.6	27.5	2.1
0	4	4	1.1191	87.253	0.288	13.8	13.7	0.1
4	0	4	1.1072	88.172	0.291	17	17.3	-0.3
2	4	3	1.106	88.288	0.292	9.9	10.3	-0.4
4	0	4	1.1072	88.438	0.292	8.5	8.6	-0.2
2	4	3	1.106	88.555	0.293	5.3	5.1	0.2
1	0	7	1.0797	91.03	0.302	7.1	7.1	-0.1
1	5	1	1.067	92.426	0.308	8.6	7.5	1.1
3	4	2	1.0516	94.197	0.315	8.2	7.2	0.9
1	5	2	1.0377	95.864	0.322	6.8	5.7	1.2
2	4	4	1.0341	96.301	0.324	20.4	18.8	1.6
1	3	6	1.033	96.438	0.325	13.2	12.4	0.8
2	4	4	1.0341	96.609	0.326	10.2	9.4	0.8
1	3	6	1.033	96.746	0.326	6.9	6.2	0.7
3	1	6	1.0283	97.031	0.328	25.7	23.9	1.8

$x = 0.10$

h	*k*	*l*	*D(A)*	*2T*	*HW*	*Iobs*	*Icalc*	*io-ic*
4	2	4	1.027	97.191	0.328	12.8	12.5	0.4
0	4	5	1.0261	97.299	0.329	5.6	5.6	0
3	1	6	1.0283	97.343	0.329	11.8	12	-0.2
4	2	4	1.027	97.504	0.33	5.9	6.2	-0.3
5	1	2	1.0234	97.644	0.33	27	28.7	-1.7
5	1	2	1.0234	97.959	0.332	15.1	14.4	0.8
1	5	3	0.9937	101.648	0.35	7.8	6.6	1.2
5	1	3	0.9812	103.46	0.359	5.5	4.4	1.1
0	0	8	0.9641	106.059	0.373	6.9	5.2	1.8
4	4	0	0.9639	106.099	0.374	11.5	8.7	2.8
4	4	0	0.9639	106.466	0.376	5.3	4.3	0.9
1	5	4	0.9405	109.97	0.397	6.4	4.9	1.5
3	5	0	0.9387	110.294	0.399	7.3	6.5	0.8
4	4	2	0.9351	110.922	0.403	7.1	6.1	1
3	5	2	0.912	115.254	0.432	23.2	24.7	-1.5
3	5	2	0.912	115.69	0.435	13.4	12.4	0.9
0	2	8	0.9098	115.704	0.435	22.2	20.6	1.6
3	3	6	0.9089	115.886	0.437	16.6	15.3	1.3
2	0	8	0.9082	116.032	0.438	19.5	18.2	1.2
0	2	8	0.9098	116.143	0.439	10.8	10.4	0.4
3	3	6	0.9089	116.327	0.44	7.8	7.7	0.1
2	0	8	0.9082	116.474	0.441	9.2	9.2	0
5	3	2	0.9055	116.565	0.442	40.9	40.8	0.1
5	3	2	0.9055	117.011	0.445	22	20.6	1.4
3	2	7	0.8896	119.97	0.469	6.7	5.9	0.8
4	3	5	0.8891	120.071	0.47	8.7	7.6	1.2
1	6	2	0.8795	122.287	0.489	7.2	7	0.2
2	6	0	0.8677	125.173	0.517	6.8	6.4	0.5
6	1	2	0.8669	125.392	0.519	5.2	5.1	0.1
2	2	8	0.8623	126.581	0.531	18.4	14.7	3.8
4	4	4	0.8622	126.617	0.532	16.4	13.2	3.3
2	2	8	0.8623	127.131	0.537	8.5	7.4	1
4	4	4	0.8622	127.167	0.537	7.6	6.7	0.9
3	5	4	0.844	131.759	0.591	8.6	7.6	1
0	6	4	0.8275	137.137	0.669	9.3	8.5	0.9
1	5	6	0.8257	137.773	0.679	7.9	7.8	0.1
2	4	7	0.8193	140.176	0.722	9.6	8.9	0.7
5	1	6	0.8185	140.474	0.727	32.6	29.9	2.6
4	4	5	0.8174	140.894	0.735	8.1	7.4	0.7
3	6	0	0.8168	141.155	0.74	5.2	4.8	0.4
6	0	4	0.8167	141.193	0.741	5.9	5.4	0.5
5	1	6	0.8185	141.248	0.742	16.6	15.2	1.4
4	5	3	0.8097	144.123	0.803	7.9	6.8	1.2
1	2	9	0.809	144.428	0.81	5.1	4.3	0.8

x = 0.2

Composition Na0.82K0.18MgF3

Space Group ***Pbnm***

Cell Dimensions

a	5.4473	(5)	ap (mean)	3.8765	
b	5.5102	(5)	ap (volume)	3.8765	Na
c	7.7628	(5)	*Z*	4	K
a'	3.8518				Mg
b'	3.8962998				F(1)
c'	3.8814				F(2)

Crystallographic Parameters

Wyck	*x*		*y*		*z*		*B*	
4*c*	0.9929	(8)	0.0242	(7)	0.25		2.0	(1)
4*c*	0.9929	(8)	0.0242	(7)	0.25		2.0	(1)
4*b*	0.0000		0.5		0		0.8	(1)
4*c*	0.0781	(11)	0.4850	(10)	0.25		0.7	(1)
8*d*	0.7090	(6)	0.2877	(6)	0.0289	(6)	1.4	(2)

Polyhedral Data

V	V/Z (Vap)	*VA* Ivton	*VA* calc	*VB*	*f*
233.006	58.251	49.543	47.940	10.311	4.65

Interatomic Distances

Na		Mg	
1st C.S.		F1	1.9869
F1	3.0120	F1	1.9869
F1	2.5740	F2	1.9794
F1	3.0972	F2	1.9696
F1	2.3703	F2	1.9794
F2	2.7322	F2	1.9696
F2	2.4079	mean	1.9786
F2	3.2128		
F2	2.6748		
F2	3.2128		
F2	2.6748		
F2	2.7322		
F2	2.4079		
m	2.7591		

Bond Angles

B-X1-B	155.3
B-X2-B	157.6

Octahedral Tilts

Method 1 (Cell Par

ϕ	7.08
θ	8.67
Φ	11.17

Method 2 (*B* - *X* -

ϕ	8.75
ϕz	7.02
θ	12.35
Φ	15.10

Method 3 (*X*, *Y*, *Z*

ϕ	8.93
θ	12.59
Φ	15.40

Agreement Parameters

Rp:	14.0
Rwp:	17.9
Rexp:	12.1
Chi2:	2.2
R-Bragg	**5.0**
DW-Stat.:	0.9

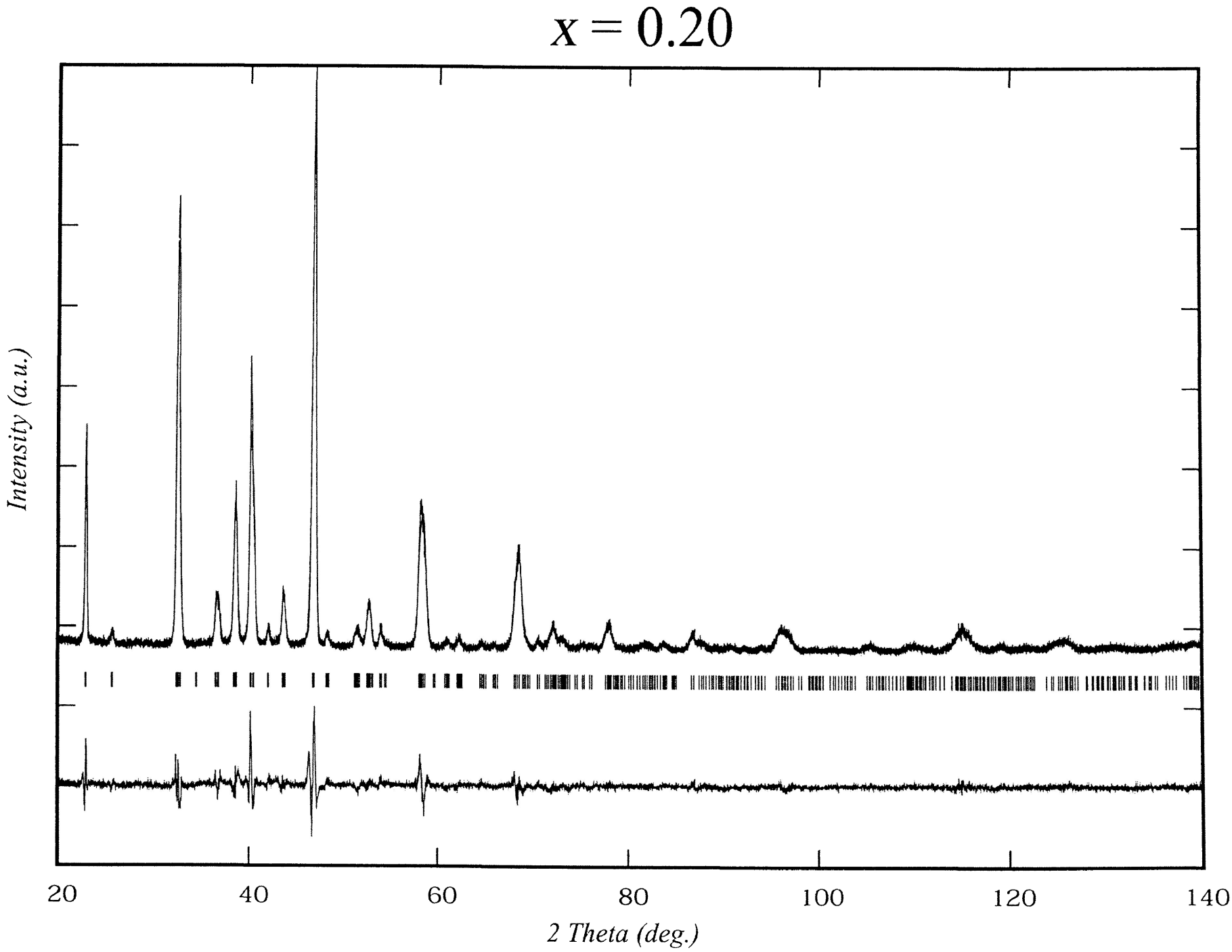
x = 0.20
Intensity (a.u.)
20
40
60
80
100
120
140
2 Theta (deg.)

Phase $x = 0.20$

h	*k*	*l*	*D(A)*	*2T*	*HW*	*Iobs*	*Icalc*	*io-ic*
0	0	2	3.8801	22.902	0.234	56.1	52.3	3.8
1	1	0	3.8745	22.935	0.234	90.6	83.7	6.9
0	0	2	3.8801	22.957	0.234	28.4	26	2.4
1	1	0	3.8745	22.991	0.234	46	41.6	4.4
1	1	1	3.4665	25.678	0.246	8.8	10.1	-1.2
1	1	1	3.4665	25.741	0.247	5.1	5	0.1
0	2	0	2.7551	32.472	0.284	99.8	98.9	0.9
0	2	0	2.7551	32.552	0.285	49	49.2	-0.1
1	1	2	2.7417	32.635	0.285	307.4	311.7	-4.3
1	1	2	2.7417	32.716	0.286	150.3	155.1	-4.7
2	0	0	2.7246	32.846	0.287	58.5	63.8	-5.2
2	0	0	2.7246	32.927	0.287	28.6	31.7	-3.1
1	2	0	2.4587	36.516	0.311	28.1	23.6	4.5
1	2	0	2.4587	36.607	0.312	13.5	11.8	1.8
2	1	0	2.4423	36.77	0.313	47.3	43.9	3.4
2	1	0	2.4423	36.861	0.314	25.1	21.8	3.2
1	2	1	2.3438	38.373	0.325	36.1	35.5	0.6
1	2	1	2.3438	38.469	0.325	17.9	17.6	0.3
1	0	3	2.3368	38.494	0.325	69.1	67.7	1.3
1	0	3	2.3368	38.59	0.326	35.6	33.7	1.9
2	1	1	2.3296	38.617	0.326	74.8	69.8	5
2	1	1	2.3296	38.713	0.327	40.5	34.7	5.8
0	2	2	2.2464	40.108	0.337	216.1	198	18.1
0	2	2	2.2464	40.209	0.338	108.3	98.5	9.8
2	0	2	2.2297	40.42	0.34	135.5	135.1	0.4
2	0	2	2.2297	40.522	0.341	66.7	67.2	-0.5
1	1	3	2.1513	41.962	0.352	19.6	16	3.6
1	1	3	2.1513	42.068	0.353	11.3	8	3.3
1	2	2	2.0768	43.543	0.364	45.4	41.3	4.1
1	2	2	2.0768	43.653	0.365	22.3	20.5	1.7
2	1	2	2.0669	43.762	0.366	32	29.3	2.7
2	1	2	2.0669	43.872	0.367	16.6	14.6	2
0	0	4	1.94	46.788	0.391	258.3	246.1	12.2
2	2	0	1.9373	46.86	0.392	417.4	399.6	17.8
0	0	4	1.94	46.907	0.392	127.9	122.4	5.5
2	2	0	1.9373	46.979	0.393	205.8	198.8	7.1
0	2	3	1.8858	48.218	0.404	6.3	6	0.3
2	2	1	1.8796	48.388	0.405	6.4	5	1.4
2	1	3	1.7758	51.414	0.432	16.1	18	-1.9
2	1	3	1.7758	51.547	0.434	7.7	8.9	-1.2
3	0	1	1.7686	51.641	0.434	12.4	14	-1.7
3	0	1	1.7686	51.774	0.436	6.6	7	-0.4
1	3	0	1.7405	52.536	0.443	23	22.9	0.1

x = 0.20

h	*k*	*l*	*D(A)*	*2T*	*HW*	*Iobs*	*Icalc*	*io-ic*
1	3	0	1.7405	52.672	0.444	11.6	11.4	0.2
1	1	4	1.7347	52.725	0.445	20.2	19.6	0.6
2	2	2	1.7332	52.774	0.445	23.9	22.9	1
1	1	4	1.7347	52.861	0.446	10.3	9.7	0.6
2	2	2	1.7332	52.91	0.446	12.2	11.4	0.8
1	3	1	1.6983	53.946	0.456	22.3	18.9	3.4
1	3	1	1.6983	54.086	0.457	11.8	9.4	2.4
3	1	1	1.684	54.443	0.461	5.4	3.9	1.5
1	3	2	1.588	58.033	0.496	86	78.1	7.9
0	2	4	1.5862	58.106	0.497	56.3	51.3	5
1	3	2	1.588	58.186	0.498	42.2	38.9	3.3
0	2	4	1.5862	58.259	0.498	27.2	25.5	1.6
2	0	4	1.5803	58.343	0.499	39.1	37.9	1.3
2	0	4	1.5803	58.497	0.501	18.6	18.8	-0.2
3	1	2	1.5763	58.507	0.501	142.3	144.3	-2.1
3	1	2	1.5763	58.662	0.502	71.6	71.8	-0.2
2	1	4	1.5191	60.939	0.526	6	7.7	-1.7
2	3	1	1.4945	62.053	0.538	6.9	7.7	-0.7
1	0	5	1.4927	62.136	0.539	5.8	6	-0.2
1	3	3	1.444	64.475	0.564	7.4	5.1	2.3
2	3	2	1.4177	65.825	0.579	7.3	7.6	-0.3
0	4	0	1.3775	67.999	0.604	50.4	46.5	3.8
0	4	0	1.3775	68.185	0.606	23.9	23.2	0.7
2	2	4	1.3708	68.378	0.608	167.5	168.4	-0.9
2	2	4	1.3708	68.565	0.611	81.6	83.8	-2.2
4	0	0	1.3623	68.867	0.614	22.7	24.2	-1.5
4	0	0	1.3623	69.056	0.616	11.4	12	-0.7
1	4	0	1.3355	70.449	0.633	11.6	10.7	0.9
1	4	0	1.3355	70.643	0.635	5.8	5.3	0.5
4	1	0	1.3225	71.25	0.643	6.5	7.6	-1.1
1	2	5	1.3124	71.879	0.65	15.7	18.1	-2.4
2	3	3	1.3124	71.881	0.65	8.8	10.1	-1.3
2	1	5	1.3099	72.038	0.652	7.8	8.7	-0.9
1	2	5	1.3124	72.079	0.653	8.2	9	-0.8
3	2	3	1.3082	72.146	0.653	11.9	13	-1.1
3	2	3	1.3082	72.346	0.656	6	6.5	-0.5
4	1	1	1.3037	72.438	0.657	7.4	8	-0.6
1	3	4	1.2955	72.965	0.664	14.3	14.4	0
1	3	4	1.2955	73.169	0.666	7.1	7.2	0
4	0	2	1.2854	73.638	0.672	6.6	7.6	-1.1
1	4	2	1.2628	75.177	0.692	9.1	6.9	2.2
4	1	2	1.2518	75.959	0.702	11.5	12.5	-0.9
4	1	2	1.2518	76.174	0.705	6.2	6.2	0
2	4	0	1.2293	77.599	0.724	15.7	14.6	1.1

x = 0.20

h	*k*	*l*	*D(A)*	*2T*	*HW*	*Iobs*	*Icalc*	*io-ic*
2	4	0	1.2293	77.599	0.724	15.7	14.6	1.1
1	1	6	1.2268	77.789	0.726	22.8	21.3	1.4
2	4	0	1.2293	77.82	0.726	7.8	7.3	0.5
3	3	2	1.2254	77.895	0.727	21.4	20	1.4
1	1	6	1.2268	78.011	0.729	11.4	10.6	0.8
3	3	2	1.2254	78.118	0.73	10.8	10	0.8
4	2	0	1.2212	78.218	0.732	8.2	7.6	0.6
3	0	5	1.1799	81.51	0.778	7.7	7.1	0.6
4	1	3	1.1775	81.716	0.78	8.4	7.8	0.6
1	3	5	1.1584	83.362	0.804	5.8	5.1	0.7
3	3	3	1.1555	83.618	0.808	5.5	4.5	1
3	1	5	1.1538	83.768	0.81	6.7	5.2	1.5
0	4	4	1.1232	86.6	0.853	37.2	35.2	2
0	4	4	1.1232	86.859	0.857	18.2	17.6	0.6
4	0	4	1.1149	87.408	0.866	18.2	18.3	-0.1
4	0	4	1.1149	87.671	0.87	9.4	9.1	0.3
1	0	7	1.0863	90.32	0.913	5.2	6.4	-1.1
1	5	1	1.0698	92.111	0.943	5.4	5.2	0.2
3	4	2	1.0561	93.664	0.97	6.6	6.3	0.3
1	5	2	1.0406	95.506	1.004	7.2	6.6	0.7
2	4	4	1.0384	95.771	1.009	20.4	19.1	1.3
1	3	6	1.0381	95.807	1.009	13.8	13	0.8
2	4	4	1.0384	96.076	1.014	9.8	9.5	0.3
1	3	6	1.0381	96.112	1.015	6.6	6.5	0.1
3	1	6	1.0348	96.213	1.017	24.8	24.5	0.2
4	2	4	1.0335	96.38	1.02	10.4	10.5	-0.1
3	1	6	1.0348	96.52	1.023	12.1	12.3	-0.1
4	2	4	1.0335	96.688	1.026	5.2	5.2	0
5	1	2	1.0307	96.724	1.026	30.1	30.1	0
5	1	2	1.0307	97.034	1.032	15.7	15.1	0.6
1	5	3	0.9967	101.215	1.115	6.1	4.8	1.4
0	0	8	0.97	105.142	1.2	12.8	10.2	2.6
4	4	0	0.9686	105.358	1.205	11.7	9.5	2.2
0	0	8	0.97	105.503	1.208	6.2	5.1	1.1
4	4	0	0.9686	105.72	1.213	5.7	4.7	1
3	5	0	0.9422	109.686	1.309	5.6	4.5	1.2
1	1	8	0.941	109.893	1.314	5.5	4.4	1.1
4	4	2	0.9398	110.101	1.319	6.5	5.2	1.3
0	6	0	0.9184	114.023	1.425	5.1	5.1	0.1
3	5	2	0.9156	114.562	1.44	27.9	27	0.9
0	2	8	0.915	114.681	1.443	14.9	14.3	0.6
3	3	6	0.9139	114.892	1.45	12.6	11.9	0.7
2	0	8	0.9138	114.903	1.45	12.2	11.5	0.7
3	5	2	0.9156	114.992	1.452	14.4	13.6	0.8
0	2	8	0.915	115.112	1.456	7.7	7.2	0.5

x = 0.20

h	*k*	*l*	*D(A)*	*2T*	*HW*	*Iobs*	*Icalc*	*io-ic*
3	3	6	0.9139	115.325	1.462	6.4	6	0.5
2	0	8	0.9138	115.336	1.463	6.3	5.8	0.4
5	3	2	0.911	115.453	1.466	46.6	43.1	3.5
5	3	2	0.911	115.89	1.479	23.6	21.7	1.9
3	2	7	0.895	118.794	1.569	6.9	6.7	0.1
4	3	5	0.8943	118.941	1.574	7	6.7	0.3
1	6	2	0.8819	121.729	1.669	8.7	6.8	1.9
6	1	2	0.8731	123.829	1.746	5.7	4.7	1.1
2	6	0	0.8702	124.539	1.773	12.1	10.2	1.9
2	6	0	0.8702	125.065	1.794	6	5.1	0.9
2	2	8	0.8674	125.27	1.802	32.1	27.2	4.8
4	4	4	0.8666	125.461	1.81	18.3	15.5	2.8
2	2	8	0.8674	125.804	1.824	16.5	13.8	2.7
4	4	4	0.8666	125.998	1.832	9.4	7.8	1.6
3	5	4	0.8475	130.705	2.041	7.1	7.1	0
1	3	8	0.8473	130.765	2.044	5.8	5.8	0
6	2	2	0.842	132.374	2.125	6	6.4	-0.4
0	6	4	0.8301	136.254	2.343	12.9	11.4	1.5
1	5	6	0.8291	136.599	2.364	7.3	6.5	0.8
0	6	4	0.8301	136.945	2.386	6.4	5.8	0.6
5	1	6	0.824	138.391	2.48	30.2	28.7	1.5
2	4	7	0.8233	138.666	2.498	5.2	4.8	0.3
5	1	6	0.824	139.121	2.529	16	14.6	1.4
1	2	9	0.8137	142.424	2.778	7.8	7.6	0.2
4	5	3	0.8133	142.559	2.789	6.3	6.1	0.2

x = 0.3

Composition Na0.7K0.3MgF3

Space Group ***Pbnm***

Cell Dimensions

a	5.5001	(0)	ap (mean)	3.9001
b	5.5230	(0)	ap (volume)	3.9001
c	7.8116	(0)	*Z*	4
a'	3.8892			
b'	3.9053			
c'	3.9058			

Crystallographic Parameters

	Wyck	*x*		*y*		*z*		*B*		*N*
Na	4*c*	0.9951	(1)	0.009	(1)	0.25	(0)	2.0	(1)	0.35
K	4*c*	0.9951	(1)	0.009	(1)	0.25	(0)	2.0	(1)	0.15
Mg	4*b*	0	(0)	0.5	(0)	0	(0)	0.8	(1)	0.5
F(1)	4*c*	0.0464	(2)	0.492	(2)	0.25	(0)	2.6	(1)	0.5
F(2)	8*d*	0.7172	(1)	0.281	(1)	0.015	(1)	2.0	(1)	1

Polyhedral Data

V	V/Z (Vap)	*VA* Ivton	*VA* calc	*VB*	*f*
237.293	59.323	50.909	49.069	10.254	4.8

Interatomic Distances

Na		Mg	
1st C.S.		F1	1.9752
F1	2.8725	F1	1.9752
F1	2.6952	F2	1.9821
F1	2.9918	F2	1.9668
F1	2.5329	F2	1.9821
F2	2.8318	F2	1.9668
F2	2.5214	mean	1.9747
F2	3.0649		
F2	2.6778		
F2	3.0649		
F2	2.6778		
F2	2.8318		
F2	2.5214		
m	2.7737		

Bond Angles

B-X1-B	164.9
B-X2-B	164.0

Octahedral Tilts

Method 1 (Cell Param)

ϕ	5.30
θ	5.21
Φ	7.43

Method 2 (*B* - *X* - *B*)

ϕ	5.34
ϕz	5.96
θ	7.55
Φ	9.24

Method 3 (*X*, *Y*, *Z*)

ϕ	7.22
θ	7.55
Φ	10.43

Agreement Parameters

Rp:	22.2
Rwp:	26.9
Rexp:	19.3
Chi2:	1.946
R-Bragg	**10.5**
DW-Stat.:	1.2101

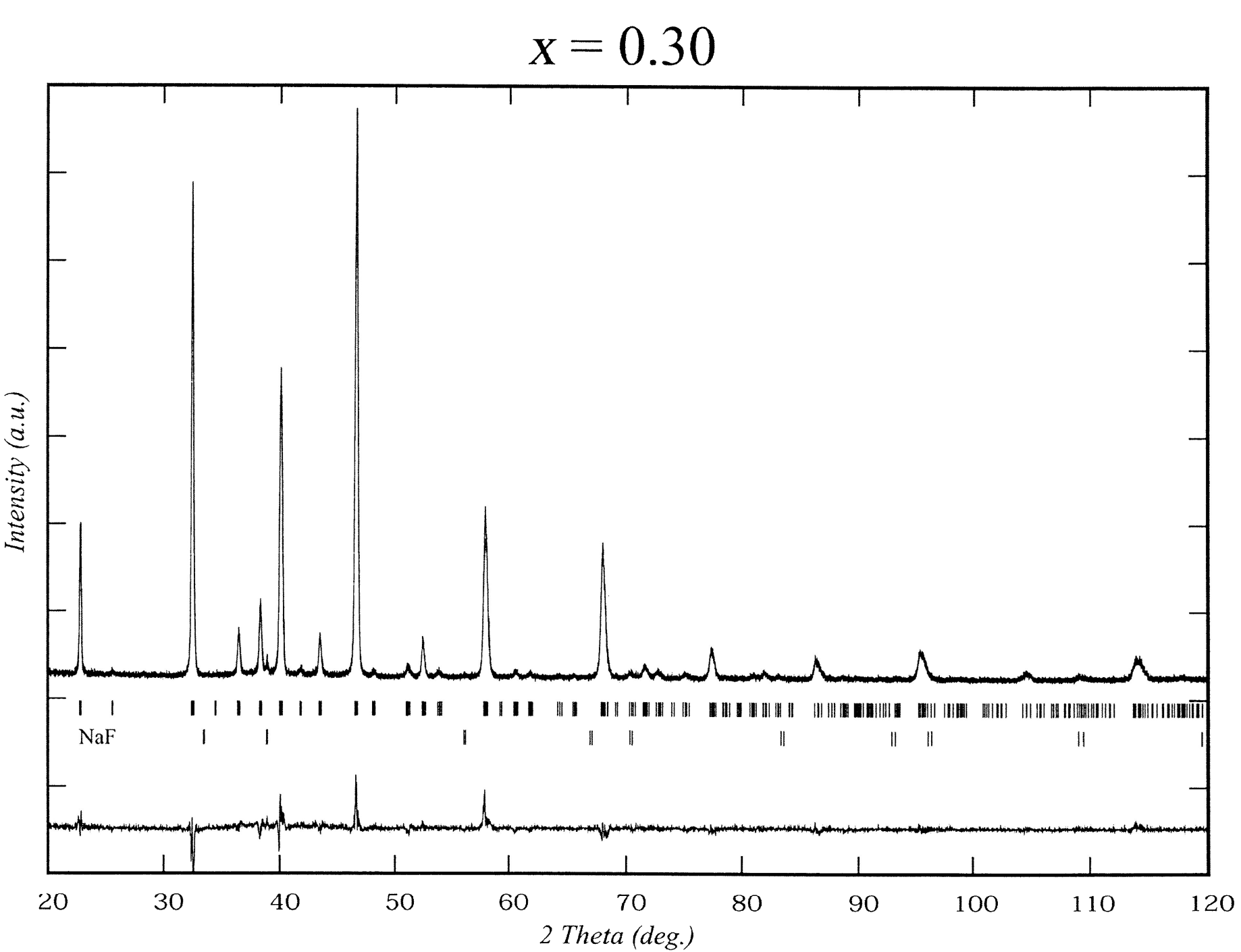
x = 0.30
Intensity (a.u.)
NaF
20
30
40
50
60
70
80
90
100
110
120
2 Theta (deg.)

Phase $x = 0.30$

h	*k*	*l*	*D(A)*	*2T*	*HW*	*Iobs*	*Icalc*	*io-ic*
0	0	2	3.9031	22.765	0.152	48.2	43.8	4.4
1	1	0	3.8942	22.817	0.152	77.1	69.3	7.8
0	0	2	3.9031	22.82	0.152	24.3	21.8	2.5
1	1	0	3.8942	22.873	0.152	39.2	34.5	4.8
0	2	0	2.7601	32.411	0.153	86.1	89.5	-3.4
1	1	2	2.7568	32.451	0.153	278.6	290.8	-12.2
0	2	0	2.7601	32.491	0.153	41.8	44.5	-2.7
1	1	2	2.7568	32.531	0.153	131.3	144.7	-13.4
2	0	0	2.7472	32.568	0.153	61.2	69.7	-8.5
2	0	0	2.7472	32.648	0.153	30.2	34.7	-4.5
1	2	0	2.4664	36.398	0.158	26.7	22.9	3.8
1	2	0	2.4664	36.488	0.158	13.4	11.4	2
2	1	0	2.4595	36.504	0.158	28.2	23.6	4.6
2	1	0	2.4595	36.595	0.159	17.2	11.7	5.5
1	2	1	2.3518	38.239	0.162	16.9	16	0.9
1	0	3	2.3517	38.241	0.162	34.8	33	1.8
1	2	1	2.3518	38.334	0.162	8.2	7.9	0.3
1	0	3	2.3517	38.336	0.162	17	16.4	0.6
2	1	1	2.3458	38.341	0.162	32.4	31.1	1.2
2	1	1	2.3458	38.436	0.162	17.5	15.5	2
0	2	2	2.2536	39.975	0.166	191	188.4	2.7
0	2	2	2.2536	40.075	0.166	97.8	93.7	4.1
2	0	2	2.2465	40.106	0.166	169.7	162.9	6.8
2	0	2	2.2465	40.206	0.166	87.5	81	6.5
1	1	3	2.1635	41.714	0.17	10.5	5.1	5.4
1	1	3	2.1635	41.819	0.17	6.5	2.5	3.9
1	2	2	2.085	43.363	0.175	32.1	27.6	4.6
2	1	2	2.0808	43.455	0.175	24.5	22	2.5
1	2	2	2.085	43.472	0.175	15.2	13.7	1.5
2	1	2	2.0808	43.565	0.175	13.9	10.9	2.9
0	0	4	1.9516	46.496	0.185	239.6	229.1	10.5
2	2	0	1.9471	46.608	0.185	426.8	403.7	23.1
0	0	4	1.9516	46.614	0.185	120.4	114	6.5
2	2	0	1.9471	46.727	0.185	211.7	200.8	10.9
2	1	3	1.7874	51.057	0.202	6.2	8	-1.8
3	0	1	1.783	51.191	0.202	6.6	8.2	-1.6
1	3	0	1.7448	52.396	0.207	14.9	14.9	0
1	1	4	1.7447	52.399	0.207	14.2	14.2	0
2	2	2	1.7423	52.477	0.208	14.8	14.9	-0.1
1	3	0	1.7448	52.532	0.208	7.2	7.4	-0.2
1	1	4	1.7447	52.535	0.208	6.8	7.1	-0.2
3	1	0	1.7383	52.609	0.208	5.8	6.2	-0.5
2	2	2	1.7423	52.612	0.208	6.8	7.4	-0.6

$x = 0.30$

h	*k*	*l*	*D(A)*	*2T*	*HW*	*Iobs*	*Icalc*	*io-ic*
1	3	1	1.7028	53.792	0.213	6.7	5.6	1.1
0	2	4	1.5935	57.816	0.232	46.1	39	7.1
1	3	2	1.5929	57.839	0.232	86	72.3	13.6
2	0	4	1.591	57.916	0.233	38.8	32.8	6.1
0	2	4	1.5935	57.968	0.233	22.6	19.4	3.2
1	3	2	1.5929	57.991	0.233	41.5	36	5.6
3	1	2	1.5879	58.038	0.233	114.2	100.3	13.8
2	0	4	1.591	58.068	0.234	18.5	16.3	2.2
3	1	2	1.5879	58.191	0.234	58.2	49.9	8.3
0	4	0	1.3801	67.858	0.288	42.6	44.9	-2.3
2	2	4	1.3784	67.952	0.289	172.5	181.2	-8.6
0	4	0	1.3801	68.043	0.289	21.2	22.4	-1.2
2	2	4	1.3784	68.137	0.29	83.3	90.2	-6.8
4	0	0	1.3736	68.221	0.29	31.3	35	-3.7
4	0	0	1.3736	68.408	0.292	15.1	17.4	-2.3
1	4	0	1.3385	70.27	0.303	8.9	7	1.9
4	1	0	1.3329	70.605	0.306	5.8	5.7	0
1	2	5	1.3192	71.455	0.311	9.7	9.7	0
3	2	3	1.3164	71.63	0.312	7.3	7.6	-0.3
4	1	1	1.3139	71.784	0.313	5.5	5.7	-0.1
1	3	4	1.3008	72.626	0.319	9.5	9.6	-0.1
1	4	2	1.2661	74.948	0.335	7.9	8.3	-0.4
4	1	2	1.2614	75.275	0.337	7.3	8.6	-1.3
1	1	6	1.234	77.252	0.352	22.5	22.5	0
2	4	0	1.2332	77.311	0.352	15.6	15.4	0.2
3	3	2	1.2317	77.42	0.353	17.3	16.8	0.5
1	1	6	1.234	77.472	0.353	11.5	11.2	0.3
2	4	0	1.2332	77.531	0.354	7.9	7.7	0.2
4	2	0	1.2297	77.57	0.354	10.7	10.5	0.2
3	3	2	1.2317	77.64	0.355	8.5	8.4	0.1
4	2	0	1.2297	77.791	0.356	5.4	5.2	0.2

x = 0.4

Composition Na0.6K0.4MgF3

Space Group ***P4/mbm***

Cell Dimensions

a	5.5444	(3)	ap (mean)	3.9209	
b	5.5444	(3)	ap (volume)	3.9209	
c	3.9217	(3)	*Z*	2	
a'	3.9205				
c'	3.9217				

Crystallographic Parameters

	Wyck	*x*		*y*		*z*	*B*		*N*
Na	2*c*	0		0.5		0	1.8	(1)	0.075
K	2*c*	0		0.5		0	1.8	(1)	0.050
Mg	2*a*	0		0		0	0.8	(1)	0.13
F(1)	2*b*	0		0		1	2.4	(1)	0.13
F(2)	4*g*	0.268	(6)	0.768	(6)	0	2.8	(4)	0.25

Polyhedral Data

V	V/Z (Vap)	*VA* Ivtcn	*VA* calc	*VB*	*f*
120.551	60.276	50.913	50.176	10.100	4.97

Interatomic Distances

Na		Mg	
1st C.S.		F1	1.9608
F1	2.7722	F1	1.9608
F1	2.7722	F2	1.9655
F1	2.7722	F2	1.9655
F1	2.7722	F2	1.9655
F2	2.6729	F2	1.9655
F2	2.6729	mean	1.9639
F2	2.6729		
F2	2.6729		
F2	2.8761		
F2	2.8761		
F2	2.8761		
F2	2.8761		
m	2.7737		

Bond Angles

B-X1-B	180
B-X2-B	171.6

Octahedral Tilts

Method 1 (Cell Param)

ϕ 0
θ 0
Φ 0

Method 2 (*B* - *X* - *B*)

ϕ 0
ϕz 4.20
θ 0
Φ 0

Method 3 (*X*, *Y*, *Z*)

ϕ 4.19
θ 0
F 0

Agreement Parameters

Rp:	23
Rwp:	26.6
Rexp:	16.7
Chi2:	2.53
R-Bragg	**11.6**
DW-Stat.:	1.01

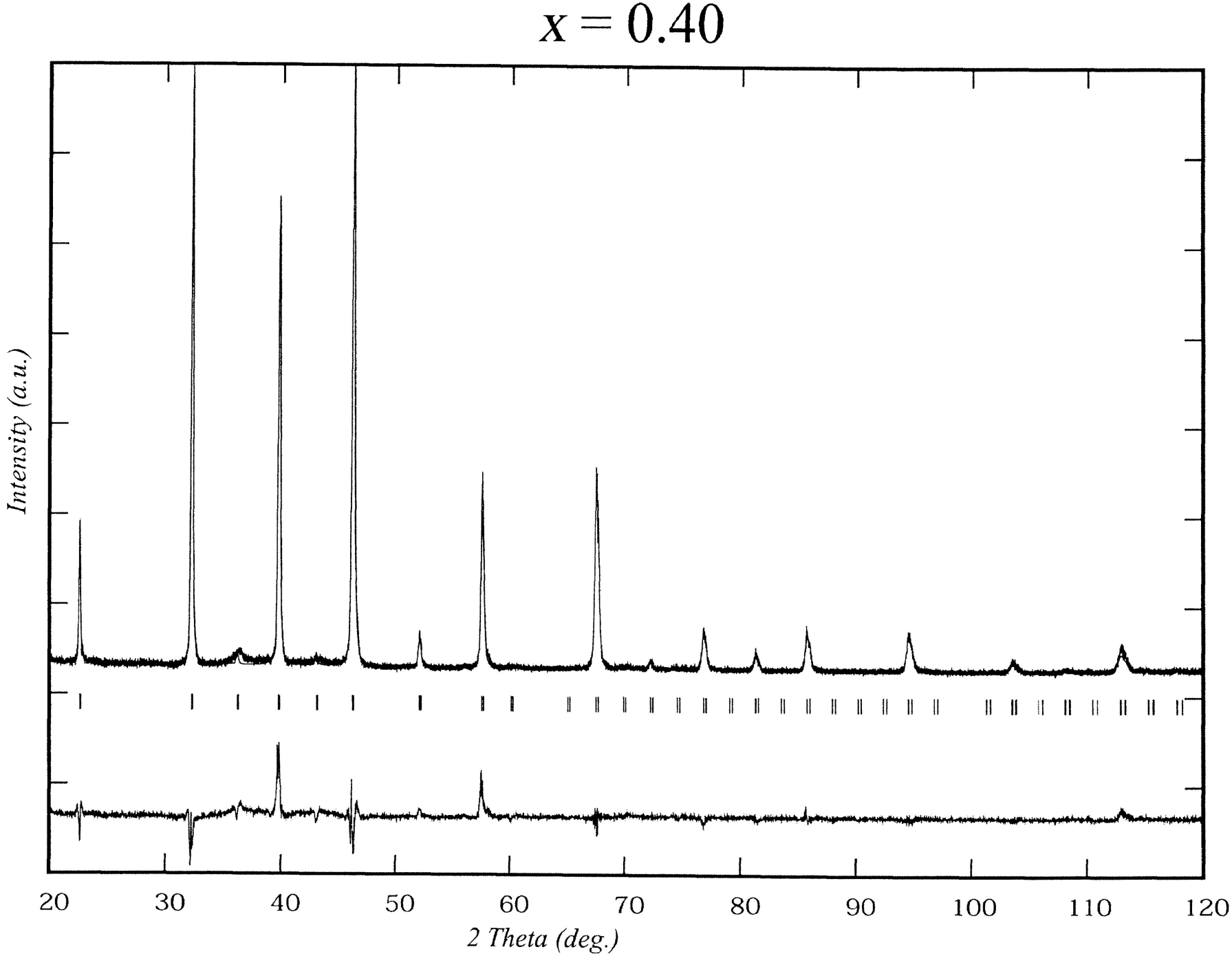
x = 0.40
Intensity (a.u.)
20
30
40
50
60
70
80
90
100
110
120
2 Theta (deg.)

Phase $x = 0.40$

h	*k*	*l*	*D(A)*	*2T*	*HW*	*Iobs*	*Icalc*	*io-ic*
0	0	1	3.9232	22.646	0.21	31.9	29.4	2.5
1	1	0	3.9215	22.656	0.21	56.9	53.1	3.8
0	0	1	3.9232	22.701	0.21	15.5	14.6	0.9
1	1	0	3.9215	22.712	0.21	28.4	26.4	2
1	1	1	2.7735	32.25	0.212	248.1	276.9	-28.8
2	0	0	2.7729	32.257	0.212	131.7	146.8	-15.2
1	1	1	2.7735	32.329	0.212	122.4	137.7	-15.3
2	0	0	2.7729	32.337	0.212	64.7	73	-8.4
2	1	0	2.4802	36.189	0.215	33.5	10.2	23.3
2	1	0	2.4802	36.278	0.215	20.7	5.1	15.6
2	0	1	2.2644	39.775	0.218	416.7	345	71.7
2	0	1	2.2644	39.875	0.218	209.7	171.6	38.1
2	1	1	2.0964	43.115	0.222	21.9	10.7	11.2
2	1	1	2.0964	43.224	0.222	12.1	5.3	6.8
0	0	2	1.9616	46.243	0.226	190.4	193.3	-2.8
2	2	0	1.9608	46.265	0.226	367.1	373.1	-6
0	0	2	1.9616	46.361	0.226	93.3	96.1	-2.8
2	2	0	1.9608	46.382	0.226	179.7	185.6	-5.9
1	1	2	1.7544	52.09	0.236	8.9	8.2	0.7
2	2	1	1.7539	52.104	0.236	8.5	7.7	0.7
3	1	0	1.7538	52.109	0.236	11.5	10.4	1
3	1	0	1.7538	52.244	0.236	6	5.2	0.8
2	0	2	1.6014	57.503	0.247	67.8	54.9	12.9
3	1	1	1.6011	57.517	0.247	144.1	116.9	27.2
2	0	2	1.6014	57.654	0.248	33.8	27.3	6.5
3	1	1	1.6011	57.668	0.248	72.1	58.2	13.9
2	2	2	1.3868	67.485	0.274	165.7	169	-3.3
4	0	0	1.3865	67.502	0.274	80.3	81.8	-1.5
2	2	2	1.3868	67.669	0.275	84.1	84.1	0
4	0	0	1.3865	67.686	0.275	40.9	40.7	0.2
4	1	0	1.3451	69.875	0.282	5.9	2.4	3.5
3	1	2	1.3074	72.196	0.29	10.1	6.2	3.9
4	1	1	1.2724	74.516	0.298	5.7	3.5	2.1
1	1	3	1.2406	76.766	0.307	21.3	22.1	-0.8
3	3	1	1.2401	76.798	0.307	18.7	19.5	-0.8
4	2	0	1.2401	76.802	0.307	23.6	24.6	-1
1	1	3	1.2406	76.984	0.308	10.8	11	-0.2
3	3	1	1.2401	77.017	0.308	9.6	9.7	-0.1
4	2	0	1.2401	77.021	0.308	12.1	12.2	-0.1
2	0	3	1.1828	81.271	0.326	11.5	11.4	0.1
4	2	1	1.1824	81.303	0.326	19.3	19.5	-0.2
2	0	3	1.1828	81.508	0.327	5.2	5.7	-0.5
4	2	1	1.1824	81.539	0.327	8.8	9.7	-0.9

$x = 0.40$

h	*k*	*l*	*D(A)*	*2T*	*HW*	*Iobs*	*Icalc*	*io-ic*
4	0	2	1.1322	85.742	0.347	70.2	64.7	5.5
4	0	2	1.1322	85.998	0.348	34.1	32.3	1.8
3	1	3	1.0484	94.574	0.396	27.6	27.4	0.2
4	2	2	1.0482	94.594	0.396	28.2	27.9	0.2
5	1	1	1.0481	94.605	0.396	25	24.8	0.2
3	1	3	1.0484	94.873	0.398	14	13.7	0.3
4	2	2	1.0482	94.892	0.398	14.3	14	0.4
5	1	1	1.0481	94.904	0.398	12.8	12.4	0.4
0	0	4	0.9808	103.51	0.458	8.9	10	-1.1
4	4	0	0.9804	103.574	0.459	16.2	18.1	-1.9
4	4	0	0.9804	103.924	0.461	8.5	9.1	-0.6
2	0	4	0.9247	112.827	0.541	13.9	10.1	3.8
3	3	3	0.9245	112.857	0.541	13.4	9.6	3.8
5	3	1	0.9243	112.89	0.541	34.8	24.7	10.1
6	0	0	0.9243	112.895	0.541	8.4	6	2.4
2	0	4	0.9247	113.243	0.545	7.7	5.1	2.6
3	3	3	0.9245	113.272	0.545	7.4	4.8	2.6
5	3	1	0.9243	113.306	0.545	19.2	12.4	6.8
4	2	3	0.8998	117.749	0.594	7.9	4.5	3.4
2	2	4	0.8772	122.839	0.659	29.6	31.3	-1.7
4	4	2	0.877	122.895	0.66	27.8	29.2	-1.4
6	2	0	0.8769	122.914	0.66	27.1	28.4	-1.3
2	2	4	0.8772	123.347	0.666	15.2	15.6	-0.3
4	4	2	0.877	123.403	0.667	14.2	14.5	-0.3
6	2	0	0.8769	123.422	0.667	13.8	14.1	-0.3

x = 0.5

Composition Na0.5K0.5MgF3

Space Group ***Pm-3m***

Cell Dimensions

a	3.9403	(1)			
a'	3.9403	(1)	ap (volume)	3.9403	
			Z	1	

Crystallographic Parameters

	Wyck	*x*	*y*	*z*	*B*		N
Na	1b	1	0.5	1	2.10	(3)	0.01042
K	1b	1	0.5	1	2.10	(3)	0.01042
Mg	1a	0	0	0	0.90	(2)	0.02083
F(1)	3d	0	0	1	1.6	(4)	0.02083

Polyhedral Data

V	*VA* Ivton	*VA* calc	*VB*	*f*
61.177	50.981	50.981	10.1900	5.00

Interatomic Distances

Na		Mg	
F1	2.7862	F1	1.9702
F1	2.7862	F1	1.9702
F1	2.7862	F1	1.9702
F1	2.7862	F1	1.9702
F1	2.7862	F1	1.9702
F1	2.7862	F1	1.9702
F1	2.7862	mean	1.9702
F1	2.7862		
F1	2.7862		
F1	2.7862		
F1	2.7862		
F1	2.7862		
m	2.7862		

Bond Angles

B-X1-B 180

B-X2-B 180

Agreement Parameters

Rp:	22.5
Rwp:	24.6
Rexp:	17.9
Chi2:	1.883
R-Bragg	**9.51**
DW-Stat.:	1.2892

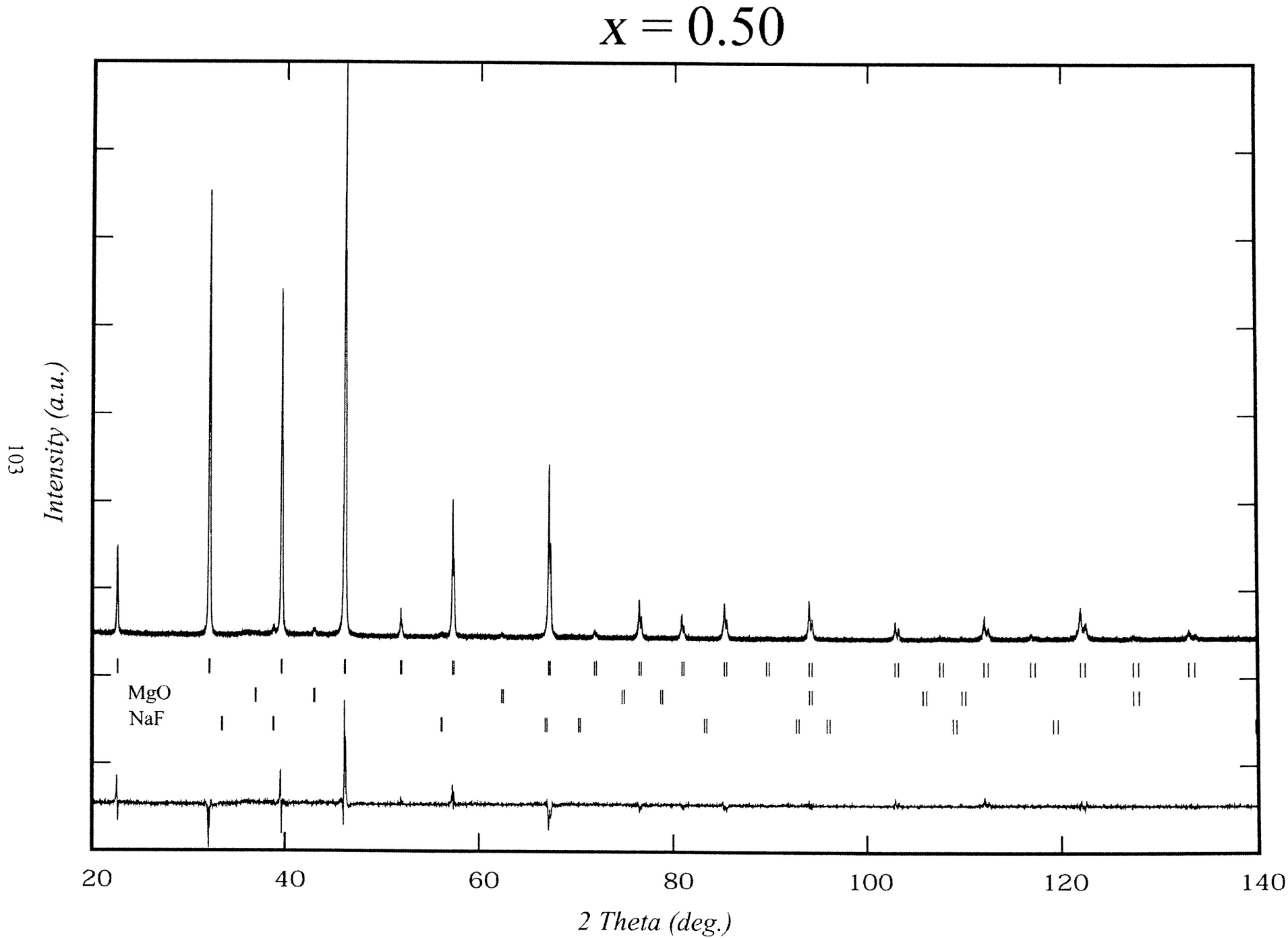
x = 0.50
Intensity (a.u.)
MgO
NaF
20
40
60
80
100
120
140
2 Theta (deg.)

Phase $x = 0.50$

h	*k*	*l*	*D(A)*	*2T*	*HW*	*Iobs*	*Icalc*	*io-ic*
1	0	0	3.9403	22.547	0.117	88.2	69	19.2
1	0	0	3.9403	22.602	0.117	37	34.3	2.7
1	1	0	2.7862	32.099	0.121	399.6	442.2	-42.5
1	1	0	2.7862	32.178	0.121	203.3	220	-16.7
1	1	1	2.2749	39.583	0.125	394.1	376.5	17.6
1	1	1	2.2749	39.683	0.125	187.4	187.2	0.2
2	0	0	1.9702	46.032	0.129	639.2	586.3	52.9
2	0	0	1.9702	46.148	0.129	337.5	291.6	45.8
2	1	0	1.7622	51.842	0.133	24.5	24.2	0.3
2	1	0	1.7622	51.976	0.133	12.5	12	0.5
2	1	1	1.6086	57.221	0.138	176.4	158.9	17.4
2	1	1	1.6086	57.372	0.138	86.3	79.1	7.3
2	2	0	1.3931	67.137	0.148	239.4	261.4	-22
2	2	0	1.3931	67.32	0.148	113.5	130.1	-16.6
2	2	1	1.3134	71.815	0.153	11.2	7.8	3.4
2	2	1	1.3134	72.014	0.153	5.6	3.9	1.7
3	1	0	1.246	76.37	0.159	57.8	61.3	-3.6
3	1	0	1.246	76.586	0.159	27.3	30.5	-3.2
3	1	1	1.188	80.838	0.165	41.3	39.4	1.9
3	1	1	1.188	81.073	0.165	18.3	19.6	-1.3
2	2	2	1.1375	85.251	0.172	64.4	67.3	-2.9
2	2	2	1.1375	85.505	0.172	28.9	33.6	-4.7
3	2	1	1.0531	94.019	0.188	74.1	68.8	5.4
3	2	1	1.0531	94.314	0.189	34.7	34.4	0.3
4	0	0	0.9851	102.882	0.208	34.4	28.8	5.6
4	0	0	0.9851	103.228	0.209	17	14.4	2.6
3	3	0	0.9287	112.075	0.235	18.4	13.2	5.3
4	1	1	0.9287	112.075	0.235	36.9	26.3	10.6
3	3	0	0.9287	112.485	0.236	9.5	6.6	2.8
4	1	1	0.9287	112.485	0.236	18.9	13.2	5.7
3	3	1	0.904	116.888	0.252	14.3	9.9	4.4
3	3	1	0.904	117.338	0.253	7.1	5	2.2
4	2	0	0.8811	121.917	0.272	102.1	92	10.1
4	2	0	0.8811	122.414	0.275	49.2	46.4	2.8
3	3	2	0.8401	132.965	0.334	26.4	27.6	-1.2
3	3	2	0.8401	133.602	0.339	12.1	14	-1.9

x = 0.6
Composition Na0.4K0.6MgF3

Space Group ***Pm-3m***

Cell Dimensions

a	3.9545	(0)		
a'	3.9545		ap (volume)	3.9545
			Z	1

Crystallographic Parameters

	W	*x*	*y*	*z*	*B*	N
Na	1b	0.5	1	0.5	2	(1) 0.00833
K	1b	0.5	1	0.5	0	(1) 0.01250
Mg	1a	0	0	0	1	(1) 0.02083
F(1)	3d	0	0	0.5	2	(1) 0.02083

Polyhedral Data

V	*VA* Ivton	*VA* calc	*VB*	*f*
61.841	51.534	51.534	10.196	5.05

Interatomic Distances

Na		Mg	
F1	2.7963	F1	1.9773
F1	2.7963	F1	1.9773
F1	2.7963	F1	1.9773
F1	2.7963	F1	1.9773
F1	2.7963	F1	1.9773
F1	2.7963	F1	1.9773
F1	2.7963	mean	1.9773
F1	2.7963		
F1	2.7963		
F1	2.7963		
F1	2.7963		
F1	2.7963		
m	2.7963		

Bond Angles

B-X1-B 180

Agreement Parameters

Rp:	13.3
Rwp:	17
Rexp:	13
Chi2:	1.688
R-Bragg	**4.68**
DW-Stat.:	1.597

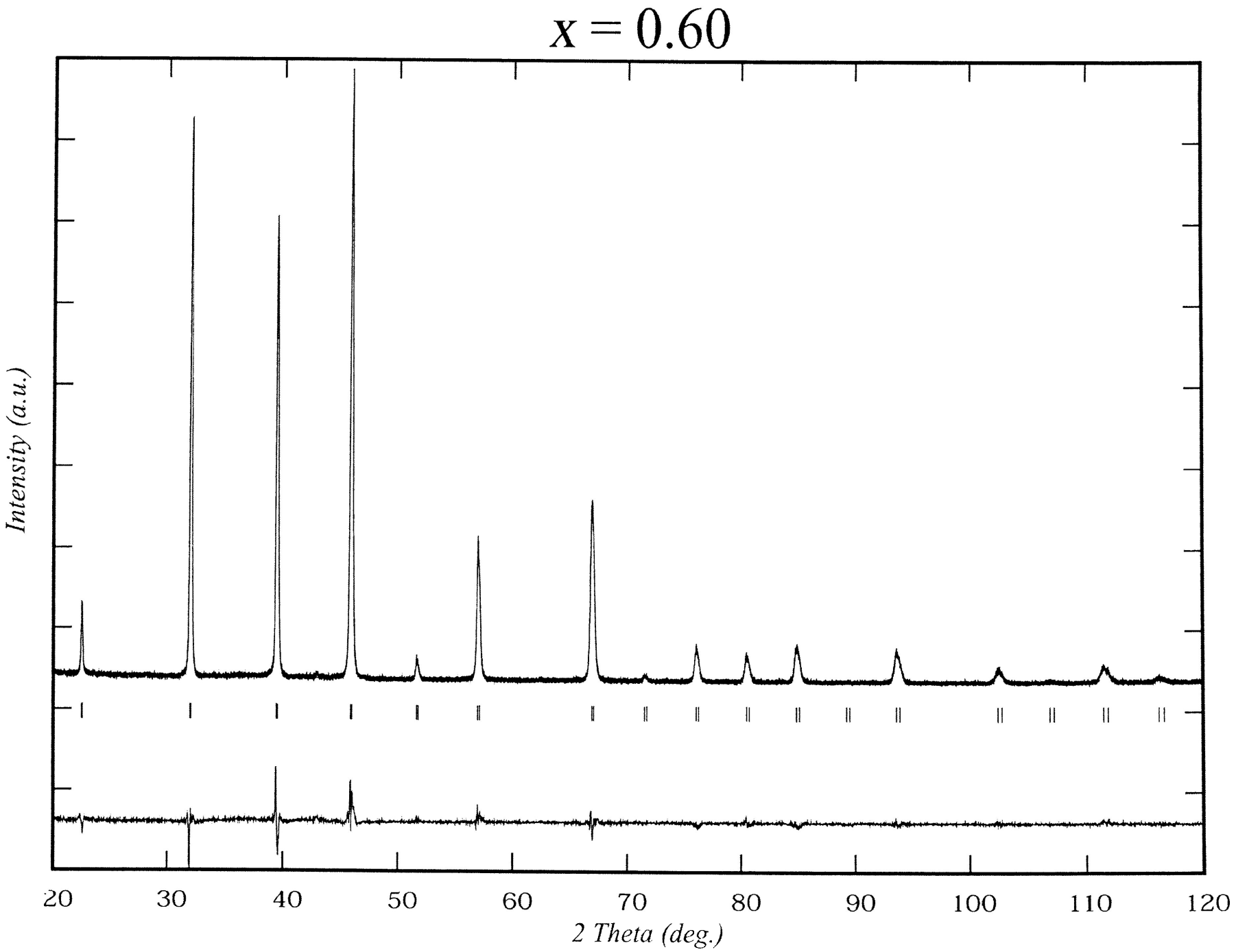
x = 0.60
Intensity (a.u.)
20
30
40
50
60
70
80
90
100
110
120
2 Theta (deg.)

Phase $x = 0.60$

h	*k*	*l*	*D(A)*	*2T*	*HW*	*Iobs*	*Icalc*	*io-ic*
1	0	0	3.9545	22.465	0.154	77.6	71	6.6
1	0	0	3.9545	22.52	0.154	36.4	35.3	1.1
1	1	0	2.7963	31.981	0.17	597.3	637.1	-39.8
1	1	0	2.7963	32.06	0.17	308.6	316.9	-8.3
1	1	1	2.2831	39.435	0.189	606.6	577.8	28.8
1	1	1	2.2831	39.534	0.19	279.2	287.4	-8.2
2	0	0	1.9773	45.857	0.21	876.4	842.3	34.1
2	0	0	1.9773	45.973	0.21	444.2	418.9	25.3
2	1	0	1.7685	51.642	0.231	31.2	28.4	2.9
2	1	0	1.7685	51.776	0.232	16.4	14.1	2.3
2	1	1	1.6144	56.997	0.253	246.8	236.9	9.9
2	1	1	1.6144	57.147	0.254	127.8	117.8	9.9
2	2	0	1.3981	66.864	0.3	394.5	396.5	-2.1
2	2	0	1.3981	67.046	0.301	200.1	197.3	2.8
2	2	1	1.3182	71.517	0.325	11.9	10	1.9
2	2	1	1.3182	71.715	0.326	6.4	5	1.5
3	1	0	1.2505	76.047	0.351	88.3	90.8	-2.5
3	1	0	1.2505	76.262	0.352	42.9	45.2	-2.3
3	1	1	1.1923	80.488	0.379	76.6	72.6	4
3	1	1	1.1923	80.722	0.38	35.2	36.2	-1
2	2	2	1.1416	84.873	0.408	108.9	111.6	-2.7
2	2	2	1.1416	85.125	0.41	53.2	55.7	-2.5
3	2	1	1.0569	93.578	0.475	110.4	106.4	4
3	2	1	1.0569	93.872	0.478	56.4	53.2	3.3
4	0	0	0.9886	102.368	0.556	51.1	48	3.1
4	0	0	0.9886	102.71	0.559	25.9	24.1	1.8
3	3	0	0.9321	111.467	0.659	24.4	20.5	3.9
4	1	1	0.9321	111.467	0.659	49.6	41.7	7.9
3	3	0	0.9321	111.872	0.664	12.8	10.3	2.5
4	1	1	0.9321	111.872	0.664	26.1	20.9	5.1
3	3	1	0.9072	116.222	0.723	25	22.4	2.5
3	3	1	0.9072	116.665	0.729	11.6	11.3	0.4

x = 0.7

Composition Na0.3K0.7MgF3

Space Group ***Pm-3m***

Cell Dimensions

a	3.9659	(2)		
a'	3.9659		ap (volume)	3.9659
			Z	1

Crystallographic Paramet

	Wyck	*x*	*y*	*z*	*B*	N
Na	1b	0.5	1	0.5	2.3	(1) 0.00625
K	1b	0.5	1	0.5	2.3	(0) 0.01458
Mg	1a	0	0	0	1.3	(2) 0.02083
F(1)	3d	0	0	0.5	2.2	(6) 0.02083

Polyhedral Data

V	*VA* Ivton	*VA* calc	*VB*	*f*
62.377	51.981	51.981	10.396	5.00

Interatomic Distances

Na		Mg	
F1	2.8043	F1	1.9830
F1	2.8043	F1	1.9830
F1	2.8043	F1	1.9830
F1	2.8043	F1	1.9830
F1	2.8043	F1	1.9830
F1	2.8043	F1	1.9830
F1	2.8043	mean	1.9830
F1	2.8043		
F1	2.8043		
F1	2.8043		
F1	2.8043		
F1	2.8043		
m	2.8043		

Bond Angles

B-X1-B	180

Agreement Parameters

Rp:	15
Rwp:	18
Rexp:	13
Chi2:	1.8
R-Bragg	**4.2**
DW-Stat.:	1.2

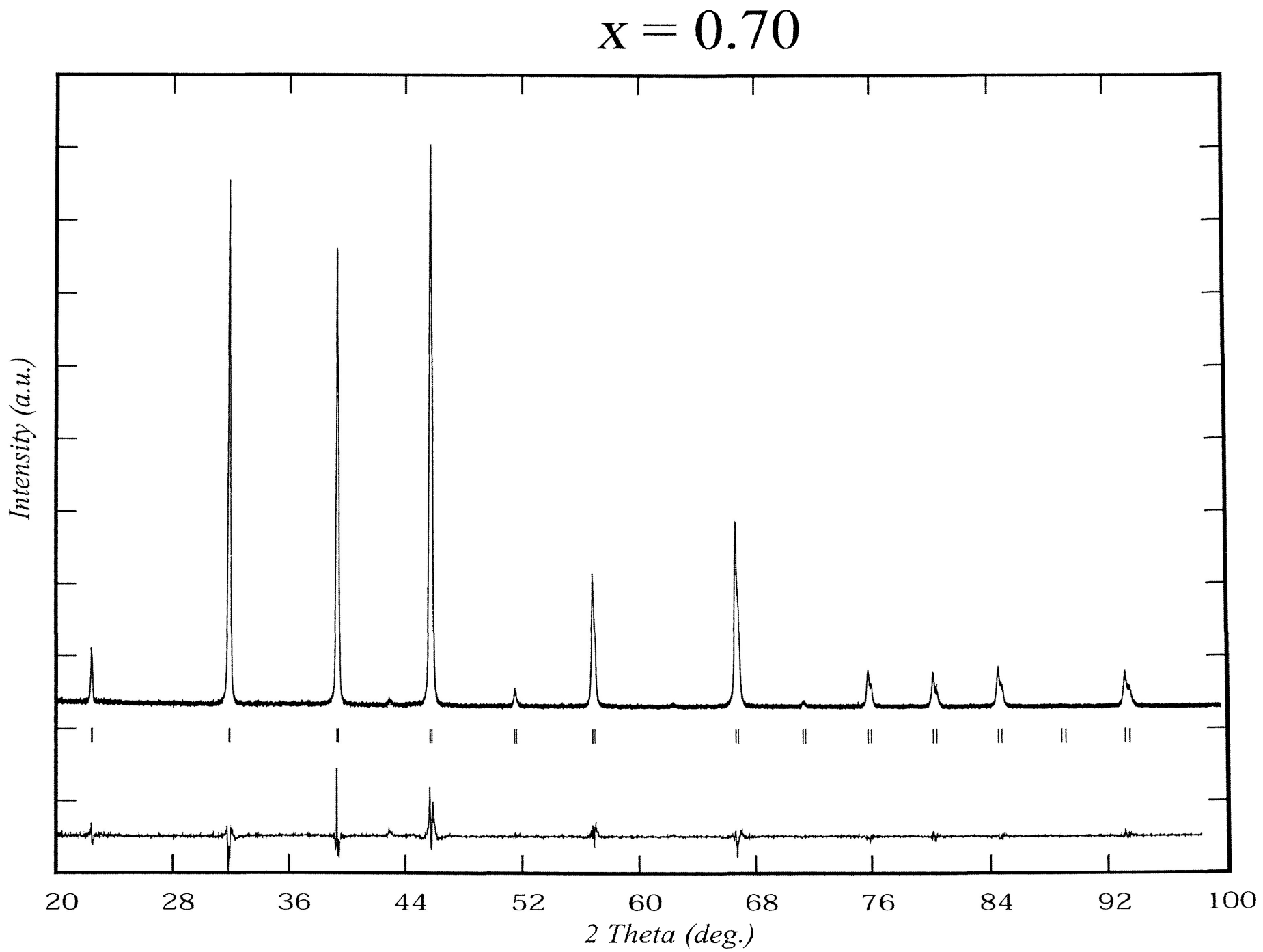
x = 0.70
Intensity (a.u.)
20
28
36
44
52
60
68
76
84
92
100
2 Theta (deg.)

Phase $x = 0.70$

h	*k*	*l*	*D(A)*	*2T*	*HW*	*Iobs*	*Icalc*	*io-ic*
1	0	0	3.9659	22.4	0.134	60.5	51.7	8.8
1	0	0	3.9659	22.454	0.134	25.9	25.7	0.1
1	1	0	2.8043	31.886	0.139	637.4	669.2	-31.7
1	1	0	2.8043	31.965	0.139	327.2	332.9	-5.7
1	1	1	2.2897	39.317	0.146	596.9	586.6	10.3
1	1	1	2.2897	39.416	0.146	280.8	291.8	-11
2	0	0	1.983	45.718	0.153	891.6	846.6	45
2	0	0	1.983	45.834	0.154	448.5	421.1	27.4
2	1	0	1.7736	51.483	0.161	23.8	22.3	1.5
2	1	0	1.7736	51.616	0.162	11.8	11.1	0.7
2	1	1	1.6191	56.818	0.17	241.4	232	9.4
2	1	1	1.6191	56.967	0.17	127.1	115.4	11.7
2	2	0	1.4022	66.647	0.189	381.2	393.9	-12.8
2	2	0	1.4022	66.828	0.19	194	196	-2
2	2	1	1.322	71.28	0.2	7.8	7.7	0.1
3	1	0	1.2541	75.789	0.212	84.6	87.7	-3.1
3	1	0	1.2541	76.004	0.212	43.8	43.7	0.1
3	1	1	1.1958	80.21	0.224	81.4	77.6	3.8
3	1	1	1.1958	80.442	0.225	40.3	38.7	1.6
2	2	2	1.1449	84.572	0.237	103.2	106.4	-3.2
2	2	2	1.1449	84.823	0.238	52	53.1	-1.1
3	2	1	1.0599	93.228	0.268	103.2	98.2	4.9
3	2	1	1.0599	93.52	0.269	53.5	49.1	4.4

$x =$ 0.8

Composition Na0.8K0.2MgF3

Space Group ***Pm-3m***

Cell Dimensions

a	3.9740	(1)		
a'	3.9740		ap (volume)	3.9740
			Z	1

Crystallographic Parameters

	Wyck	*x*	*y*	*z*	*B*		N
Na	1b	0.5	1	0.5	1.5	(3)	0.00417
K	1b	0.5	1	0.5	1.5	(3)	0.01667
Mg	1a	0	0	0	0.8	(3)	0.02083
F(1)	3d	0	0	0.5	1.43	(3)	0.06250

Polyhedral Data

V	*VA* Ivton	*VA* calc	*VB*	*f*
62.760	52.300	52.300	10.460	5.00

Interatomic Distances

Na		Mg	
F1	2.8100	F1	1.9870
F1	2.8100	F1	1.9870
F1	2.8100	F1	1.9870
F1	2.8100	F1	1.9870
F1	2.8100	F1	1.9870
F1	2.8100	F1	1.9870
F1	2.8100	mean	1.9870
F1	2.8100		
F1	2.8100		
F1	2.8100		
F1	2.8100		
F1	2.8100		
m	2.8100		

Bond Angles

B-X1-B	180

Agreement Parameters

Rp:	19.2
Rwp:	22.4
Rexp:	18.8
Chi2:	1.4
R-Bragg	**5.8**
DW-Stat.:	1.5

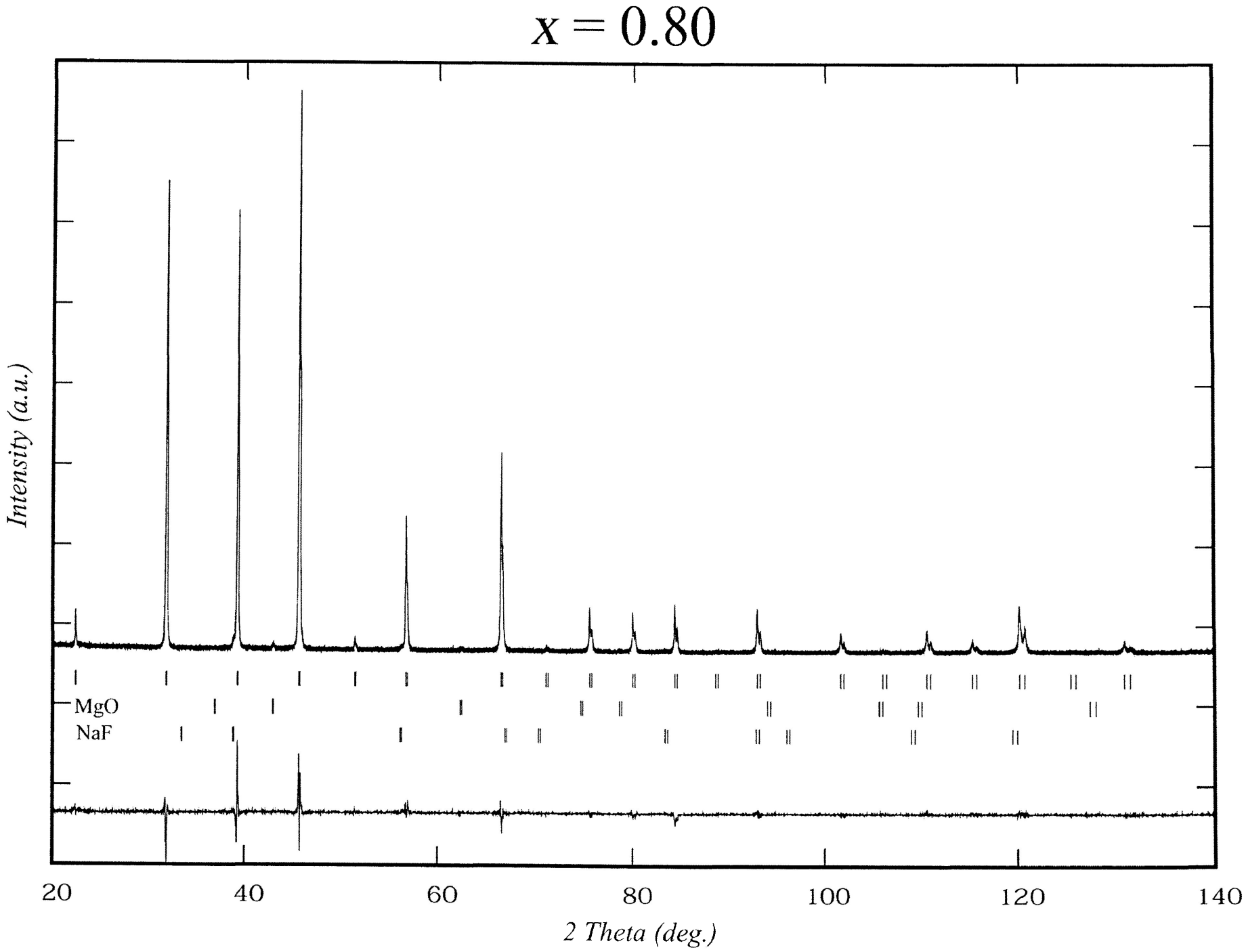
x = 0.80
Intensity (a.u.)
MgO
NaF
20
40
60
80
100
120
140
2 Theta (deg.)

Phase $x = 0.80$

h	*k*	*l*	*D(A)*	*2T*	*HW*	*Iobs*	*Icalc*	*io-ic*
1	0	0	3.974	22.353	0.134	28.5	21.3	7.3
1	0	0	3.974	22.408	0.134	12.8	10.6	2.2
1	1	0	2.81	31.82	0.134	406.4	428	-21.6
1	1	0	2.81	31.898	0.134	201.6	212.9	-11.3
1	1	1	2.2944	39.234	0.135	388.1	374.6	13.5
1	1	1	2.2944	39.332	0.135	198.9	186.3	12.5
2	0	0	1.987	45.619	0.136	563.7	532.3	31.4
2	0	0	1.987	45.735	0.136	278.3	264.7	13.5
2	1	0	1.7772	51.371	0.138	12.1	10.1	2
2	1	0	1.7772	51.503	0.138	5.4	5	0.4
2	1	1	1.6224	56.692	0.14	158.3	149.2	9.1
2	1	1	1.6224	56.841	0.141	81.6	74.2	7.4
2	2	0	1.405	66.494	0.146	254.5	258.8	-4.3
2	2	0	1.405	66.675	0.147	125.4	128.8	-3.4
3	1	0	1.2567	75.608	0.154	59.3	58.3	1
3	1	0	1.2567	75.822	0.154	29.3	29	0.3
3	1	1	1.1982	80.014	0.159	57.7	58.5	-0.8
3	1	1	1.1982	80.245	0.159	27	29.2	-2.1
2	2	2	1.1472	84.361	0.164	60.3	72.2	-12
2	2	2	1.1472	84.61	0.165	28	36	-8.1
3	2	1	1.0621	92.982	0.178	71.5	66.9	4.6
3	2	1	1.0621	93.272	0.178	33.1	33.4	-0.4
4	0	0	0.9935	101.672	0.195	34.2	33.1	1.1
4	0	0	0.9935	102.011	0.196	16.4	16.6	-0.2
3	3	0	0.9367	110.646	0.219	15.1	13.1	2.1
4	1	1	0.9367	110.646	0.219	30.3	26.1	4.1
3	3	0	0.9367	111.045	0.22	7.4	6.6	0.8
4	1	1	0.9367	111.045	0.22	14.7	13.1	1.6
3	3	1	0.9117	115.324	0.234	26.9	22.6	4.4
3	3	1	0.9117	115.76	0.236	13.7	11.4	2.3
4	2	0	0.8886	120.191	0.254	118.4	112.2	6.2
4	2	0	0.8886	120.671	0.256	59.8	56.6	3.2
3	3	2	0.8473	130.781	0.31	27.3	27.5	-0.2
3	3	2	0.8473	131.386	0.314	13.9	13.9	-0.1
4	2	2	0.8112	143.462	0.423	145.6	136.3	9.2
4	2	2	0.8112	144.305	0.434	71.5	66.5	5

x = 0.9

Composition Na0.1K0.9MgF3

Space Group ***Pm-3m***

Cell Dimensions

a	3.9823	(1)		
a'	3.9823	ap (volume)	3.9823	
		Z	1	

Crystallographic Parameters

	Wyck	*x*	*y*	*z*	*B*		N
Na	1b	0.5	1	0.5	1	(3)	0.00208
K	1b	0.5	1	0.5	1	(3)	0.01875
Mg	1a	0	0	0	1	(4)	0.02083
F(1	3d	0	0	0.5	1	(3)	0.06250

Polyhedral Data

V	*VA* Ivton	*VA* calc	*VB*	*f*
63.152	52.627	52.6	10.525	5.00

Interatomic Distances

Na		Mg	
F1	2.81589	F1	1.99113
F1	2.81589	F1	1.99113
F1	2.81589	F1	1.99113
F1	2.81589	F1	1.99113
F1	2.81589	F1	1.99113
F1	2.81589	F1	1.99113
F1	2.81589	mean	1.9911
F1	2.81589		
F1	2.81589		
F1	2.81589		
F1	2.81589		
F1	2.81589		
m	2.8159		

Bond Angles

B-X1-B	180

Agreement Parameters

Rp:	17.5
Rwp:	22.0
Rexp:	19.0
Chi2:	1.3
R-Bragg	**3.8**
DW-Stat.:	1.6

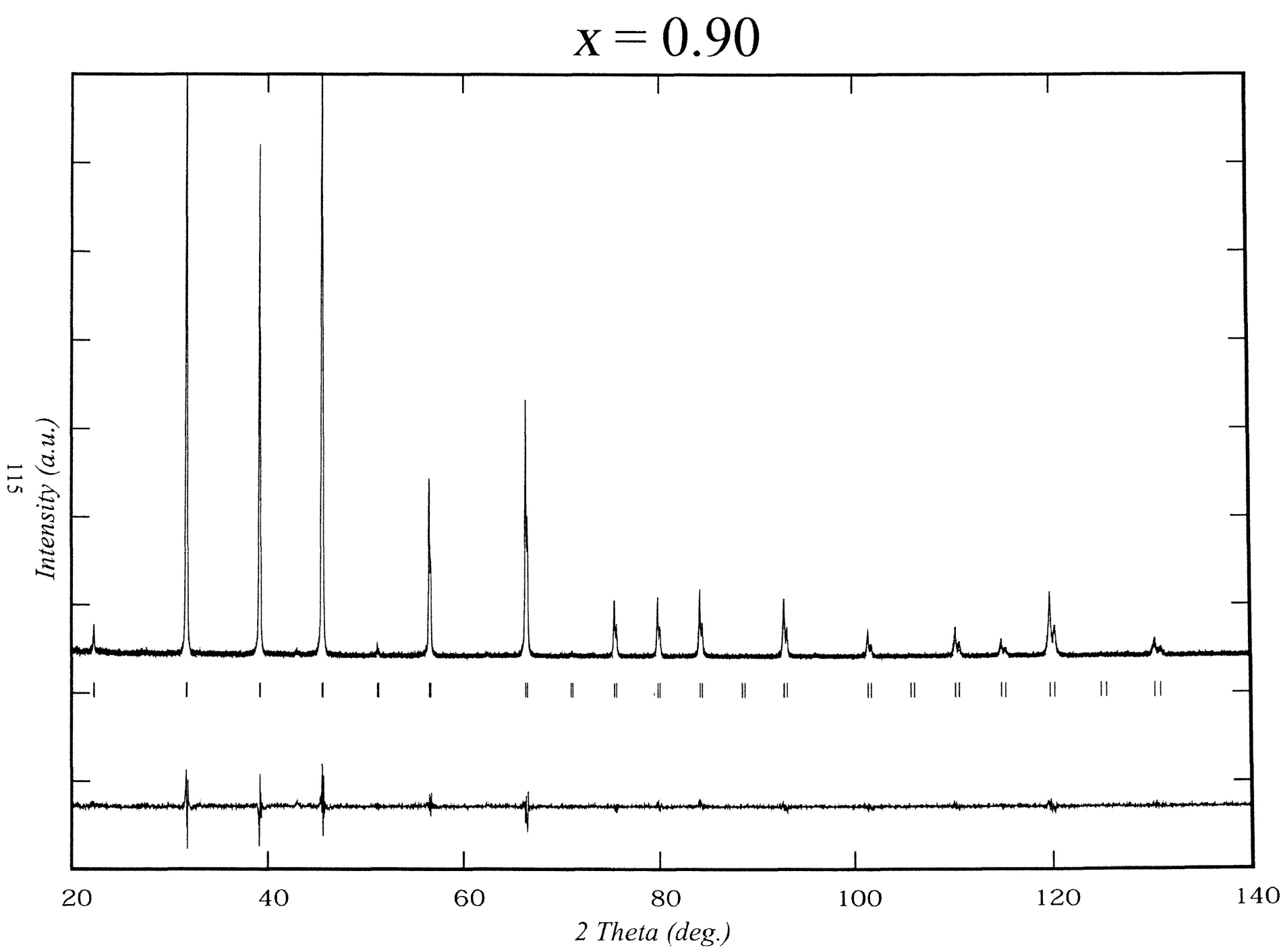
x = 0.90
Intensity (a.u.)
20
40
60
80
100
120
140
2 Theta (deg.)

Phase $x = 0.90$

h	*k*	*l*	*D(A)*	*2T*	*HW*	*Iobs*	*Icalc*	*io-ic*
1	0	0	3.9822	22.307	0.127	18.7	13.3	5.5
1	0	0	3.9822	22.361	0.127	8.7	6.6	2.1
1	1	0	2.8158	31.753	0.126	434.3	423.4	11
1	1	0	2.8158	31.831	0.126	212.4	210.6	1.8
1	1	1	2.2991	39.15	0.127	353.9	363.5	-9.6
1	1	1	2.2991	39.248	0.127	181.4	180.8	0.5
2	0	0	1.9911	45.52	0.129	526.2	508.4	17.8
2	0	0	1.9911	45.636	0.129	255.8	252.9	2.9
2	1	0	1.7809	51.258	0.131	6.9	6.8	0.1
2	1	1	1.6257	56.566	0.134	158.6	150.2	8.3
2	1	1	1.6257	56.714	0.134	77.6	74.7	2.8
2	2	0	1.4079	66.34	0.142	245.6	252.8	-7.2
2	2	0	1.4079	66.52	0.143	118.7	125.8	-7.1
3	1	0	1.2593	75.426	0.153	59.5	60.2	-0.7
3	1	0	1.2593	75.638	0.153	28.4	30	-1.6
3	1	1	1.2007	79.816	0.16	64.6	60.8	3.8
3	1	1	1.2007	80.047	0.16	30.7	30.3	0.4
2	2	2	1.1496	84.148	0.167	79.4	72.2	7.2
2	2	2	1.1496	84.396	0.167	37.3	36	1.3
3	2	1	1.0643	92.734	0.185	71.6	71	0.6
3	2	1	1.0643	93.023	0.185	33.6	35.5	-1.8
4	0	0	0.9955	101.384	0.207	34.6	33.9	0.7
4	0	0	0.9955	101.72	0.208	15.7	17	-1.2
3	3	0	0.9386	110.307	0.238	15.9	14.3	1.6
4	1	1	0.9386	110.307	0.238	31.8	28.5	3.2
3	3	0	0.9386	110.703	0.24	7.6	7.2	0.4
4	1	1	0.9386	110.703	0.24	15.2	14.3	0.9
3	3	1	0.9136	114.954	0.258	30.1	25.2	4.9
3	3	1	0.9136	115.387	0.26	14.7	12.7	2
4	2	0	0.8904	119.783	0.282	122.6	117.1	5.5
4	2	0	0.8904	120.26	0.284	58.1	59.1	-1
3	3	2	0.849	130.27	0.351	34	30.8	3.2
3	3	2	0.849	130.868	0.356	15.6	15.6	-0.1
4	2	2	0.8129	142.756	0.485	154.9	145.6	9.3
4	2	2	0.8129	143.582	0.497	76.9	73.4	3.5

x = 1

Composition Na0.0K1.0MgF3

Space Group ***Pm-3m***

Cell Dimensions

a	3.9903	(0)			
a'	3.9903		ap (volume)	3.9903	
			Z	1	

Crystallographic Parameters

	Wyck	*x*	*y*	*z*	*B*	N
Na	1b	0.5	1	0.5	1.5 (5)	0.00000
K	1b	0.5	1	0.5	1.5 (5)	0.02083
Mg	1a	0	0	0	0.9 (6)	0.02083
F(1)	3d	0	0	0.5	1.3 (5)	0.06250

Polyhedral Data

V	*VA* Ivton	*VA* calc	*VB*	*f*
63.537	52.946	52.946	10.589	5.00

Interatomic Distances

Na		Mg	
F1	2.8216	F1	1.9952
F1	2.8216	F1	1.9952
F1	2.8216	F1	1.9952
F1	2.8216	F1	1.9952
F1	2.8216	F1	1.9952
F1	2.8216	F1	1.9952
F1	2.8216	mean	1.9952
F1	2.8216		
F1	2.8216		
F1	2.8216		
F1	2.8216		
F1	2.8216		
m	2.8216		

Bond Angles

B-X1-B	180

Agreement Parameters

Rp:	18.1
Rwp:	23.0
Rexp:	19.0
Chi2:	1.5
R-Bragg	**3.2**
DW-Stat.:	1.5

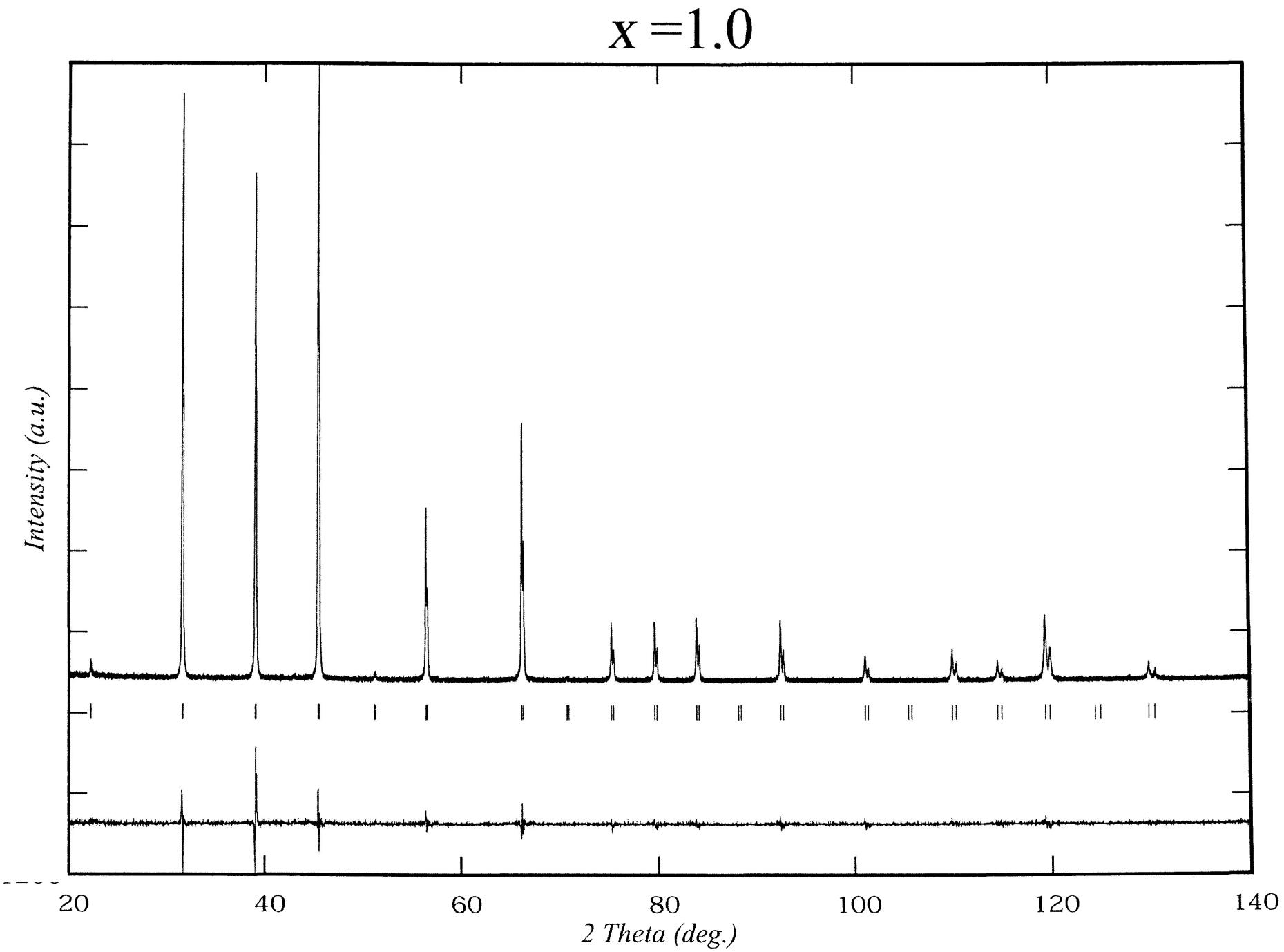
x =1.0
Intensity (a.u.)
20
40
60
80
100
120
140
2 Theta (deg.)

Phase $x = 1.0$

h	*k*	*l*	*Mult*	*D(A)*	*2T*	*HW*	*Iobs*	*Icalc*	*io-ic*
1	0	0	6	3.9903	22.261	0.124	10.9	6.9	4.1
1	0	0	6	3.9903	22.315	0.124	6	3.4	2.6
1	1	0	12	2.8216	31.686	0.123	432.2	425.9	6.3
1	1	0	12	2.8216	31.764	0.123	203.6	211.9	-8.3
1	1	1	8	2.3038	39.067	0.123	357.5	358.8	-1.3
1	1	1	8	2.3038	39.165	0.123	199.3	178.5	20.8
2	0	0	6	1.9952	45.422	0.123	498.2	486.7	11.5
2	0	0	6	1.9952	45.537	0.123	240.3	241.9	-1.6
2	1	1	24	1.629	56.439	0.125	155.7	147.6	8.1
2	1	1	24	1.629	56.587	0.125	74.1	73.4	0.7
2	2	0	12	1.4108	66.187	0.129	237.1	241.2	-4.1
2	2	0	12	1.4108	66.366	0.129	118.8	120	-1.2
3	1	0	24	1.2619	75.244	0.135	58.9	58.5	0.4
3	1	0	24	1.2619	75.457	0.135	28.6	29.1	-0.5
3	1	1	24	1.2031	79.621	0.138	63	61.9	1.1
3	1	1	24	1.2031	79.85	0.139	29.4	30.8	-1.5
2	2	2	8	1.1519	83.936	0.142	70.3	68.8	1.5
2	2	2	8	1.1519	84.184	0.143	33.3	34.3	-1
3	2	1	48	1.0665	92.489	0.153	69.8	68.4	1.4
3	2	1	48	1.0665	92.777	0.153	33.7	34.2	-0.5
4	0	0	6	0.9976	101.098	0.167	31.5	32.2	-0.7
4	0	0	6	0.9976	101.433	0.168	14.1	16.1	-2
3	3	0	12	0.9405	109.971	0.187	15	13.6	1.4
4	1	1	24	0.9405	109.971	0.187	30	27.3	2.7
3	3	0	12	0.9405	110.365	0.188	7.6	6.9	0.7
4	1	1	24	0.9405	110.365	0.188	15.1	13.7	1.4
3	3	1	24	0.9154	114.587	0.2	28.7	26.5	2.2
3	3	1	24	0.9154	115.017	0.201	15.1	13.3	1.8
4	2	0	24	0.8923	119.38	0.216	115.3	110.6	4.7
4	2	0	24	0.8923	119.853	0.217	56.1	55.8	0.3
3	3	2	24	0.8507	129.767	0.263	30.5	29.1	1.4
3	3	2	24	0.8507	130.357	0.266	15.5	14.8	0.7
4	2	2	24	0.8145	142.067	0.354	145.1	137.3	7.8
4	2	2	24	0.8145	142.876	0.363	75.9	70.4	5.5

Appendix A – 2

This appendix contains crystallographic parameters for natural and synthetic cryolite and synthetic simmonsite. The simmonsite refinement contained minor amounts of cryolite and LiF_3.

Composition

Na2LiAlF6 simmonsite

Space Group ***P121/n1***

Cell Dimensions

a	5.2861	(1)	ap (mean)	3.7641
b	5.3732	(1)	ap (volume)	3.7640
c	7.5100	(2)	*Z*	4
b	89.970	(9)		
a'	3.7379			
b'	3.7995			
c'	3.7550			

Crystallographic Parameters

	Wyck	*x*		*y*		*z*		*B*	*N*
Li	2*c*	0.5		0.0		0.5		1.2 (1)	0.5
Na	4*e*	0.5052	(8)	0.5388	(4)	0.2514	(6)	2.6 (1)	1.0
Al	2*d*	0.5		0.0		0.0		1.0 (1)	0.5
F(1)	4*e*	0.2228	(8)	0.1928	(8)	-0.0371	(8)	1.9 (1)	1.0
F(2)	4*e*	0.3104	(7)	0.7243	(7)	-0.0430	(6)	1.7 (1)	1.0
F(3)	4*e*	0.4259	(6)	0.9770	(5)	0.241	(1)	2.4 (1)	1.0

Polyhedral Data

V	V/Z (Vap)	*VA* Ivton	*VD*	*VA* calc	*VBLi*	*VBAl*	*f*
213.31	53.327	35.824	7.826	43.650	11.175	8.179	4.5107

Interatomic Distances

Na			**Al**				**Li**			
1st C.S.			F1	1.8309			F1	2.0303		
F1	2.5895		F1	1.8309			F1	2.0303		
F1	2.5954		F2	1.8310			F2	2.0515		
F1	2.3206		F2	1.8310			F2	2.0515		
F2	2.6429		F2	1.8299			F3	2.0146		
F2	2.3155		F2	1.8299			F3	2.0146		
F2	2.5629		mean	1.8306	Δ =	#####		2.0321	Δ =	0.05546
F2	2.3941									
F2	3.0523		**Al**				**Li**			
F2	2.3107	F1 -	F2	89.827		F1 -	F2	89.322		
F2	3.0204	F1 -	F2	90.173		F1 -	F2	90.678		
m1	2.5804	F1 -	F3	90.782		F1 -	F3	88.416		
		F1 -	F3	89.218		F1 -	F3	91.584		
F2	3.2280	F1 -	F2	90.173		F1 -	F2	90.678		
F1	3.2408	F1 -	F2	89.827		F1 -	F2	89.322		
m2	3.2344	F1 -	F3	89.218		F1 -	F3	91.584		
		F1 -	F3	90.782		F1 -	F3	88.416		
m3	2.6894	F2 -	F3	90.184		F2 -	F3	92.136		
		F2 -	F3	89.816		F2 -	F3	87.864		
		F2 -	F3	89.816		F2 -	F3	87.864		
		F2 -	F3	90.184		F2 -	F3	92.136		
			δ =	0.2458			δ =	2.7391		

Agreement Parameters

Rp:	14.5
Rwp:	18.4
Rexp:	13.5
Chi2:	1.853
R-Bragg	**4.7**
DW-Stat.	1.1804

Octahedral Tilts

A =	0.165	ϕ	B' (Li) [001] = 9.10
B =	0.156	ϕ	B (AL) [001] = 10.33
C =	0.187	θ	B' (Li) [110] = 11.93
D =	0.178	θ	B (AL) [110] = 12.79
E =	0.392	Φ	B' (Li) [111] = 14.96
F =	0.124	Φ	B (AL) [111] = 16.38

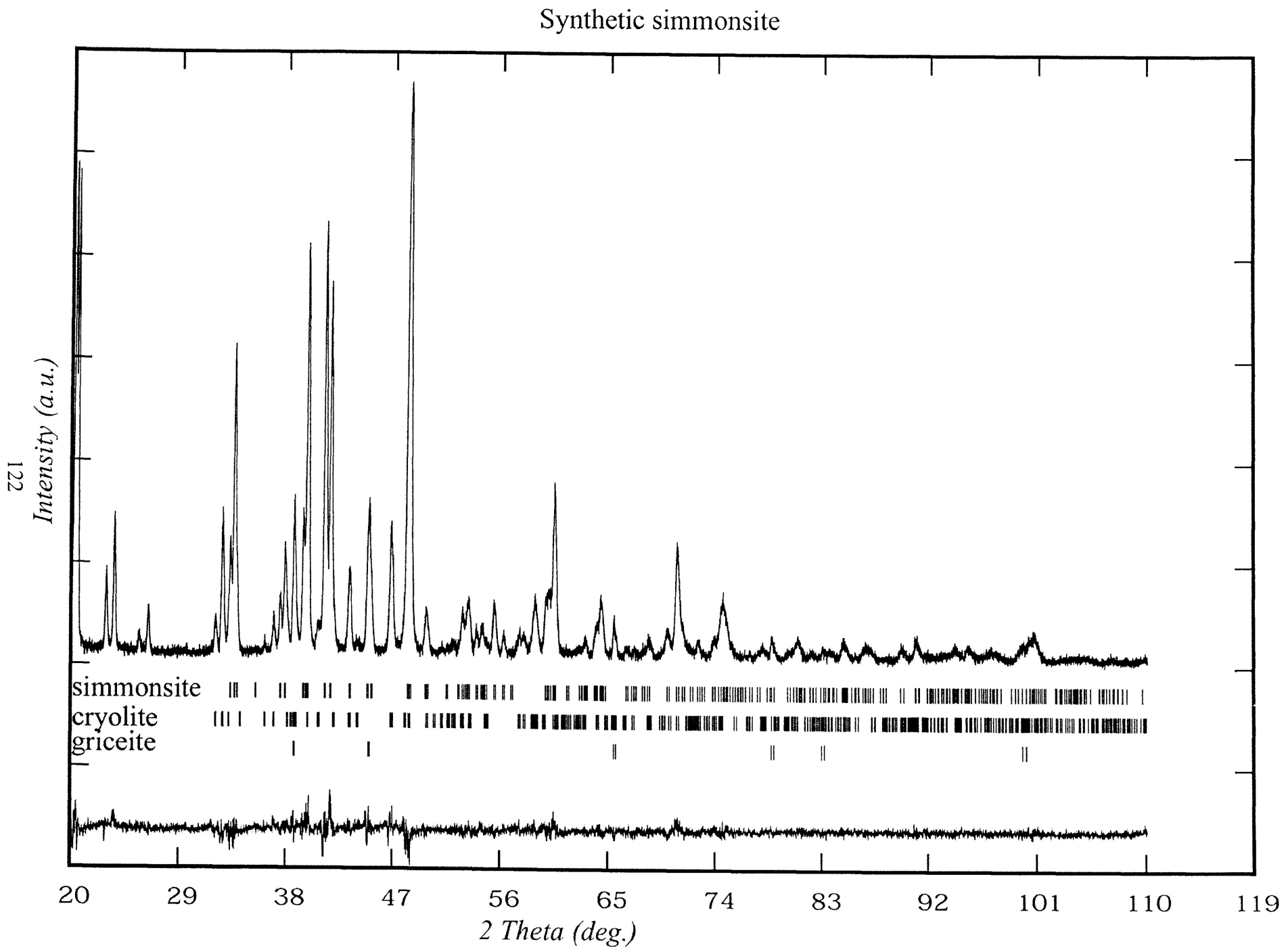
Synthetic simmonsite
Intensity (a.u.)
simmonsite
cryolite
griceite
20
29
38
47
56
65
74
83
92
101
110
119
2 Theta (deg.)

Simmonsite

h	*k*	*l*	*D(A)*	*2T*	*HW*	*Iobs*	*Icalc*	*io-ic*
0	1	1	4.3699	20.306	0.155	189.2	187.3	1.9
0	1	1	4.3699	20.355	0.155	94.7	93.2	1.5
1	0	1	4.3235	20.526	0.156	69.9	69.1	0.7
1	0	-1	4.3218	20.534	0.156	105.7	104.4	1.3
1	0	1	4.3235	20.576	0.156	34.7	34.4	0.3
1	0	-1	4.3218	20.584	0.156	52.3	52	0.3
1	1	0	3.7682	23.591	0.164	48.6	38.7	9.8
1	1	0	3.7682	23.648	0.164	23.6	19.3	4.3
0	0	2	3.755	23.675	0.164	20.6	16.6	3.9
0	0	2	3.755	23.733	0.165	11.1	8.3	2.8
1	1	1	3.3684	26.439	0.172	9.7	10.9	-1.3
1	1	-1	3.3676	26.445	0.172	9	10.3	-1.2
0	2	0	2.6866	33.323	0.194	42.9	46.8	-3.9
0	2	0	2.6866	33.406	0.194	21.9	23.3	-1.4
1	1	2	2.6603	33.663	0.195	70.2	72.6	-2.4
1	1	-2	2.6595	33.673	0.195	76.1	79	-2.9
1	1	2	2.6603	33.746	0.196	34	36.1	-2.1
1	1	-2	2.6595	33.757	0.196	36.9	39.3	-2.4
2	0	0	2.643	33.889	0.196	28.8	30.6	-1.9
2	0	0	2.643	33.973	0.196	13.9	15.2	-1.3
1	2	0	2.395	37.522	0.209	32.1	30.5	1.5
1	2	0	2.395	37.616	0.209	15.8	15.2	0.7
2	1	0	2.3716	37.906	0.21	61.5	54.9	6.5
2	1	0	2.3716	38.001	0.21	30.8	27.3	3.5
1	2	1	2.2819	39.457	0.216	58.2	57.6	0.6
1	2	-1	2.2817	39.462	0.216	6.7	6.6	0.1
1	2	1	2.2819	39.556	0.216	28.7	28.6	0.1
0	1	3	2.2692	39.689	0.216	9.4	9.3	0.1
1	0	3	2.2628	39.804	0.217	28.2	27.7	0.5
1	0	-3	2.2621	39.818	0.217	102	99.8	2.3
2	1	1	2.2618	39.823	0.217	71.1	69.4	1.7
2	1	-1	2.2613	39.832	0.217	11.3	11	0.3
1	0	3	2.2628	39.904	0.217	14.5	13.8	0.8
1	0	-3	2.2621	39.917	0.217	52.7	49.6	3.1
2	1	1	2.2618	39.923	0.217	36.7	34.5	2.2
2	1	-1	2.2613	39.932	0.217	5.9	5.5	0.4
0	2	2	2.185	41.286	0.222	237.3	235.9	1.5
0	2	2	2.185	41.39	0.223	119.6	117.3	2.3
2	0	2	2.1617	41.75	0.224	108.5	100.6	7.8
2	0	-2	2.1609	41.767	0.224	93.3	86	7.3
2	0	2	2.1617	41.855	0.224	55.2	50	5.1
2	0	-2	2.1609	41.872	0.225	47.2	42.8	4.4
1	1	3	2.0854	43.354	0.23	16.1	14.9	1.2

Simmonsite

h	*k*	*l*	*D(A)*	*2T*	*HW*	*Iobs*	*Icalc*	*io-ic*
I	1	-3	2.0849	43.366	0.23	23.4	21.7	1.7
1	1	3	2.0854	43.463	0.231	8	7.4	0.6
1	1	-3	2.0849	43.475	0.231	11.6	10.8	0.9
1	2	2	2.0194	44.846	0.236	29	26.9	2.1
1	2	-2	2.0191	44.854	0.236	23.1	21.5	1.5
1	2	2	2.0194	44.96	0.236	13.7	13.4	0.3
1	2	-2	2.0191	44.968	0.236	10.9	10.7	0.2
2	1	2	2.0055	45.175	0.237	16.1	15.7	0.3
2	1	-2	2.0048	45.19	0.237	14	13.7	0.3
2	1	2	2.0055	45.289	0.238	8	7.8	0.2
2	1	-2	2.0048	45.305	0.238	7	6.8	0.1
2	2	0	1.8841	48.264	0.25	292.2	305.9	-13.8
2	2	0	1.8841	48.387	0.25	146.5	152.2	-5.6
0	0	4	1.8775	48.445	0.25	156.9	163.6	-6.6
0	0	4	1.8775	48.568	0.251	77.2	81.4	-4.1
0	2	3	1.8315	49.743	0.256	15.8	16.4	-0.6
2	2	1	1.8276	49.856	0.256	6.9	7.2	-0.3
2	2	-1	1.8274	49.863	0.256	6.1	6.3	-0.2
0	2	3	1.8315	49.871	0.256	7.9	8.2	-0.3
1	2	3	1.7307	52.856	0.269	15	16	-1
1	2	3	1.7307	52.993	0.269	7.5	8	-0.5
2	1	-3	1.7214	53.166	0.27	12.5	12.8	-0.3
2	1	-3	1.7214	53.304	0.271	6.4	6.4	0.1
3	0	1	1.7156	53.359	0.271	11.5	11.4	0.1
3	0	-1	1.7153	53.37	0.271	5.3	5.3	0
3	0	1	1.7156	53.497	0.272	5.4	5.7	-0.3
1	3	0	1.6963	54.013	0.274	14.4	15.6	-1.2
1	3	0	1.6963	54.154	0.274	7.7	7.8	-0.1
2	2	2	1.6842	54.434	0.276	10.9	9.4	1.6
1	1	-4	1.6803	54.573	0.276	8.3	7.2	1.1
2	2	2	1.6842	54.576	0.276	5.4	4.7	0.7
1	3	1	1.6547	55.488	0.28	30.7	30.1	0.6
1	3	-1	1.6546	55.491	0.28	10.2	10.1	0.2
1	3	1	1.6547	55.633	0.281	14.6	15	-0.4
3	1	-1	1.634	56.252	0.284	13.9	12	1.9
3	1	-1	1.634	56.399	0.284	6.2	6	0.3
1	3	2	1.546	59.769	0.3	25.4	24.1	1.3
1	3	-2	1.5458	59.776	0.3	13.4	12.7	0.7
1	3	2	1.546	59.928	0.301	12.5	12	0.5
1	3	-2	1.5458	59.934	0.301	6.6	6.3	0.3
0	2	4	1.539	60.071	0.301	37.7	36.6	1.1
0	2	4	1.539	60.23	0.302	18.6	18.2	0.4
2	0	4	1.5309	60.419	0.303	7.7	7.4	0.3
2	0	-4	1.5303	60.445	0.303	25.7	24.6	1.1

Simmonsite

h	*k*	*l*	*D(A)*	*2T*	*HW*	*Iobs*	*Icalc*	*io-ic*
3	1	2	1.5294	60.485	0.303	54.9	52.7	2.2
3	1	-2	1.5289	60.505	0.304	36.4	35.1	1.3
2	0	-4	1.5303	60.605	0.304	12.3	12.3	0.1
3	1	2	1.5294	60.646	0.304	25.9	26.2	-0.3
3	1	-2	1.5289	60.665	0.304	17.1	17.4	-0.4
3	2	0	1.4734	63.041	0.316	7	6.9	0.1
2	3	1	1.4547	63.948	0.32	20.5	20	0.5
2	3	1	1.4547	64.119	0.321	10.5	10	0.5
0	1	5	1.4466	64.35	0.322	8.5	8	0.5
3	2	1	1.4459	64.381	0.322	17.5	16.5	1
1	0	-5	1.4447	64.445	0.323	18.4	17.2	1.2
3	2	1	1.4459	64.554	0.323	8.9	8.2	0.7
1	0	-5	1.4447	64.618	0.324	9.3	8.6	0.7
1	3	-3	1.4042	66.537	0.333	9.2	6.9	2.3
0	4	0	1.3433	69.98	0.352	25.9	25.6	0.3
0	4	0	1.3433	70.173	0.353	12.9	12.7	0.1
2	2	4	1.3301	70.777	0.356	54.8	51.4	3.3
2	2	-4	1.3297	70.801	0.356	44.3	41.9	2.5
2	2	4	1.3301	70.973	0.357	26.6	25.6	1
2	2	-4	1.3297	70.997	0.357	21.6	20.8	0.8
4	0	0	1.3215	71.308	0.359	16.7	16	0.7
4	0	0	1.3215	71.506	0.36	8.4	8	0.4
1	4	0	1.3019	72.55	0.366	10.8	11.1	-0.3
1	4	0	1.3019	72.752	0.367	5.3	5.5	-0.2
4	1	0	1.2833	73.777	0.373	7.5	7.2	0.3
2	3	-3	1.2756	74.296	0.376	14.9	14.8	0.2
1	2	5	1.2726	74.502	0.377	24.7	25.1	-0.4
2	3	-3	1.2756	74.505	0.377	7.2	7.3	-0.1
3	2	-3	1.2696	74.707	0.378	19.2	19.5	-0.3
1	2	5	1.2726	74.711	0.378	12.3	12.5	-0.2
2	1	5	1.2691	74.738	0.378	10.9	11	-0.1
3	2	-3	1.2696	74.917	0.379	9.8	9.7	0.1
2	1	5	1.2691	74.948	0.379	5.5	5.5	0.1
4	1	1	1.265	75.023	0.38	11.8	11.6	0.2
4	1	1	1.265	75.235	0.381	5.7	5.8	0
4	1	2	1.2145	78.732	0.402	6.8	7.5	-0.7
2	4	0	1.1975	80.069	0.41	6.7	6.3	0.4
1	1	6	1.188	80.846	0.415	6.6	6.1	0.5
1	1	-6	1.1878	80.863	0.415	7	6.5	0.5
1	4	-3	1.155	83.66	0.434	6.2	6.3	-0.1
3	0	5	1.1433	84.715	0.441	7.4	6.7	0.6
4	1	-3	1.1418	84.853	0.442	11	9.8	1.1
4	1	-3	1.1418	85.105	0.443	5.8	4.9	0.8
3	3	-3	1.1225	86.661	0.454	5.1	5.2	-0.1

Simmonsite

h	*k*	*l*	*D(A)*	*2T*	*HW*	*Iobs*	*Icalc*	*io-ic*
3	1	-5	1.1178	87.119	0.457	5.8	5.9	0
0	4	4	1.0925	89.674	0.476	16.6	14.7	1.9
0	4	4	1.0925	89.948	0.478	8.8	7.3	1.4
4	0	4	1.0809	90.905	0.485	7	5.8	1.2
4	0	-4	1.0805	90.95	0.485	5.5	4.6	0.9
1	5	-1	1.0429	95.229	0.519	8.1	7.7	0.4
2	4	-4	1.0095	99.462	0.556	8	8.1	0
3	1	6	1.0027	100.391	0.564	10	9.3	0.7
4	2	-4	1.0024	100.428	0.565	7.1	6.6	0.5
3	1	6	1.0027	100.722	0.567	5.3	4.7	0.6
5	1	2	1	100.765	0.568	8.4	7.5	1
5	1	-2	0.9998	100.794	0.568	9	8	1

Composition

Natural Na2NaAlF6

Space Group ***P121/n1***

Cell Dimensions

a	5.4047	(2)	ap (mean)	3.8866	
b	5.5914	(2)	ap (volume)	3.8862	
c	7.7684	(3)	*Z*	4	
b	89.806	(4)			
a'	3.8217				
b'	3.9537				
c'	3.8842				

Crystallographic Parameters

	Wyck	***x***		***y***		***z***	***B***		***N***
Na(1)	2*c*	0.5		0.0		0.5	1.4	(1)	0.5
Na	4*e*	0.5124	(5)	0.5511	(4)	0.2512	2.3	(1)	1.0
Al	2*d*	0.5		0.0		0.0	0.9	(1)	0.5
F(1)	4*e*	0.2252	(7)	0.1738	(7)	-0.0420	1.9	(1)	1.0
F(2)	4*e*	0.3304	(7)	0.7316	(7)	-0.0610	1.7	(1)	1.0
F(3)	4*e*	0.3961	(6)	0.9559	(6)	0.2194	1.2	(1)	1.0

Polyhedral Data

V	V/Z (Vap)	*VA* Ivton	*VD*	*VA* calc	*VBNa*	*VBAl*	*f*
234.760	58.690	25.2410	21.882	47.1235	15.1460	7.9870	4.0741

Interatomic Distances

Na (2)			**Al**			**Na (1)**		
1st C.S.			F1	1.805	(4)	F1	2.216	(4)
F1	2.6838	(4)	F1	1.805	(4)	F1	2.216	(4)
F1	2.6466	(4)	F2	1.822	(5)	F2	2.255	(5)
F1	2.3445	(4)	F2	1.822	(5)	F2	2.255	(5)
F2	2.8083	(5)	F3	1.809	(6)	F3	2.266	(6)
F2	2.3227	(5)	F3	1.809	(6)	F3	2.266	(6)
F2	2.5642	(5)	mean	1.812	Δ = 0.043		2.246	Δ = 0.107
F3	2.3627	(6)						
F3	2.2812	(6)						
m1	2.5018							
F1	3.47439	(4)						
F2	3.5191	(5)						
F3	3.3956	(6)						
F3	3.2501	(6)						
m2	3.4098							
m3	2.8044							

Interatomic Angles

Al			**Na (1)**		
F1 - F2	88.927	(2)	F1 - F2	90.439	(2)
F1 - F2	91.073	(2)	F1 - F2	89.561	(2)
F1 - F3	89.458	(2)	F1 - F3	85.088	(2)
F1 - F3	90.542	(2)	F1 - F3	94.912	(2)
F1 - F2	91.073	(2)	F1 - F2	89.561	(2)
F1 - F2	88.927	(2)	F1 - F2	90.439	(2)
F1 - F3	90.542	(2)	F1 - F3	94.912	(2)
F1 - F3	89.458	(2)	F1 - F3	85.088	(2)
F2 - F3	88.743	(2)	F2 - F3	93.782	(2)
F2 - F3	91.257	(2)	F2 - F3	86.218	(2)
F2 - F3	91.257	(2)	F2 - F3	86.218	(2)
F2 - F3	88.743	(2)	F2 - F3	93.782	(2)
δ =	1.10		δ =	14.04	

Agreement Parameters

Rp:	12.9
Rwp:	15.3
Rexp:	8.05
Chi2:	3.596
R-Bragg	**6.41**
DW-Stat.:	0.6808

Octahedral Tilts

A =	0.189	ϕ	B' (Li) [001] =	10.2
B =	0.170	ϕ	B (AL) [001] =	12.7
C =	0.238	θ	B' (Li) [110] =	15.7
D =	0.213	θ	B (AL) [110] =	19.8
E =	0.562	Φ	B' (Li) [111] =	18.6
F =	0.246	Φ	B (AL) [111] =	23.4

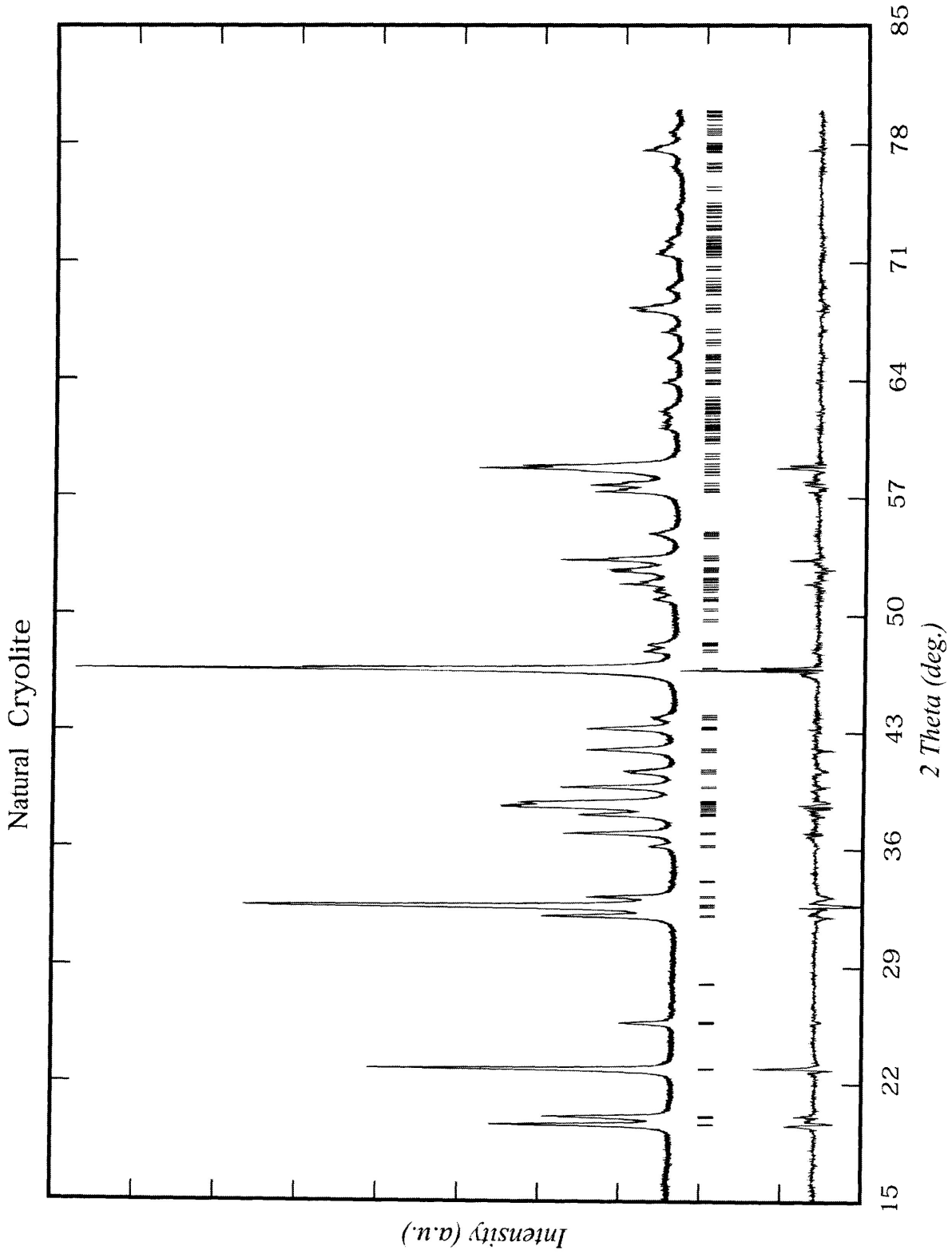
Natural Cryolite
Intensity (a.u.)
15
22
29
36
43
50
57
64
71
78
85
2 Theta (deg.)

Composition

Synthetic Na2NaAlF6

Space Group ***P121/n1***

Cell Dimensions

a	5.4054	(1)	ap (mean)	3.8870	
b	5.5934	(1)	ap (volume)	3.8866	
c	7.7672	(1)	*Z*	4	
b	89.807	(0)			
a'	3.8222				
b'	3.9552				
c'	3.8836				

Crystallographic Parameters

	Wyck	***x***		***y***		***z***		***B***		***N***
Na(1)	*2c*	0.5		0.0		0.5		1.6	(1)	0.5
Na	*4e*	0.5138	(5)	0.5520	(4)	0.2518	(5)	2.3	(1)	1.0
Al	*2d*	0.5		0.0		0.0		1.8	(1)	0.5
F(1)	*4e*	0.2255	(7)	0.1765	(7)	0.9530	(6)	1.6	(1)	1.0
F(2)	*4e*	0.3353	(7)	0.7285	(7)	0.9362	(6)	1.4	(1)	1.0
F(3)	*4e*	0.3970	(6)	0.9564	(6)	0.2182	(6)	1.4	(1)	1.0

Polyhedral Data

V	V/Z (Vap)	*VA* Ivton	*VD*	*VA* calc	*VBNa*	*VBAl*	*f*
234.839	58.710	25.241	21.902	47.143	15.146	7.987	4.08

Interatomic Distances

Na (2)

1st C.S.		
F1	2.7193	(4)
F1	2.6091	(4)
F1	2.3236	(4)
F2	2.8165	(5)
F2	2.2914	(5)
F2	2.5678	(5)
F3	2.3630	(6)
F3	2.2954	(6)
m1	2.4982	
F1	3.4962	(4)
F2	3.5565	(5)
F3	3.3996	(6)
F3	3.2462	(6)
m2	3.4246	
m3	2.8070	

Al

F1	1.820	(4)
F1	1.820	(4)
F2	1.830	(5)
F2	1.830	(5)
F3	1.799	(6)
F3	1.799	(6)
mean	1.816	Δ = 0.051

Na (1)

F1	2.211	(4)
F1	2.211	(4)
F2	2.271	(5)
F2	2.271	(5)
F3	2.273	(6)
F3	2.273	(6)
	2.252	Δ = 0.163

Interatomic Angles

Al

F1 - F2	89.896	(2)
F1 - F2	90.104	(2)
F1 - F3	90.715	(2)
F1 - F3	89.285	(2)
F1 - F2	90.104	(2)
F1 - F2	89.896	(2)
F1 - F3	89.285	(2)
F1 - F3	90.715	(2)
F2 - F3	89.623	(2)
F2 - F3	90.377	(2)
F2 - F3	90.377	(2)
F2 - F3	89.623	(2)
	δ = 0.24	

Na (1)

F1 - F2	89.163	(2)
F1 - F2	90.837	(2)
F1 - F3	86.235	(2)
F1 - F3	93.765	(2)
F1 - F2	90.837	(2)
F1 - F2	89.163	(2)
F1 - F3	93.765	(2)
F1 - F3	86.235	(2)
F2 - F3	94.176	(2)
F2 - F3	85.824	(2)
F2 - F3	85.824	(2)
F2 - F3	94.176	(2)
	δ = 11.75	

Agreement Parameters

Rp:	14.30
Rwp:	16.80
Rexp:	8.73
Chi2:	3.71
R-Bragg	**5.93**
DW-Stat.:	0.76

A =	0.20	ϕ	B' (Li) [001] =	10.4	
B =	0.17	ϕ	B (AL) [001] =	13.0	
C =	0.24	θ	B' (Li) [110] =	15.5	
D =	0.22	θ	B (AL) [110] =	19.7	
E =	0.56	Φ	B' (Li) [111] =	18.6	
F =	0.24	Φ	B (AL) [111] =	23.5	

Octahedral Tilts

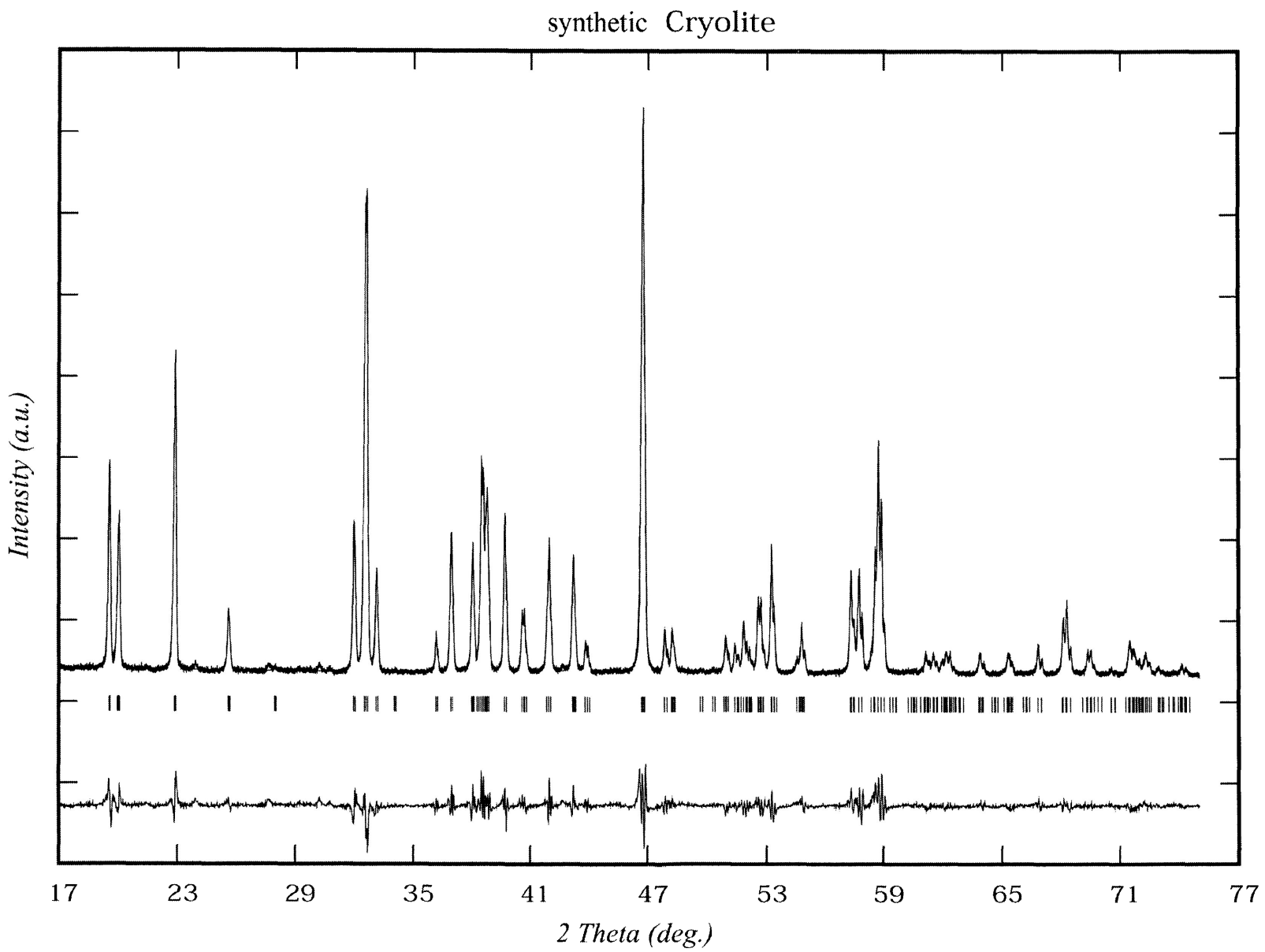
synthetic Cryolite
Intensity (a.u.)
17
23
29
35
41
47
53
59
65
71
77
2 Theta (deg.)